UNIVERSITY OF CALIFORNIA, SAN DIEGO

Ecology of Flows and Drift Wave Turbulence: Reduced Models and Applications

A dissertation submitted in partial satisfaction of the
requirements for the degree
Doctor of Philosophy

in

Engineering Sciences (Engineering Physics)

by

Rima Hajjar

Committee in charge:

Professor George R. Tynan, Chair
Professor Patrick H. Diamond, Co-Chair
Professor Farhat Beg
Professor Kevin Quest
Professor Daniel Tartakovsky

2018

The dissertation of Rima Hajjar is approved, and it is acceptable in quality and form for publication on microfilm and electronically:

_____

_____

_____

_____
Co-Chair

_____
Chair

University of California, San Diego

2018

DEDICATION

To my father *Joseph*, my mother *Bernadette*,

to my sisters *Nisrine, Rosine, Nelly, Soha* and *Nicole*,

and most importantly, to my husband *Avram*.

EPIGRAPH

Alice: Would you tell me, please, which way I ought to go from here?

The Cheshire Cat: That depends a good deal on where you want to get to.

Alice: I don't much care where.

The Cheshire Cat: Then it doesn't much matter which way you go.

Alice: ...So long as I get somewhere.

The Cheshire Cat: Oh, you're sure to do that, if only you walk long enough.

—Lewis Caroll, Alice in wonderland

TABLE OF CONTENTS

LIST OF FIGURES

LIST OF TABLES

ACKNOWLEDGEMENTS

Firstly, I would like to express my sincere gratitude to Prof. Patrick H. Diamond and Prof. George R. Tynan for their continuous support of my PhD study, for their patience, motivation and immense knowledge. Their guidance helped me complete a successful PhD degree and present a decent scientific research. I would like to thank them for welcoming me into their research group. My deepest appreciation goes to my lead academic advisor Patrick Diamond. Not only was he the perfect PhD advisor, but also the best academic mentor I could have ever imagined. His deep knowledge and sharp and constructive critic helped me become a better scientist. I will be forever grateful for his patience and his help.

I would like to thank the members of my dissertation committee: Prof. Farhat Beg, Prof. Kevin Quest, and Prof. Daniel Tartakovsky. Special gratitude goes to Prof. Tartakovsky. I will always remember the fluid course he taught me as part of the PhD course requirements.

My sincere thanks also go to people of the lunch club: Leo Chousal, Rollie Hernandez, Dr. Rongjie Hong, Dr. Saikat Thakur, Dr. Jonathan Yu, Dr. Anze Zloznik, and soon to be Dr. Shota Abe, Dr. Jiacong Li and Dr. Michael J. Simmonds. I would like to thank each and every one of them for the stimulating discussions we had, regarding both physics and non-physics topics.

I would also like to thank Zachary Dake, Patrick Mallon and Lydia Ramirez from the Mechanical and Aerospace Engineering department, as well as the assistant Dean and Director of the Students Affairs and Admissions April Bjornsen for providing an immense help overcoming many of the technical problems during my PhD. I am deeply appreciative of their assistance.

Of course, my deepest gratitude goes to my family: my father Joseph, my mother Berandette, and my sisters: Nisrine, Rosine, Nelly, Soha and Nicole. Despite not being physically present around me, I am sure they kept me in their hearts and minds. My family played a major and important role in supporting all the decisions I took, decisions that allowed me to reach the point of defending my PhD. I would also like to thank my mother-in-law for her assistance and

support.

Lastly and most importantly, I am forever grateful to my husband Avram Dalton. Avram was my source of motivation during the lonely times I spent wondering when I will finish my PhD, or if I will ever finish it. I feel he shared with me the hurdles, the efforts, the good and the bad of this PhD. I thank him for being the ONLY constant sound of reason and sanity during the seven years I spent at UCSD, and I dedicate this degree to him.

Chapter 2 is a reprint of the material as it appears in the publication "The Ecology of Flows and Drift Wave Turbulence in CSDX: a Model" in the Journal of Physics of Plasmas **25**, 022301 (2018). Hajjar R. J., Diamond P.H., Tynan G.R., American Institute of Physics, 2018. The dissertation author was the primary investigator and author of this article.

Chapter 3 is a reprint of the material as it appears in the publication "Modeling Enhanced Confinement in Drift-Wave Turbulence" in the Journal of Physics of Plasmas **24**, 062106 (2017). Hajjar R. J., Diamond P. H., Ashourvan A., Tynan G. R, American Institute of Physics, 2017. The dissertation author was the primary investigator and author of this article.

Chapter 4 is currently being prepared for submission for publication in "On the Dynamics of Zonal Shear Layer Collapse at High Density" in the Journal of Physics of Plasmas 2018. Hajjar R. J., Diamond P. H., Malkov M., American Institute of Physics, 2018. The dissertation author was the primary investigator and author of this article.

VITA

2007	B. S. in Physics, Lebanese University, Beirut, Lebanon.
2010	M. S. in Physics, American University of Beirut, Beirut, Lebanon.
2011-2018	Graduate Research Assistant and Teaching Assistant, University of California, San Diego, USA.
2018	Ph. D. in Engineering Sciences (Engineering Physics), University of California, San Diego, USA.

PUBLICATIONS

R. J. Hajjar, P. H. Diamond, M. Malkov, "On the Dynamics of Zonal Shear Layer Collapse at High Density", Journal of Physics of Plasmas, (under preparation for submission for publication)

R. J. Hajjar, P. H. Diamond, G. R. Tynan, "The Ecology of Flows and Drift Wave Turbulence in CSDX: a Model", Journal of Physics of Plasmas, 25, 022301, 2018.

R. J. Hajjar, P. H. Diamond, A. Ashourvan, G. R. Tynan,"Modeling Enhanced Confinement in Drift Wave Turbulence", Journal Physics of Plasmas, 24, 062106, 2017.

R. Hajjar, E. M. Hollmann, S. I. Krashenninikov, R. P. Doerner, "Modeling of Aluminum Impurity Entrainment in the PISCES-A He^+ Plasma", Journal of Nuclear Materials, 463, 664-667, 2015.

R. Hong, J. C. Li, S. Chakraborty Thakur, R. J. Hajjar, P. H. Diamond, G. R. Tynan, "Tracing the Pathway from Drift-Wave Turbulence with Broken Symmetry to the Production of Sheared Axial Mean Flow", Physical Review Letters (Accepted for publication)

R. Hong, J. C. Li, R. J. Hajjar, S. Chakraborty Thakur, P. H. Diamond, G. R. Tynan, "Generation of Parasitic Axial Flow by Drift Wave Turbulence with Broken Symmetry: Theory and Experiment", Journal of Physics of Plasmas (Submitted for publication)

ABSTRACT OF THE DISSERTATION

Ecology of Flows and Drift Wave Turbulence: Reduced Models and Applications

by

Rima Hajjar

Doctor of Philosophy in Engineering Sciences (Engineering Physics)

University of California, San Diego, 2018

Professor George R. Tynan, Chair
Professor Patrick H. Diamond, Co-Chair

In this dissertation, we present advances in turbulence modeling for magnetically confined plasmas. We investigate the ecology of microscopic drift wave turbulence and the self-generated macroscopic flows in magnetically confined plasmas. We formulate reduced models that self-consistently describe the evolution of turbulence and mean plasma profiles (including flows) and recover trends obtained from the CSDX device and HL-2A tokamak. The dissertation is divided to three parts. The first part presents a reduced model that describes the interplay between drift wave turbulence and zonal and axial flows in the adiabatic plasma of CSDX, where the electron response is Boltzmann. The model explains how free energy released from the density gradient

accelerates both axial and azimuthal flows in CSDX. A description of the interactions between the disparate scales of the plasma via the parallel and perpendicular Reynolds stresses $\langle \tilde{v}_x \tilde{v}_z \rangle$ and $\langle \tilde{v}_x \tilde{v}_y \rangle$ is presented. Expressions for these stresses are decomposed into a diffusive component that relaxes the flow profile, and a residual stress responsible for accelerating the corresponding flow. Moreover, parallel and perpendicular flow dynamics are described using an extended mixing length approach. This accounts for the degree of symmetry breaking in the parallel direction and parametrizes the efficiency of ∇n in driving the axial flow. In the second part of the dissertation, the relationship between drift waves and zonal flows is examined in depth via a more specific model. Analytical results obtained from this model confirm the published experimental data showing a suppression of turbulence with the increase in magnitude of the magnetic field **B**. A new criterion for access to enhanced confinement is introduced. This criterion captured by the dimensionless quantity R_{DT}, compares the production rate of turbulent enstrophy due to relaxation of the mean profiles, to the corresponding destruction rate via coupling to the mean flow. When $R_{DT} > 1$, the profiles steepen and enhanced confinement is accessible. In the third paper, a novel idea for understanding the physics of the density limit problem in low β tokamaks is presented. The collapse of the zonal shear flow when the electron response transitions from Boltzmann to hydrodynamic scaling, along with cooling of the edge and the onset of MHD activity is predicted by the observation that the zonal flow drive will drop as the electron parallel diffusion time increases with density. This leads to a simple, verified understanding of the density limit phenomenon in *L*-modes.

Chapter 1

INTRODUCTION

1.1 Nuclear Fusion: Concepts and Definitions

The greatest increase in demand for energy is envisaged to come from developing countries where, with rapid urbanization, large-scale electricity generation will be required. With environmental requirements for zero or low CO_2 emission sources and the need to invest in a viable energy mix, new energy sources must be developed. Since the 1950s, nuclear fusion has been investigated as a means for humans to generate sustainable energy. As an alternative to burning fossil fuels, nuclear fusion has the potential of producing high outputs of clean energy that can be easily converted to electric power. In contrast to nuclear fission reactions, controlled fusion reactions safely release high amount of energy while producing fewer radioactive particles. In spite of currently remaining an experimental technology for power production, nuclear fusion will be available as a future energy option, and should acquire a significant role in providing a sustainable, secure and safe solution to tackle the global energy needs.

Plasma, also referred to as the fourth state of matter, is a hot ionized and charged gas that can be classified into two categories: a natural plasma that occurs in the Sun, the stars and the interstellar clouds..., and a laboratory or a man-made plasma. The latter is currently being studied

as a potential route to fusion energy. The primary fuel used in experimental fusion power plants is composed of Hydrogen isotopes. The three nuclear reactions involving hydrogen isotopes are:

$$ {}^{2}_{1}H + {}^{2}_{1}H \rightarrow {}^{3}_{2}He + {}^{1}_{0}n + 3.27MeV \tag{1.1} $$

$$ {}^{2}_{1}H + {}^{2}_{1}H \rightarrow {}^{3}_{1}H + {}^{1}_{1}H + 4.03MeV \tag{1.2} $$

$$ {}^{2}_{1}H + {}^{3}_{1}H \rightarrow {}^{4}_{2}He + {}^{1}_{0}n + 17.59MeV \tag{1.3} $$

Of these, the reaction with the highest cross section is a D-T reaction, where a nucleus of deuterium $({}^{2}_{1}H)$ fuses with a nucleus of tritium $({}^{3}_{1}H)$ to produce an alpha particle $({}^{4}_{2}He)$ and a neutron. Because of the mass difference between the reactants and products, this reaction produces an energy excess of 17.6 MeV, carried mostly by the light neutron. In advanced nuclear reactor designs, the resultant neutron escapes the electromagnetic fields, and reacts with a plasma breeder blanket composed mainly of Lithium $({}^{6}_{3}Li)$ composites according to the following reaction:

$$ {}^{1}_{0}n + {}^{6}_{3}Li \rightarrow {}^{4}_{2}He + {}^{3}_{1}H + 4.8MeV \tag{1.4} $$

This reaction produces an additional alpha particle and another tritium nucleus, which is recycled back to fuel the original (D-T) mixture in the reactor core. Conventional energy conversion methods are then used to produce electric power out of the $4.8MeV$ exothermic energy yielded by the Lithium reaction. Macroscopically, 1 kg of the D-T fuel produces $10^8 kWh$ of energy in the nuclear fusion process, enough to provide the requirement of a $1GW$ electric power station per day [Wes04]. This means that, while a 10^3 MW coal-fired power plant requires 2.7 million tons of coal per year, a fusion plant will only require 250 kg of D-T fuel per year, half of it being deuterium, the other half being tritium [ite].

For the Deuterium-Tritium reaction to occur, the D-T mixture needs to be heated to a sufficiently high temperature to overcome the Coulomb repulsive force. At a sufficiently high temperature (roughly > 10 keV), the cross section of the D-T reaction is optimal as shown in

figure (1.1), inter-particle collisions are frequent, and both electrons and ions coexist together.

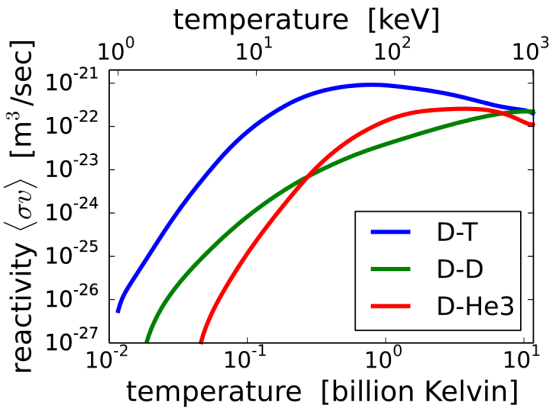

Figure 1.1: Fusion reaction rates versus temperature.

A crucial step after creating the plasma is keeping the ionized gas spatially confined for a long time, in order to achieve a sufficient number of fusion reactions. The goal is to exceed break-even, meaning the fusion energy output exceeds the energy required to heat the plasma. As a D-T plasma is heated to thermonuclear conditions, the alpha particle provides an increasing fraction of the total heating. When adequate confinement conditions are provided, a point is reached where the plasma temperature can be maintained against the energy losses, solely by alpha particle heating. The applied heating can then be removed and the plasma temperature is sustained by internal heating. This is called ignition.

A promising and well-known approach for plasma confinement is by using externally imposed magnetic field lines to keep the ionized particles inside the fusion device. Toroidal devices, like tokamaks (Fig.(1.2)) and stellerators, or linear devices, such as the Controlled Shear Decorrelation eXperiment (CSDX) (Fig.(1.3)) rely on the concept of magnetic confinement to shape the plasma. While confining the plasma is an important and necessary first step, it remains limited by thermal conduction and convection and radiation processes. Moreover, Coulomb collisions cause major losses of particles and energy from the plasma.

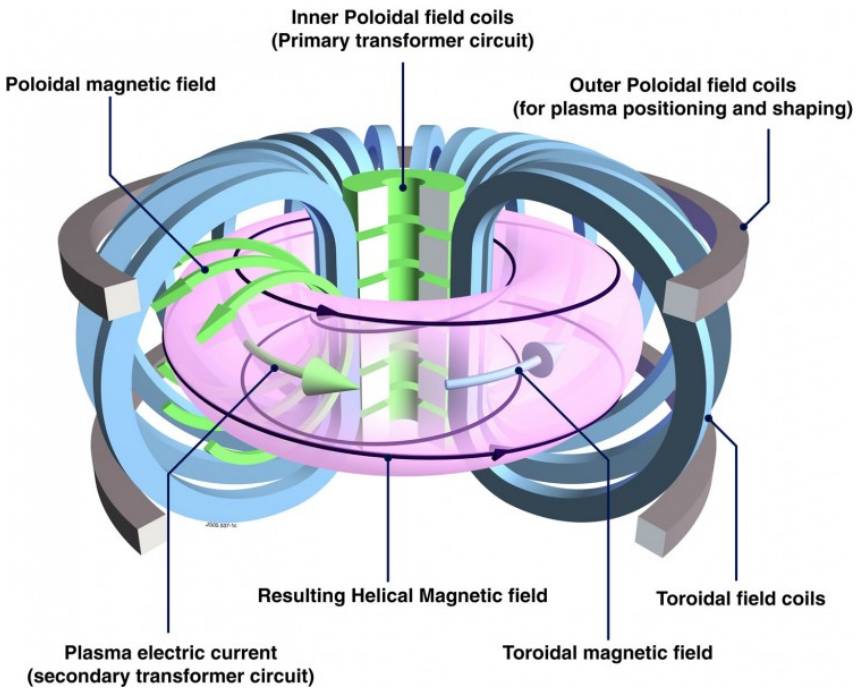

Figure 1.2: Magnetic configuration inside a tokamak.

1.2 Classical, Neoclassical, and Anomalous Transport

A main issue limiting the confinement of energy and particles in fusion devices are the strong thermal and particle losses that exceed both the classical and neoclassical estimates. According to the *classical theory of diffusion*, an estimate of the particle transport scale length in a plasma column is the corresponding Larmor radius ρ. For a characteristic collision time τ_c, the total plasma confinement time is: $\tau \sim \tau_c(a/\rho)^2$, where a is the plasma radius. Since both τ_c and ρ are mass dependent, the total confinement time of the electrons is higher than that of ions by $(m_i/m_e)^{1/2}$. Like-particle collisions do not produce any diffusion because the particles simply shift around in the center of mass reference frame. Therefore, electrons and ions diffuse at a rate equal to the electron-ion collision frequency $\nu_{ei} \sim n/T_e^{3/2}$. The classical theory of diffusion hence predicts a confinement time: $\tau_c \propto 1/\nu_{ei}$.

In tokamaks, however, this argument does not hold and significant modification is required, as diffusion of particles is enhanced by the complex magnetic topology. Accounting

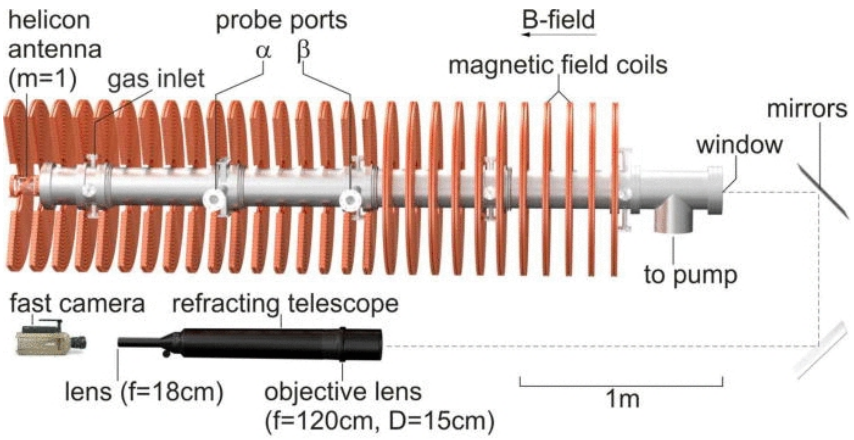

Figure 1.3: Controlled Sheared Decorrelation eXperiment (CSDX)

for the effects of the outward force that results from the presence of a pressure gradient has given rise to the study of *neoclassical transport*. Depending on the plasma collision frequency, the particle diffusion coefficient is further enhanced compared to the classical coefficient D^c [Wes04]. Despite taking neoclassical effects into consideration, experimental transport rates remain much higher that those calculated, even for cases of low plasma temperatures where Coulomb collisions are more frequent.

To reiterate, predicted particle and energy transport rates, which would naturally occur in the absence of instabilities, are much lower than those reported experimentally. Data obtained from various devices show that the actual ion thermal conductivity is larger by an order of magnitude when compared to the neoclassical ion conductivity κ_{neo}. In addition, both the electron thermal conduction and the particle diffusion coefficients are greater by about two orders of magnitude than what is expected neoclassically [IIFY99, Sta05]. In order to reconcile the experimental data to the theoretical calculations, it is thought that anomalous plasma transport is due to the presence of instabilities that cause particles and energy to escape at a higher rate. These micro-instabilities are generated by turbulent fluctuations in the plasma pressure and/or in the electric and magnetic fields. Their presence is almost unavoidable in most fusion devices, so much so that one focus of nuclear fusion research is now directed towards understanding how to

control and stabilize them.

1.3 Turbulence and Instabilities

Turbulence in plasma has several characteristic features. Indeed, the level of fluctuations and the spectrum of turbulence are strongly influenced by the configuration of the plasma and its thermodynamic state [YII03]. Although the most conspicuous instabilities observed in tokamaks are of long wavelength, low-m MHD modes, such as those responsible for disruptions, there appears to be little correlation between the intensity of these modes and the observed electron loss rates in macroscopically stable plasmas. Such modes affect local transport in the vicinity of their resonant surface, but do not appear to contribute to the overall electron loss rate. Consequently, investigations have focused on short wavelength fluctuations, referred to as micro-turbulence [Sta05]. In particular, investigations distinguished between turbulence along the magnetic field **B** and turbulence perpendicular to **B** (in the radial direction), which induces a variety of plasma responses, i.e., various plasma instabilities. There are two ways for micro-turbulence to enhance the radial transport: the $E \times B$ drift across the confining field lines resulting from the fluctuating electric fields, or parallel plasma motion along the magnetic field lines with a fluctuating radial component. Most effort has been devoted to understanding turbulent transport arising from $E \times B$ drifts.

One type of instability frequently observed in almost all fusion devices is that caused by drift waves (DWs). Driven by radial inhomogeneities in the plasma density, drift waves are inherently stable. However, a simple dissipation mechanism - such as parallel resistivity caused by eletron-ion collisions - can drive them to be unstable. The transport of particles and energy would then grow, leading to a loss of the plasma confinement in some cases.

1.4 Drift Waves and Drift Wave Instabilities

In this section, we introduce the drift waves, which are the main topic of investigation in this dissertation. Drift waves are low-frequency electrostatic waves ($\omega \ll \omega_i \ll \omega_e$) associated with the presence of density gradients ∇n. They propagate in a direction almost perpendicular to the magnetic field, so the **B**-parallel component of the wave vector k is small in such a way that $v_{th,i} \ll \omega/k_z \ll v_{th,e}$. Here, the ion and electron thermal velocities are $v_{th,i}$ and $v_{th,e}$, respectively and ω is the frequency of the drift waves. Driven by the pressure gradient $\nabla p = T\nabla n$ (assuming

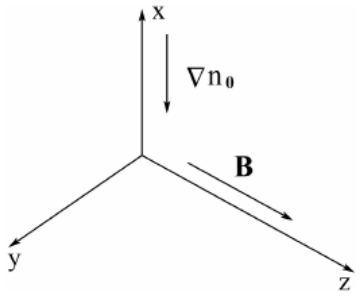

Figure 1.4: Geometry of the problem, showing the density gradient and the magnetic field vector.

a constant temperature), these waves drift across the plasma at a velocity of:

$$v_i = \frac{K_B T_i}{eB}\frac{d\ln n(x)}{dx}\hat{y} \tag{1.5a}$$

$$v_e = -\frac{K_B T_e}{eB}\frac{d\ln n(x)}{dx}\hat{y} \tag{1.5b}$$

where K_B is the Boltzmann constant, and $\hat{y}$ is the direction perpendicular to both **B** and ∇n (see Fig.(1.4)).

1.4.1 Linear Analysis and Linear Solutions

The expressions for the drift velocities are obtained by examining the density and momentum equations of both electrons and ions. Considering the electrons first, and neglecting

their inertia in the parallel direction, we obtain the Boltzmann isothermal relation from the momentum equation:

$$\frac{\partial \ln n_e}{\partial z} \approx \frac{e}{K_B T_e} \frac{\partial \phi}{\partial z} \tag{1.6}$$

or

$$n_e = n_0(x) \exp[e\phi / K_B T_e] \tag{1.7}$$

The quasistatic process described by eq.(1.7) shows how the electrons respond instantaneously to the drift waves, moving almost spontaneously from a wave crest to a wave trough to establish an equilibrium in the parallel direction. As for the ions, their velocity perpendicular to the magnetic field is approximated by the $E \times B$ drift: $u_i = \frac{\hat{z} \times \nabla \phi}{B}$, where the electrostatic potential $\mathbf{E} = -\nabla \phi$ is introduced. The ion continuity equation then becomes:

$$\frac{\partial n_i}{\partial t} + \nabla . (\frac{\hat{z} \times \nabla \phi}{B} n_i) = 0 \tag{1.8}$$

Keeping in mind the quasi-neutrality condition $n_e \approx n_i$, combining eq.(1.7) and eq.(1.8) gives:

$$\frac{\partial \phi}{\partial t} - \frac{K_B T_e}{e} \frac{\nabla \phi \times \hat{z}}{B} . \frac{\nabla n_0(x)}{n_0(x)} = 0 \tag{1.9}$$

Note that, for a plasma with constant magnetic field $\mathbf{B}$, the ion perpendicular motion is incompressible since $\nabla . (\nabla \phi \times B) = 0$. The plasma fluctuations are thus associated with variations in the density profile, as the ions move in and out along a density gradient taken in the $\hat{x}$-direction according to fig.(1.4). In order to obtain the corresponding dispersion relation of these perturbations, we write the fluctuating electric potential as: $\phi = \phi_0(x) \exp(i\omega t + ik_y y)$, where ω and k_y are the frequency and the wavenumber of the corresponding turbulent mode. From eq.(1.9), we obtain:

$$\omega = \omega^\star = u_{De}(x) k_y \tag{1.10}$$

where the electron diamagnetic velocity in the $\hat{x}$ direction is:

$$u_{De}(x) = -\frac{K_B T_e}{eB}.\frac{\nabla n_0(x)}{n_0(x)} \tag{1.11}$$

Eq.(1.10) is a dispersion relation with only a real component. Therefore, it describes a *local* and *stable* drift wave fluctuation. This peculiar result is a consequence of ignoring the ion inertia in both parallel and perpendicular directions, which makes eq.(1.9) linear in $\phi(x)$ although no linearization assumptions were actually made.

A general form of the dispersion relation is obtained by keeping the ion inertia in the momentum equation for cold ions:

$$M(\frac{\partial u_i}{\partial t} + u_i.\nabla u_i) = e(-\nabla\phi + u_i \times B) \tag{1.12}$$

The perpendicular ion velocity is then:

$$u_{i\perp} = -\frac{\nabla\phi \times \hat{z}}{B} - \frac{M}{eB^2}[\frac{\partial}{\partial t}(u_i \times B) + u_i.\nabla(u \times B)] \tag{1.13a}$$

$$= -\frac{\nabla\phi \times \hat{z}}{B} - \frac{M}{eB^2}\Big[\frac{\partial}{\partial t} - \frac{1}{B}\nabla\phi \times \hat{z}.\nabla\Big]\nabla_\perp\phi \tag{1.13b}$$

The first term in eq.(1.13) represents the lowest order $E \times B$ drift. The second term represents the ion polarization drift that makes $\nabla.u_i \neq 0$. The parallel component of the momentum equation remains:

$$M(\frac{\partial u_{i\|}}{\partial t} + u_i.\nabla u_{i\|}) = -e\frac{\partial\phi}{\partial z} \tag{1.14}$$

Using the quasi-neutrality condition $n_e \approx n_i$, and assuming isothermal Boltzmann electrons, we obtain the following nonlinear equation in $\phi(x)$:

$$\frac{\partial\phi}{\partial t} + \frac{K_B T_e}{e}\nabla.u + u.\nabla\phi + \frac{K_B T_e}{en_0(x)}\frac{dn_0(x)}{dx}u.\hat{x} = 0 \tag{1.15}$$

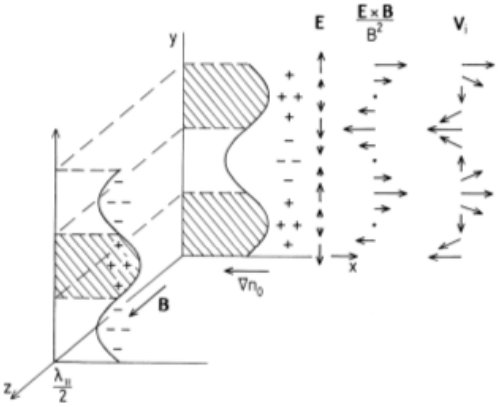

Figure 1.5: Drift wave perturbation reproduced from [Pec13]. The solid line indicates a contour of constant density, while the electric fields and the ion velocities are indicated by small arrows. Charge densities are indicated by + and - symbols. Regions with enhanced density are shaded for clarity.

where $u = \{u_\perp, u_\parallel\}$. A linear solution to the set of eqs.(1.13-1.15) gives the following dispersion relation in a collisionless plasma [Pec13]:

$$\omega^2(1+\rho_s^2 k_y^2) - \omega k_y u_{De} - c_s^2 k_z^2 = 0 \tag{1.16}$$

Here $\rho_s = c_s/\omega_{ci} = (c\sqrt{T_e M_i})/(eB)$ is the effective ion Larmor radius with an electron temperature T_e, where $c_s = \sqrt{T_e/M_i}$ is the plasma sound speed and $\omega_{ci} = eB/M_i c$ is the ion Larmor gyrofrequency. For a homogeneous plasma, $k_y = 0$ and one easily recovers the dispersion relation for an acoustic wave $\omega = c_s k_z$. The second term inside the parenthesis of eq.(1.16) represents the contribution of the polarization drift and results from considering the ion inertia. For small ρ_s and k_z, the initial dispersion relation $\omega = \omega^\star = k_y u_{De}$ is recovered, and the wave propagates in the direction of the electron diamagnetic drift. In the limit $k_z \to 0$, the DW dispersion relation becomes:

$$\omega = \frac{k_y u_{De}}{1+\rho_s^2 k_y^2} \tag{1.17}$$

Fig.(1.5) illustrates the basic mechanism of the drift wave perturbation. A solid line represents the contours of constant plasma density, i.e., the contours of constant electric potential

(because of the Boltzmann equilibrium relation). When the polarization drift induced by the ion inertia is neglected, the ion drift velocities are approximated to the lowest order by the $E \times B$ drift. If the electric fields were steady, ions would drift with the local $E \times B$ velocity. However, because of the fluctuating density, the plasma electric potential, and thus, the corresponding electric field E are also fluctuating. Since E fluctuates in the $\hat{y}$ direction, ions are accelerated in the $\hat{x}$-direction, and their lowest order velocity is equal to $v_x = E_y/B = -ik_y\phi/B$. The corresponding dispersion relation is then that given by eq.(1.10). Because eq.(1.10) gives a non-imaginary frequency: $\omega = k_y u_{De}$, there is no growth rate associated with such waves, which are considered to be inherently *stable*.

To see how drift waves become unstable, one must realize that the ion drift velocity is not really equal to the $E \times B$ drift, and that there are corrections due to the ion polarization drift. When accounting for this additional drift, the electric potential lags the density fluctuations, forcing u_i to be outward where the plasma has already been shifted outward, and causing the perturbations to grow. Without this polarization drift, n and ϕ would simply be 90° out of phase and the motion of the waves would be purely diffusive [Che84]. An analytical derivation of the corresponding dispersion relation for a drift wave instability is obtained by considering the effects of the parallel plasma resistivity on the electron adiabatic response. Because the plasma current is divergence free:

$$\nabla . j = \nabla_\perp . j_\perp + \nabla_\parallel . j_\parallel = 0$$

the perpendicular ion polarization drift will necessarily affect the electron parallel response via the parallel plasma resistivity $\eta_\parallel$. When writing the density and momentum equations for both electrons and ions, it is essential to consider the momentum exchange terms that result from electron-ion collisions. Such terms are directly proportional to the electron collision frequency ν_{ei}. An analytical derivation by [HW83] shows that the electron linear response is no longer

adiabatic, but rather equal to:

$$\frac{n}{n_0} = \frac{e\phi}{K_B T_e} \frac{\omega^\star + ib\sigma_\parallel}{\omega + ib\sigma_\parallel} \tag{1.18}$$

where we have used the conventional notation $b = \rho_s^2 k_\perp^2$ and $\sigma_\parallel = (k_z^2/k_y^2)(\omega_{ce}\omega_{ci}/\nu_{ei})$. The density n_0 is the average plasma density used as a normalization constant. Proceeding as above, the linear dispersion relation that describes the evolution of the drift wave perturbation is equal to:

$$\omega^2 + i\sigma_\parallel \Big(\omega(1+b) - \omega^\star \Big) = 0 \tag{1.19}$$

This quadratic equation bears a damped solution:

$$\omega_{damped} = \frac{1}{2} \Big(-i\sigma_\parallel (1+b) - \sqrt{4i\sigma_\parallel \omega^\star - \sigma_\parallel^2 (1+b)^2} \Big) \tag{1.20}$$

as well as an unstable solution that describes the character of a drift wave instability:

$$\omega_{unstable} = \frac{1}{2} \Big(-i\sigma_\parallel (1+b) + \sqrt{4i\sigma_\parallel \omega^\star - \sigma_\parallel^2 (1+b)^2} \Big) \tag{1.21}$$

The analysis used to derive the previous dispersion relations was a *linear* analysis that remains valid only for waves with small amplitudes. Moreover, two approximations were made to derive these linear equations: the assumption of quasi-neutrality (plasma approximation) and the omission of ion polarization drifts (ion inertia) in certain cases. The relaxation of these two assumptions leads to weakly nonlinear physics described by the Hasegawa-Mima (HM) equation and the nonlinear Hasegawa-Wakatani (HW) equations. In the following subsections, we relax these two approximations, and perform a nonlinear analysis to get the corresponding dispersion relation.

1.4.2 Hasegawa-Mima Equation

The Hasegawa-Mima equation describes a turbulent plasma regime where time scales are fast ($\omega_{ci}^{-1}\partial/\partial t \ll 1$), and parallel distance scale is long. Using this ordering, the perpendicular ion velocity is still given by eq.(1.13), and the nonlinear equation for $\phi(x)$, i.e., eq.(1.15) is re-written as:

$$\frac{\partial\phi}{\partial t} - \frac{K_B T_e}{e}.\frac{\nabla_\perp\phi\times\hat{z}}{B}.\nabla_\perp \ln n_0 - \frac{c_s^2}{\omega_{ci}^2}\Big(\frac{\partial}{\partial t} - \frac{\nabla_\perp\phi\times\hat{z}}{B}.\nabla_\perp\Big)\nabla_\perp^2\phi = 0 \tag{1.22}$$

The previous equation is known as the Hasegawa-Mima equation. Upon normalization, it becomes:

$$\frac{\partial}{\partial t}\Big(\nabla_\perp^2\phi - \phi\Big) + \hat{z}\times\nabla_\perp\phi.\nabla_\perp\Big(\nabla_\perp^2\phi\Big) - \beta\frac{\partial\phi}{\partial y} = 0 \tag{1.23}$$

where the constant $\beta = -d\ln n_0/dx$ measures the electron diamagnetic drift. The notation is eased by introducing the Poisson brackets: $\{f,g\} = \partial_x f\partial_y g - \partial_x g\partial_y f$, giving the final form of the Hasegawa-Mima equation:

$$\frac{\partial}{\partial t}\Big(\nabla_\perp^2\phi - \phi\Big) - \beta\frac{\partial\phi}{\partial y} + \{\phi,\nabla_\perp^2\phi\} = 0 \tag{1.24}$$

In its linear form, the Poisson brackets are dropped from the (HM) equation which becomes:

$$\frac{\partial}{\partial t}\Big(\nabla_\perp^2\phi - \phi\Big) - \beta\frac{\partial\phi}{\partial y} = 0 \tag{1.25}$$

The corresponding linear dispersion relation is then obtained as: $\omega = \beta k_y/(1+k_\perp^2) = \omega^\star/(1+k_\perp^2)$. This is the same dispersion relation given by eq.(1.17).

1.4.3 Hasegawa-Wakatani Equations

A self-evident restriction of the Hasegawa-Mima equation is that it describes linearly stable waves or fluctuations, i.e. any perturbation has to be imposed initially. This feature violates the basic property of drift waves being unstable. The Hasegawa-Mima equation can however readily be generalized to include this feature. For a divergence free electric current: $\nabla.\mathbf{J} = 0 \Longrightarrow \nabla_\perp.J_{\perp,i} = -\nabla_\parallel.J_{\perp,e}$. Here the perpendicular current driven by the ions is balanced in the parallel direction by the electrons motion. The ion velocity is equal to:

$$v_{\perp,i} = \frac{\mathbf{E}\times\mathbf{B}}{B^2} - \frac{1}{\omega_{ci}B}\frac{d\nabla_\perp\phi}{dt} + \frac{\mu_{ii}}{\omega_{ci}B}\nabla^2(\nabla_\perp\phi) \tag{1.26}$$

where an ion viscosity term μ_{ii} has been added. Noting the plasma average density and resistivity as n_0 and η respectively:

$$\nabla_\perp J_{\perp,i} = en_0\nabla_\perp v_{\perp,i} = en_0\nabla_\perp\Big[-\frac{1}{\omega_{ci}B}\frac{d\nabla_\perp\phi}{dt} + \frac{\mu_{ii}}{\omega_{ci}B}\nabla^2(\nabla_\perp\phi)\Big]$$

In a similar way:

$$-\nabla_\parallel J_{\parallel,e} = -en_0\nabla_\parallel v_e = -\frac{T_e}{\eta e}\nabla_\parallel^2(\frac{n}{n_0} - \frac{e\phi}{T_e}),$$

therefore:

$$\frac{1}{\omega_{ci}B}\Big[\frac{d\nabla_\perp^2\phi}{dt} - \mu_{ii}\nabla^2(\nabla_\perp^2\phi)\Big] = \frac{T_e}{\eta e^2 n_0}\nabla_\parallel^2(\frac{n}{n_0} - \frac{e\phi}{T_e}) \tag{1.27}$$

The electron continuity equation on the other hand gives: $dn/dt + n\nabla.v = 0$ or:

$$\frac{d}{dt}\Big[\ln n_0 + \frac{n}{n_0}\Big] = \frac{T_e}{e^2 n_0\eta}\nabla_\parallel^2\Big[\frac{n}{n_0} - \frac{e\phi}{T_e}\Big] \tag{1.28}$$

A normalization of the time scale, the plasma density, and the plasma electric potential

by the ion cyclotron frequency $t = \omega_{ci}t$, the average density: $n = n/n_0$, and $\chi = e\phi/T_e$ gives:

$$\frac{dn}{dt} + \beta\frac{\partial\chi}{\partial y} = \frac{T_e}{e^2 n_0 \eta}\frac{\partial^2}{\partial z^2}(n-\chi) \tag{1.29a}$$

$$\frac{d\nabla_\perp^2\chi}{dt} = \frac{T_e}{e^2 n_0 \eta}\frac{\partial^2}{\partial z^2}(n-\chi) + \mu_{ii}\nabla^4\chi \tag{1.29b}$$

The two previous equations constitute the Hasegawa- Wakatani (HW) equations. When linearized, the Haseawa-Wakatani equations become:

$$\frac{\partial n}{\partial t} + \beta\frac{\partial\chi}{\partial y} = \frac{T_e}{e^2 n_0 \eta}\frac{\partial^2}{\partial z^2}(n-\chi) \tag{1.30a}$$

$$\frac{\partial\nabla_\perp^2\chi}{dt} = \frac{T_e}{e^2 n_0 \eta}\frac{\partial^2}{\partial z^2}(n-\chi) + \mu_{ii}\nabla^4\chi \tag{1.30b}$$

By Fourier transform, it is readily shown that eq.(1.30a) reproduces eq.(1.18), and that the linear dispersion relation is given by eq.(1.19)

1.5 The Drift Wave- Zonal Flow Relation

The results of the previous section show that, under certain conditions, drift waves can become unstable. As the levels of turbulence inside the plasma increase, transport of particle and energy is enhanced, and confinement is easily destroyed. Fortunately, the mechanism of turbulence regulation via self-generation and amplification of zonal flows (ZFs) [DIIH05, FII$^+$04].

Formation of zonal flows is a well-known and well-documented phenomenon in 2D turbulent systems [DIIH05]. In contrast to 3D turbulent systems, vortex stretching is inhibited in 2D systems, and turbulence is characterized by an inverse energy cascade in which energy is transferred to large spatial structures. In the inertial range, a direct enstrophy cascade where turbulent energy is driven to smaller scales dominates. The turbulent energy is then dissipated

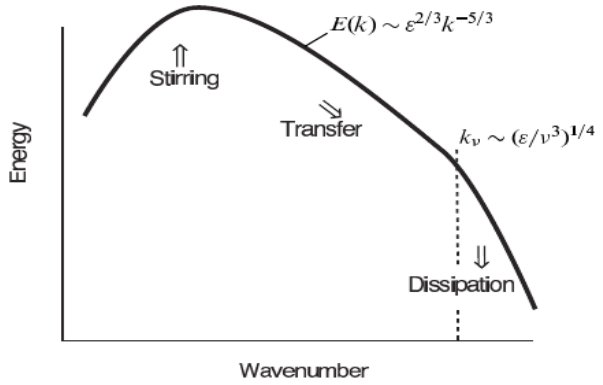

Figure 1.6: Direct energy cascade in 3D turbulent systems.

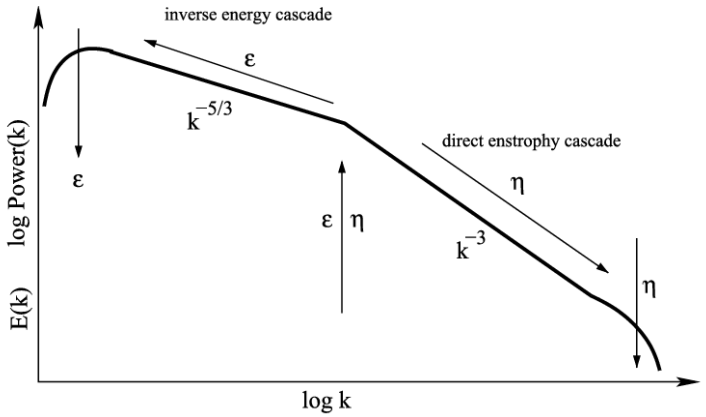

Figure 1.7: Dual cascade in 2D turbulent systems.

into heat on a Kolmogorov length scale $\eta = (\nu^3/\varepsilon)^{1/4}$ [Pop08]. Here ν is the fluid viscosity, and ε is the average rate of dissipation of the turbulent kinetic energy per unit mass. In addition to η, the Kolmogorov theory defines $\tau = (\nu/\varepsilon)^{1/2}$ and $u = (\nu\varepsilon)^{1/4}$ as the time scale and velocity scale at which viscosity dominates. Besides the direct enstrophy cascade, 2D systems also experience an inverse cascade of energy to larger scales. This inverse cascade is responsible for the generation of mesoscopic flows (see Fig.(1.7)). Examples include the famous quasi-2D geostrophic Rossby waves. These atmospheric waves result from the conservation of potential vorticity and are influenced by the Coriolis force and pressure gradient.

In plasmas, zonal flows represent linearly stable azimuthal $E \times B$ sheared layers that decorrelate the turbulent eddies, thus reducing the transport properties inside the plasma. In

the case of a smooth mean shear flow, it is well-known that shearing tilts the eddies, narrowing their radial extent and elongating them (fig.(1.8)). ZFs are radially localized flow structures with

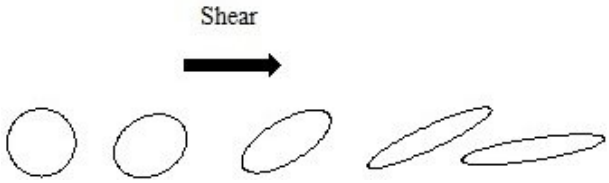

Figure 1.8: Tilting and shearing of the eddies.

azimuthal mode number $n = m = 0$ and finite radial wavenumber and low eigenfrequency ω. In a cylindrical plasma, ZFs are in the direction of the electron diamagnetic drift velocity (azimuthal direction). Because of their symmetry, zonal flows do not generate additional energy or particle transport, and are not subject to Landau damping. They are primarily damped by collisional processes. This is why ZFs are thought of as an ideal reservoir for the free plasma energy. Experiments show a suppression of turbulence through the zonal flows when the $E \times B$ shearing rate becomes greater than the linear growth rate of the drift wave instability, γ_l [HB95, TKE$^+$99]. Numerous theoretical, experimental, and numerical studies describing the relation between DWs and ZFs have been published, so much so that the problem is now referred to as "the problem of ZF/DW turbulence."

From a theoretical point of view, the formation of zonal flows results from direct nonlinear energy transfer between different unstable modes in the plasma. It is a consequence of non-local interaction in the wavenumber space. This process is related, but not identical, to the inverse energy cascade that occurs via non-local coupling [DIIH05]. Zonal flows are thought of as being generated by triad coupling, $\vec{k}_1 + \vec{k}_2 = \vec{k}_{ZF}$, according to fig.(1.9). Here $\vec{k}_1$, $\vec{k}_2$, and $\vec{k}_{ZF}$ are the wavenumbers of turbulence and zonal flow, respectively. According to the geometry of fig.(1.9), $\vec{k}_{ZF}$ is smaller than both $\vec{k}_1$ and $\vec{k}_2$. In addition, the zonal flow frequency is much lower than that of the individual waves.

The turbulence drive mechanism of zonal flows has been described by a simple fluid

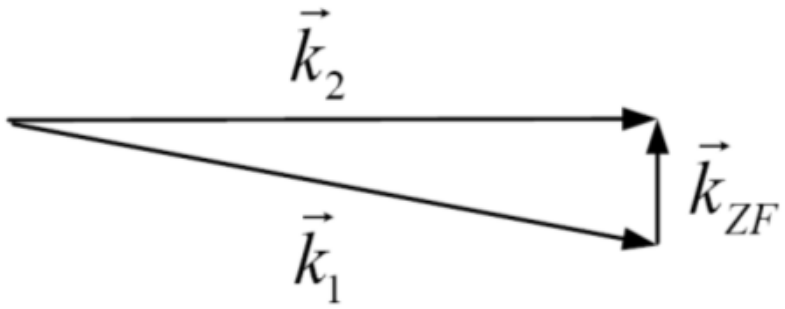

Figure 1.9: Generation of zonal flows by triad coupling. The wavenumbers of the drift waves are bigger than that of the zonal flow: $\vec{k}_1, \vec{k}_2 \gg \vec{k}_{ZF}$

model [DGH$^+$08] as:

$$\frac{\partial V_{ZF}}{\partial t} = -\frac{\partial}{\partial x}\langle \tilde{v}_x \tilde{v}_y \rangle - \nu_d V_{ZF} \tag{1.31}$$

where V_{ZF} is the zonal flow velocity, and ν_d is the zonal flow damping rate. The quantity $\langle \tilde{v}_x \tilde{v}_y \rangle$ is the turbulent Reynolds stress that redistributes momentum among different spatial locations. The divergence of the Reynolds stress is related to the vorticity flux via the Taylor identity [Tay15]:

$$-\frac{\partial}{\partial x}\langle \tilde{v}_x \tilde{v}_y \rangle = \langle \tilde{v}_x \nabla^2 \phi \rangle \tag{1.32}$$

The Reynolds stress plays a major role in the saturation process of turbulence. It is through $\langle \tilde{v}_x \tilde{v}_y \rangle$ that the plasma self-organizes into zonal flows, and energy is exchanged between its different turbulent components [DIIH05, Sco05].

A predator-prey relation exists between drift waves and zonal flows. Several analytical models have been developed to describe the nonlinear energy exchange between the disparate scales of the plasma. In these models, the zonal flows, i.e., the predators, feed on the prey population, i.e., the drift waves. The population of the predators is thus determined by that of the prey, as well as by the collisional damping rate of the zonal flows. The drift wave population on the other hand is determined by the predator-prey relation, as well as by the drift wave growth rate. This predator-prey relation has been verified experimentally, theoretically and

numerically [DIIH05, MRS09].

1.6 The Drift Wave-Axial Flow Relation

In addition to the drift wave-zonal flow relation, theoretical studies supported by experimental results reveal a similar relation between drift waves and the axial (parallel) flows in both toroidal and linear plasmas [KIIe5, KIK$^+$16, IKI$^+$16]. Measurements from Alcator C-Mod tokamak show that the observed intrinsic flow is proportional to the edge temperature gradient [RHD$^+$11]. The plasma behaves like a heat engine that uses the free energy to produce an intrinsic flow. During this process, the temperature gradient excites turbulence, which not only relaxes ∇T, but also drives a non-diffusive residual stress [KDG10]. In a similar vein, measurements from PANTA linear device show a direct relation between the parallel Reynolds stress and the parallel flows. These axial flows play an important role in stabilizing the plasma and reducing certain MHD and resistive wall modes, particularly in large scale fusion devices where parallel momentum injection via external Neutral Beam Injections (NBIs) is thought to be insufficient on its own. The aforementioned experimental observations were explained by theoretical investigations, which attribute an essential role to the parallel Reynolds stress $\langle \tilde{v}_x \tilde{v}_z \rangle$ in accelerating the formation of axial flows [DMG$^+$09, KJD$^+$11, DKG$^+$13]. Similar to the perpendicular Reynolds stress, the parallel Reynolds stress redistributes the momentum in the parallel direction, and uses the ∇n free energy to accelerate v_z. Specifically, it is the presence of a non-zero parallel residual stress $\Pi_{xz}^{res} = \Pi_{xz}^{res}(\nabla n, \nabla T_e)$ when the parallel symmetry is broken that triggers the generation and acceleration of v_z. The parallel residual stress is the counterpart of the poloidal residual stress that accelerates the zonal flows. Experiments on TJ-II stellarator confirm the existence of a significant turbulent residual parallel stress that produces a toroidal intrinsic torque. An electrode biasing experiment on J-TEXT achieved a nearly zero toroidal rotation profile, thereby showing that the intrinsic torque can be explained by the measured

residual stress [GmcHP$^+$06]. Recently, a gyrokinetic simulation also predicted that the residual stress generates the intrinsic torque, which is consistent with the measured rotation profile in DIII-D [WGE$^+$17].

Besides the parallel residual stress, the turbulent diffusion of the parallel momentum χ_z also plays an important role in the dynamics of v_z, since the expression for the parallel Reynolds stress is:

$$\langle \tilde{v}_x \tilde{v}_z \rangle = -\chi_z \nabla v_z + \langle \tilde{v}_x \tilde{v}_z \rangle^{res} \tag{1.33}$$

where $\Pi^{res} = \langle \tilde{v}_x \tilde{v}_z \rangle^{res}$. The competition between Π_{xz}^{res} and χ_z may create a spectral imbalance, thus promoting the growth of certain unstable modes. A well-documented example in CSDX is

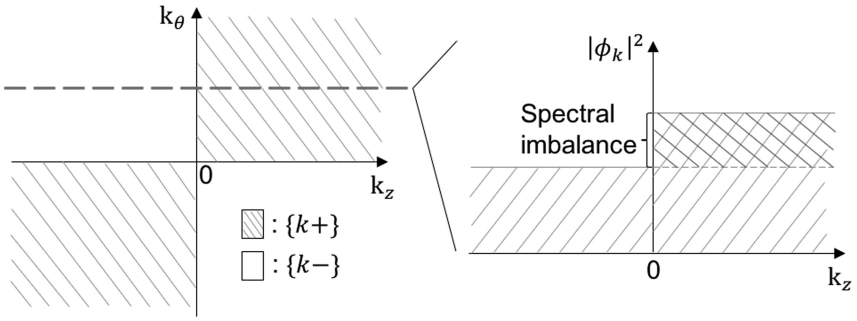

Figure 1.10: Spectral imbalance in the parallel wavenumber space [LDXT16].

that discussed in [LDXT16]. The energy released from the density gradient is used to accelerate v_z and steepen its profile. The axial flow then self-amplifies through a process of negative viscosity [LDXT16]. Nevertheless, v_z loses acceleration, as a parallel shear flow instability (PSFI) ultimately limits the growth of the plasma axial flow. This is somewhat analogous to the zonal flow saturation by tertiary instability [LDXT16].

1.7 Dissertation Outline

As discussed above, drift waves play a key role in regulating turbulence and controlling the dynamics of axial and zonal flows. To better understand and control fusion plasmas, it is essential to examine and map the relation between these three plasma components. Toroidal plasmas are complex systems that are characterized by high temperature ($\sim$ several keV). Moreover, tokamaks are usually large-scale devices, where the magnetic field **B** is not constant. This is why a magnetic shear is always present in a tokamak plasma. These aspects make the plasma diagnosis in a toroidal device difficult. To make progress, scientists reduce the problem by focusing their studies on an elementary linear plasma, such as that of CSDX. Not only is the CSDX plasma simpler to study compared to large toroidal plasmas, but also presents a unique opportunity to investigate the evolution of both turbulence and mean profiles near the plasma edge. Measurements from both Langmuir and Mach probes are easily obtained from CSDX low-temperature plasma.

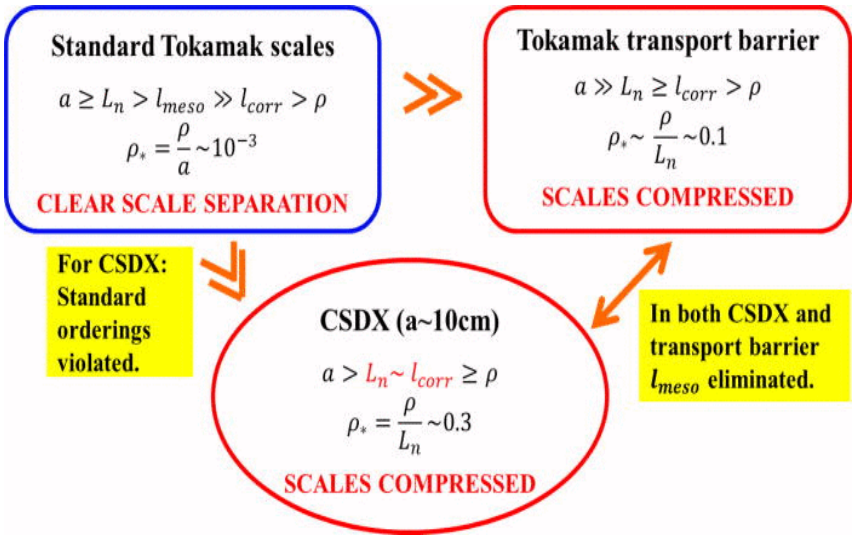

Figure 1.11: Scaling comparison between standard tokamak, tokamak transport barrier regime, and CSDX [CAT$^+$16].

CSDX is a promising testbed for exploring drift-wave physics in compressed scale regimes [CAT$^+$16]. The range of scales in CSDX is essential in formulating the appropriate

physical models used to describe turbulence and flow dynamics as shown in figure (1.11). Note that in CSDX, the normalized radius $\rho_\star = \rho/a$ is comparable to that in H-mode edge transport barrier regimes. Moreover, the mesoscopic length l_{meso} is eliminated from the scale ordering in CSDX. This shows why CSDX is a useful venue, where studies of scale compression can be performed. The characteristics of CSDX plasma are summarized in the following table:

Table 1.1: Characteristics of CSDX plasma.

Gas Type	Argon
Total Plasma Length (L)	$\approx 3\ m$
Plasma Radius (a)	$\approx 10\ cm$
Plasma density (n)	$0.9-1\times10^{13}\ cm^{-3}$
Electron Temperature (T_e)	$3.0-3.3\ eV$
Ion Temperature (T_i)	$0.5-0.7\ eV$
Ion Sound Speed ($c_s()$	$2.8\times10^{5}\ cms^{-1}$
Ion gyroradius ($\rho_s = c_s/\omega_{ci}$)	$1.1\ cm$
Ion-ion viscosity ($\mu_\perp$)	$4.6\times10^{3}\ cm^2s^{-1}$
Ion-neutral collision frequency (ν_{in})	$6\times10^{3}\ s^{-1}$

The low electron temperature T_e and high ion-neutral collision frequency ν_{in} in CSDX are comparable to existing values in the edge regions of large-scale devices. Details of the experimental device, operating regimes, plasma diagnostics, and typical radial profiles of the standard plasma parameters can be found in references [TBC$^+$14, AYT07].

In this dissertation, I investigate the relation between drift waves and plasma zonal and axial flows. In particular, I formulate reduced models that self-consistently describe the evolution of turbulence and flow dynamics in both adiabatic and hydrodynamic electron limit of the plasma. The aim is to map different relations between the fluctuations and the macroscopic flows, while also verifying the experimental results obtained in CSDX and HL-2A tokamak. A flow chart summarizing the work covered in this dissertation is shown below Fig.(1.12). In Chapter 2, we present a reduced model that describes the ecology of drift wave turbulence and flows in CSDX. The model explains how the ∇n free energy accelerates both zonal and axial flows via the Reynolds stresses, $\langle \tilde{v}_x \tilde{v}_y \rangle$ and $\langle \tilde{v}_x \tilde{v}_z \rangle$. The model describes time and space evolution of the density

n, the azimuthal and axial flows v_y and v_z, and the turbulent energy $\varepsilon = \langle \tilde{n}^2 + \tilde{v}_y^2 + \tilde{v}_z^2/2 \rangle$. The model explains how the Reynolds stresses redistribute the momentum in the axial and azimuthal directions. It also relates parallel to perpendicular flow dynamics by introducing a coupling constant σ_{vT}. This constant measures the degree of parallel symmetry breaking, as well as the correlator $\langle k_m k_z \rangle$, which is at the essence of the parallel residual stress. Chapter 2 presents a complete picture of the different interactions that occur between turbulence and mean profiles, including a detailed study of feedback loops that exist between different elements of the plasma.

In Chapter 3, I focus on the DW/ZF relation. A numerical validation and verification of the turbulence regulation phenomenon in CSDX is presented. This turbulence regulation has been observed experimentally in references [CTD$^+$15, CAT$^+$16]. For this purpose, another reduced model that describes space and time evolution of n and v_y, in addition to the usual potential enstrophy $\varepsilon = \langle (\tilde{n} - \nabla^2 \tilde{\phi})^2/2 \rangle$ is formulated. Chapter 3 focuses only on the DW/ZF relation in the adiabatic electron limit. It presents numerical results that describe the evolution of the plasma mean and turbulent profiles, as the magnitude of the magnetic field **B** is varied. In addition, a new criterion for turbulence saturation is established. This criterion is characterized by the dimensionless quantity R_{DT}, which compares the production rate of the turbulent enstrophy due to the relaxation of the mean profiles, to the destruction rate of ε via coupling to the mean flow because of the predator-prey relation.

Chapter 4 examines the relation between DWs and ZFs is examined in another plasma limiting case, known as the hydrodynamic limit. In this case, the equations that describe the behavior of the plasma density and vorticity decouple, and are essentially reduced to a 2D Navier-Stokes equation. In contrast to the adiabatic limit, zonal flows are shown to collapse in the hydrodynamic limit, and turbulence is enhanced instead of being suppressed. These changes in the plasma dynamics are interpreted from a zonal flow production perspective. As the adiabaticity parameter decreases, the particle transport increases, while the efficiency of plasma zonal flows production decreases. The edge shear layer weakens, the thermal confinement

degrades, and an MHD activity is eventually triggered. This chapter is of particular interest in the context of understanding the enhancement of turbulence and the collapse of the edge shear layer in density limit experiments - a topic of crucial importance for future magnetic fusion devices.

Lastly, Chapter 5 summarizes the findings of this dissertation, points to future work on the relation between turbulence and mean flows, and presents a list of potential experiments and recommendations to further advance the experiments of this study.

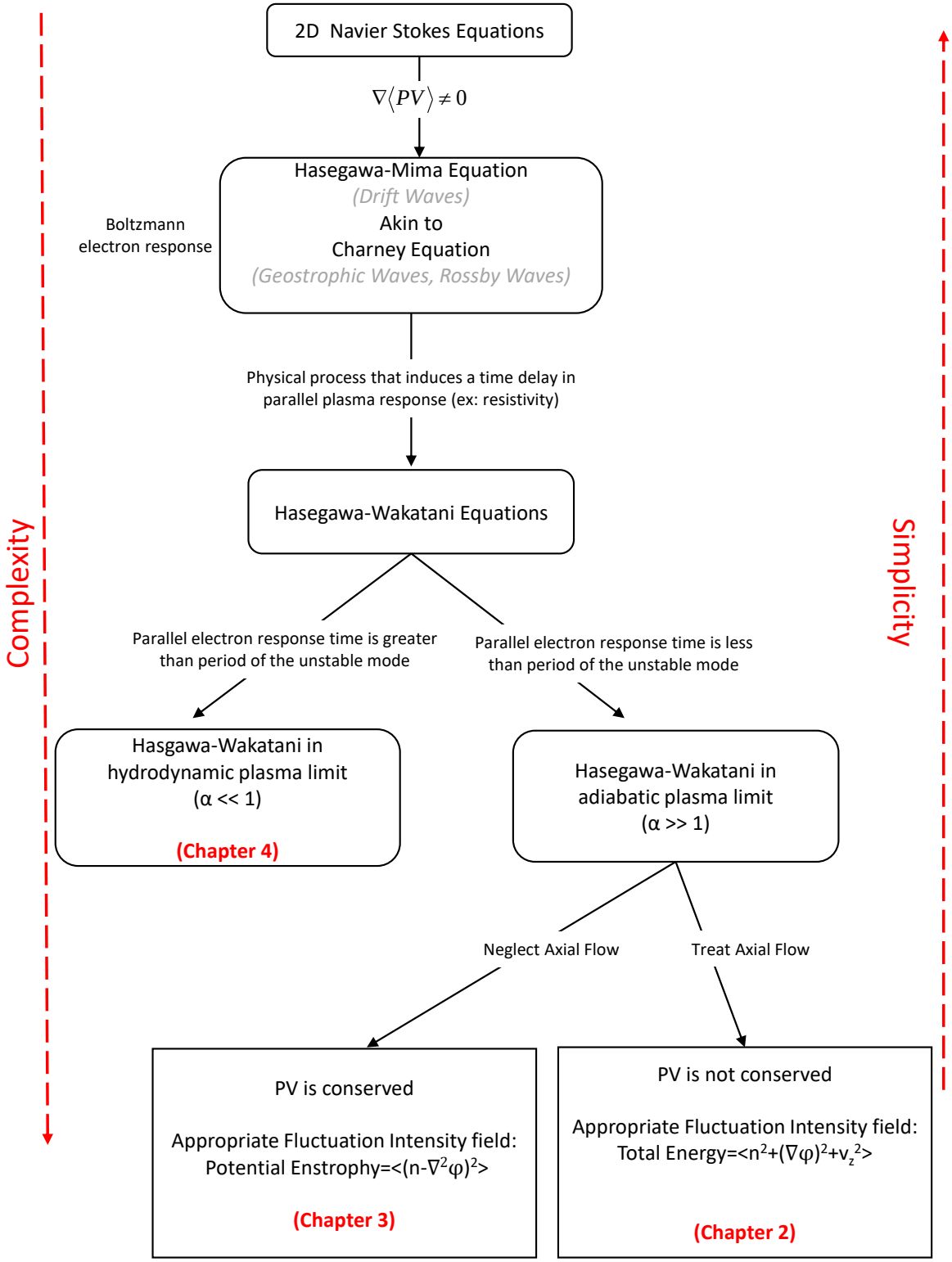

Figure 1.12: (De)-evolutionary tree of plasma models showing the organization of the dissertation.

Chapter 2

THE ECOLOGY OF FLOWS AND DRIFT WAVE TURBULENCE IN CSDX: A MODEL

2.1 INTRODUCTION

Drift wave (DW) turbulence is one of the fundamental issues in magnetically confined plasmas, and continues to be a subject of interest for many experimental and theoretical studies [Ter00, DIIH05]. Driven by radial inhomogeneities, drift wave fluctuations increase the turbulent transport of particles and energy, which leads ultimately to loss of the plasma particles, heat, etc. One mechanism that regulates these fluctuations is the self-generation and amplification of sheared $E \times B$ flows by turbulent stresses. This is related, but not identical to the inverse energy cascade in a two-dimensional fluid that occurs via local coupling in the wavenumber space. Here, the generation of zonal (azimuthal) flows occurs through non-local nonlinear energy transfer between the small and large scales of the plasma [Hor99, Sco05, MRS09]. Such flows play an important role in saturating the drift wave instabilities, in $L-H$ transition, and in the formation

of internal transport barriers (ITBs) [KD03]. Drift wave turbulence is also responsible for the generation of toroidal/axial flows, which play a crucial role in the macrostability of fusion grade tokamak plasmas. In particular, intrinsic toroidal flows are needed in large scale devices, where momentum input through NBI is not effective. Such flows stabilize some MHD and resistive wall modes, suppress turbulence, and enhance the overall particle confinement [KJD$^+$11, GTA$^+$99].

The relationship between drift waves and zonal flows has been extensively studied, so much so that the problem is now referred to as drift wave/zonal flow turbulence. Several self-regulating predator-prey models were developed, where the drift wave fluctuations correspond to the prey population and the zonal flows correspond to the predator population [DLCT94, II96, IIFY99]. As the population of drift waves grows rapidly, it supports the predator population. Zonal flows then control the drift waves by feeding on them, while being themselves regulated by a predator-prey competition and by nonlinear damping [DIIH05]. The existing versions of these models however, do not adequately address the problem of zonal flow saturation.

In a different vein, axial flow formation by turbulence requires a breaking in parallel symmetry and a non-zero correlator $\langle k_z k_m \rangle = \sum_m k_z k_m |\tilde{\phi}|^2$. In tokamaks, it is (usually) the magnetic shear that enables the parallel symmetry breaking. In linear devices however, $\mathbf{B}$ is constant and standard mechanisms do not apply. Recently, a parallel symmetry breaking mechanism that is based in drift wave turbulence and axial flow shear was developed [LDXT16]. This mechanism does not rely on complex magnetic geometry to generate a parallel residual stress $\Pi_{xz}^{res} \propto \langle k_z k_m \rangle$. The energy released from the density gradient is used to accelerate an axial flow through a negative viscosity process. For strong flows, the parallel shear flow instability (PSFI) controls the dynamics of $\bar{v}_z$.

Inverse energy cascade has been observed in both 2D and 3D systems [BMT12]. Examples include reversal of the flux of energy in geophysical flows subject to the Earth's rotation [MAP09], as well as in shallow fluid layers [XBFS11]. In plasmas, inverse energy cascade that results in the generation of broadband turbulence and large scale coherent structures from

DW fluctuations is widely accepted now. With drift waves triggering the formation of both axial and azimuthal flows (Fig.2.1), fundamental questions concerning the flow configuration arise: What mechanisms regulate the self-organization process, and ordain the final configuration of turbulence and flows in the plasma? How is energy partitioned between the fluctuations and the different flows $\bar{v}_z$ and $\bar{v}_y$ in the plasma? Moreover, since fluctuations and mean flows constitute an interdependent system, could there be a coupling relation between $\bar{v}_y$ and $\bar{v}_z$? If so, what determines the strength of this coupling? And most importantly, how does this coupling affect the energy branching ratio in the plasma?

To answer these questions, we present in this paper a 1D (in radius) reduced $k-\varepsilon$ type model that describes the evolution of the three mean fields: density $\bar{n}$, axial and azimuthal flows $\bar{v}_z$ and $\bar{v}_y$, as well as variations in the fluctuation intensity $\varepsilon = \langle \tilde{n}^2 + (\nabla_\perp \tilde{\phi})^2 + \tilde{v}_z^2 \rangle$, in the linear plasma of CSDX. The model is derived from the Hasegawa-Wakatani system with axial flow evolution included. The model self-consistently relates variations in ε to the evolution of the mean profiles via the particle flux $\langle \tilde{n}\tilde{v}_x \rangle$, and the parallel and perpendicular Reynolds stresses $\langle \tilde{v}_x \tilde{v}_z \rangle$ and $\langle \tilde{v}_x \tilde{v}_y \rangle$. Because of parallel compression, the fluctuation intensity is the relevant conserved field.

To explain the relation between $\bar{v}_y$ and $\bar{v}_z$ with respect to ε, the model uses a mixing length l_{mix} that reflects turbulence suppression by the axial and azimuthal flow shear. External particle and axial flow sources which result from injection of neutrals and axial momentum, are included in this model. When the work done by the fluctuations on the parallel flow is less than that done on the perpendicular flow, the model can be reduced to a 2-field predator-prey model, where the azimuthal flow feeds on the density population.

The model is a necessary intermediary between a 0D model that shows the structure of the flows and fluctuations, and a full DNS. For a multiscale system such as CSDX, a reduced model provides a route to an interpretation of the experimental results, and gives detailed insight into the feedback loops between the disparate scales. At the same time, it avoids the labor of

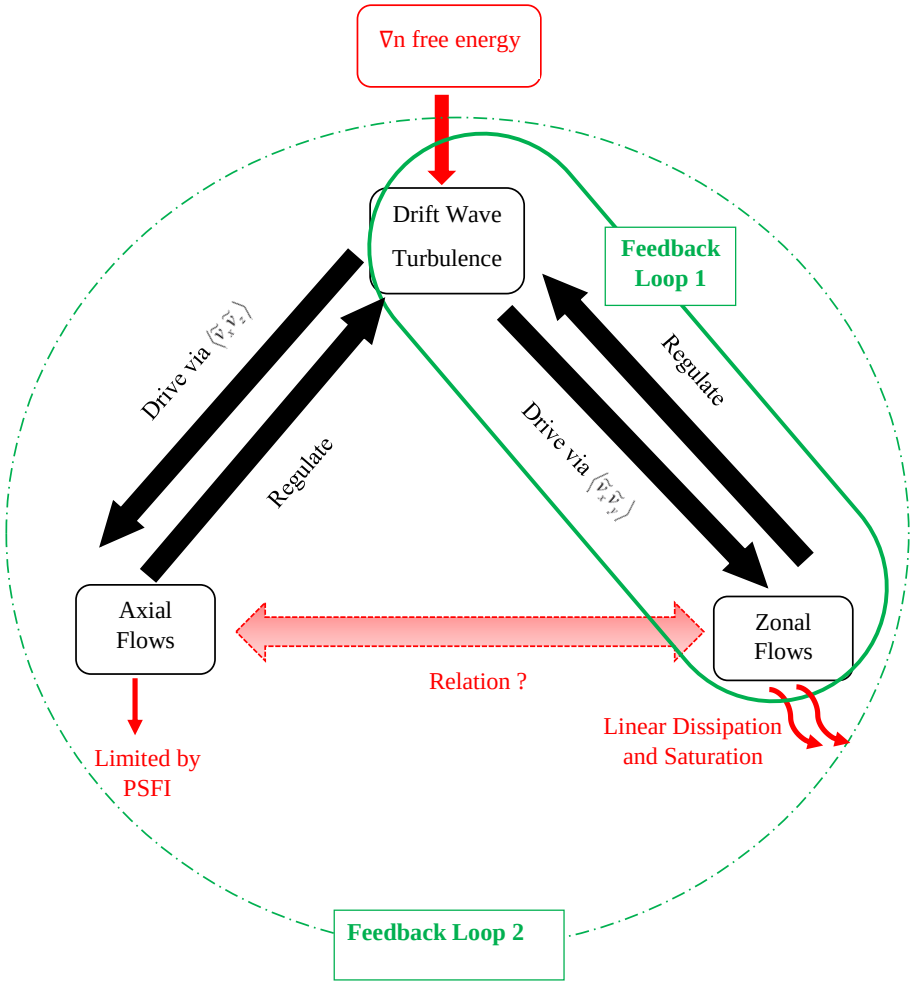

Figure 2.1: A schematic of the ecology of drift wave turbulence, zonal, and axial flows. The first feedback loop relates the drift waves to the zonal flows via $\langle \tilde{v}_x \tilde{v}_y \rangle$. A second feedback loop exists as a result of a potential relation between $\bar{v}_y$ and $\bar{v}_z$. The second loop relates the fluctuations to both mean flows.

a full DNS. The model consists of a set of compact equations that describe the evolution of the plasma stresses and flows. It shows how $\nabla \bar{n}$ free energy accelerates both $\bar{v}_y$ and $\bar{v}_z$, and investigates the coupling relation between the parallel and perpendicular flow dynamics in CSDX by introducing σ_{VT}, the empirical measure of the acoustic coupling in the plasma.

The 1D reduced model description taken here should provide a useful new intermediate approach for the simulation of self-consistent evolution edge and SOL plasma profiles, transverse and parallel flows and turbulence, and would allow the study of main plasma and

trace impurity dynamics across timescales ranging from a few turbulent correlation times up to system equilibrium timescales. When modified to include toroidal and open-field line effects, and extended to a 2D geometry along the magnetic field and binormal directions, our proposed reduced model would bridge the gap between existing time-averaged fluid codes of the edge and SOL region of confinement devices (see e.g. ref.[WRK$^+$15]) which are incapable of capturing such self-consistent dynamical phenomena, and fully turbulent direct numerical simulations (see e.g. refs. [TGT$^+$10, RMRP92]) which capture self-consistent profile and flow evolution but are computationally expensive and thus difficult to use for long time scale dynamical evolution studies. Such a new capability might be useful to study the self-consistent entrainment and transport of eroded wall impurities in flowing edge and SOL plasma and the long-time migration of these materials in the SOL and divertor regions of confinement devices. These obvious extensions are left as future work.

The rest of the paper is organized as follows. Section 2.2 presents the structure of the model, as well as a full derivation of the involved equations and an interpretation of each term of these equations. Section 2.3 elaborates on the relation between drift waves and zonal flows, and calculates the turbulent expressions for the particle flux and the vorticity flux. Expressions for the perpendicular Reynolds stress and the Reynolds work are also presented. Section 2.4 is dedicated to the parallel Reynolds stress. This sections explains how drift waves accelerate the axial flows through $\langle \tilde{v}_x \tilde{v}_z \rangle$. An empirical constant σ_{VT} is introduced in this section. By analogy to pipe flows, σ_{VT} is presented as a measure of the acoustic coupling or the efficiency of converting the $\nabla \bar{n}$ energy to drive an axial flow. σ_{VT} is then used to establish a direct relation between the axial and the azimuthal flow shear, as both residual stresses Π^{res}_{xy} and Π^{res}_{xz} are proportional to ∇n. An expression for the mixing length l_{mix} that depends on both shears is derived in section 2.5. In section 2.6, we give a summary and a discussion of the model, before reducing it to a 2-field predator-prey model in section 2.7. Finally, conclusion and discussion are given in section 4.8.

2.2 THE MODEL AND ITS STRUCTURE

The basic equations are derived from the Hasegawa-Wakatani system [HW83, HW87], with axial flow velocity $\tilde{v}_z$ evolution included. In a box of dimensions: $0 \leq x \leq L_x$, $0 \leq y < L_y$ and $0 \leq z \leq L_z$, and for a straight magnetic field $\mathbf{B} = B\hat{z}$, these equations are [LD17]:

$$\frac{d\tilde{n}}{dt} + \mathbf{v}_E.\nabla\langle n\rangle + n_0\nabla_z\tilde{v}_z = -\frac{v_{th}^2}{\nu_{ei}}\nabla_z^2(\tilde{\phi}-\tilde{n}) + D_0\nabla_\perp^2\tilde{n} + \{\tilde{n},\tilde{\phi}\} \tag{2.1a}$$

$$\frac{d\nabla_\perp^2\tilde{\phi}}{dt} + \mathbf{v}_E.\nabla\langle\nabla_\perp^2\phi\rangle = -\frac{v_{th}^2}{\nu_{ei}}\nabla_z^2(\tilde{\phi}-\tilde{n}) + \mu_0\nabla_\perp^4\tilde{\phi} - \nu_{in}(\bar{v}_y-\bar{v}_n) + \{\nabla_\perp^2\tilde{\phi},\tilde{\phi}\} \tag{2.1b}$$

$$\frac{d\tilde{v}_z}{dt} + \mathbf{v}_E.\nabla\langle v_z\rangle = -c_s^2\nabla_z\tilde{n} + \nu_0\nabla_\perp^2\tilde{v}_z - \nu_{in}(\bar{v}_z-\bar{v}_n) + \{\tilde{v}_z,\tilde{\phi}\} \tag{2.1c}$$

Here x, y and z are the radial, azimuthal and axial directions respectively. The fields are normalized as follows: $\tilde{n} \equiv \tilde{n}_e/n_0$, $\tilde{\phi} \equiv e\tilde{\phi}/T_e$, $t \equiv \omega_{ci}t$, $\tilde{v}_z \equiv \tilde{v}_z/c_s$ and $length \equiv length/\rho_s$. n_0 and T_e are the average density and electron temperature respectively, $\omega_{ci} = eB/m_i$ is the ion cyclotron frequency, $c_s = \sqrt{T_e/m_i}$ is the ion sound speed and $\rho_s = c_s/\omega_{ci}$ is the ion Larmor radius with temperature T_e. v_{th} and ν_{ei} are the electron thermal velocity and the electron-ion collision frequency, respectively. The total time derivative is: $d/dt = \partial_t + \mathbf{v}_E.\nabla$, and the axial ion pressure gradient is neglected in the $\tilde{v}_z$ equation. The neutral friction, proportional to the ion-neutral collision frequency $\nu_{in} = n_n\sqrt{8T_i/\pi m_i}$, is a natural sink for energy that inverse cascades to larger scales. This friction is especially significant near the plasma boundary. Its expression can be further simplified by taking $\bar{v}_n \approx 0$ close to the boundary. Terms that are proportional to D_0, μ_0 and ν_0 dissipate energy via viscous collisions. Finally, the nonlinear advection terms are expressed as Poisson brackets: $\{f,g\} = \partial_x f\partial_y g - \partial_x g\partial_y f$, and represent spatial scattering of fluctuations.

The system of eqs.(2.1) describes a variety of linearly unstable modes. One eigenmode of this system is the strongly damped ion drift wave with an eigenfrequency that satisfies the

relation: $|\omega| < |k_z c_s|$. Here k_z is the parallel wave number. Such a wave is heavily damped, will be difficult to excite, and thus will not be considered here. A second solution to this system describes the dynamics of the parallel shear flow instability (PSFI). The PSFI describes turbulence production due to free energy released from parallel flow shear [KIK$^+$16, KII16]. In contrast to other linear plasmas [KIIe5, IKI$^+$16], experimental results from the CSDX linear device show that the parallel flow shear $\bar{v}_z'$ is well below the critical threshold necessary to drive PSFI [LD17]. The PSFI is thus heavily damped in CSDX, and will also not be considered here. A third solution describes the dynamics of the coupled 3D drift-ion acoustic turbulence. In this paper, we are mainly concerned with the coupling between the parallel and perpendicular flow dynamics. Thus we focus only on the dynamics of the coupled drift-ion acoustic waves. We decompose each field into a mean and a fluctuating part: $f = \langle f \rangle + \tilde{f}(x,y,z,t)$, where the averaging is performed over the directions of symmetry y and z:

$$\bar{f}(x,t) = \langle f(x,t) \rangle = \frac{1}{L_z L_y} \int_0^{L_z} dz \int_0^{L_y} dy f(x,y,z,t)$$

where we assume that the plasma profiles do not change substantially along the axial direction.

In the presence of compressible parallel flows, conservation of potential vorticity (PV) - and thus that of the potential enstrophy - is broken. Coupling between the PV fluctuations and the parallel flow compression thus defines an energy transfer channel between the parallel and perpendicular flow dynamics. This energy exchange influences the wave momentum density and modifies the zonal momentum balance theorem [WDH12]. In its new form, the zonal momentum balance theorem shows that coupling between drift-acoustic waves acts as a driving source that allows stationary turbulence to excite zonal flows in the absence of any driving force or potential enstrophy flux. The coupling drive involves both perpendicular and parallel dynamics, and does not require symmetry breaking in the turbulence spectrum. Therefore, instead of using potential

enstrophy as the fluctuation intensity field, we use the mean fluctuation energy $\langle\varepsilon\rangle$ defined as:

$$\langle\varepsilon\rangle = \frac{1}{L_z L_y}\int_0^{L_\parallel} dz \int_0^{2\pi} d\theta\varepsilon(r) = \frac{1}{L_z L_y}\int_0^{L_z} dz \int_0^{L_y} dy\varepsilon(x) = \frac{\left\langle \tilde{n}^2 + (\nabla_\perp \tilde{\phi})^2 + \tilde{v}_z^2 \right\rangle}{2},$$

where z and y are the axial (parallel) and azimuthal (perpendicular) directions respectively, and $L_\parallel = L_z$ is the axial length of the plasma. Here we assume periodicity in the axial direction z. The mean fluctuating energy $\langle\varepsilon\rangle$, interpreted as a sum of internal energy $\langle\tilde{n}^2\rangle$ and kinetic energy: $\langle(\nabla_\perp\tilde{\phi})^2\rangle + \langle\tilde{v}_z^2\rangle$, is conserved up to dissipation and internal production, as demonstrated later. The time evolution of $\langle\varepsilon\rangle$ is:

$$\frac{d\langle\varepsilon\rangle}{dt} = \frac{1}{L_z L_y}\int (\tilde{n}\frac{d\tilde{n}}{dt} + \nabla_\perp\tilde{\phi}\frac{d\nabla_\perp\tilde{\phi}}{dt} + \tilde{v}_z\frac{d\tilde{v}_z}{dt})dydz \tag{2.2}$$

An expression for eq.(2.2) is obtained by multiplying the set of eqs.(2.1) by $\tilde{n}$, $-\tilde{\phi}$ and $\tilde{v}_z$ respectively, and integrating along the directions of symmetry to get:

$$\begin{aligned}\langle\frac{d\varepsilon}{dt}\rangle = &-\langle\tilde{n}\tilde{v}_x\rangle\frac{d\bar{n}}{dx} - \langle\tilde{v}_x\tilde{v}_y\rangle\frac{d\bar{v}_y}{dx} - \langle\tilde{v}_x\tilde{v}_z\rangle\frac{d\bar{v}_z}{dx} - \frac{1}{L_z L_y}\frac{v_{th,e}^2}{\nu_{ei}}\int\left[\partial_z(\tilde{\Phi}-\tilde{n})\right]^2 dz - \langle\tilde{n}\tilde{v}_z\rangle \\ &- \nu_{in}\Big(\langle\tilde{v}_y^2\rangle + \langle\tilde{v}_z^2\rangle\Big) - \frac{1}{L_z L_y}\int\Big(D_0(\nabla_\perp\tilde{n})^2 + \mu_0(\nabla_\perp^2\tilde{\phi})^2 + \nu_0(\nabla_\perp\tilde{v}_z)^2\Big)dydz \\ &+ \frac{1}{L_z L_y}\int\Big(\tilde{n}\{\tilde{n},\tilde{\phi}\} - \tilde{\phi}\{\nabla_\perp^2\tilde{\phi},\tilde{\phi}\} + \tilde{v}_z\{\tilde{v}_z,\tilde{\phi}\}\Big)dydz\end{aligned} \tag{2.3}$$

Here we have used periodic boundary conditions in the y direction to obtain the fourth term of the RHS of eq.(2.3). The first three terms on the RHS of eq.(2.3) are direct mean-fluctuation coupling terms. They relate the variations of ε to the variations of the mean profiles of $\bar{n}$, $\bar{v}_y$ and $\bar{v}_z$ via $\langle\tilde{n}\tilde{v}_x\rangle$, $\langle\tilde{v}_x\tilde{v}_y\rangle$ and $\langle\tilde{v}_x\tilde{v}_z\rangle$.

A common issue that arises while using such reduced models is the closure problem. To obtain equations that contain only the mean quantities, we simplify the energy equation by examining each term of eq.(2.3), in order to properly construct the equation for ε. In the case of

pure drift wave turbulence, the $d\bar{v}_z/dx$ term is absent and $\omega < \omega^\star \propto \nabla\bar{n}$. The density gradient term is then the only source of energy production. It is positive definite, and represents the rate at which free energy is extracted from the density gradient $\nabla\bar{n}$. The second term on the RHS of eq.(2.3) is the Reynolds power. It represents the free energy coupled to the azimuthal flow $\bar{v}_y$ via the Reynolds stress $\langle\tilde{v}_x\tilde{v}_y\rangle$. For pure DWs and stable Kelvin-Helmholtz (KH) modes, this energy is transfered to the mean flow and the Reynolds power is negative. The third term, on the other hand, can represent either an energy source or an energy sink. Depending on the sign of the cross phase between $\tilde{v}_x$ and $\tilde{v}_z$, this term can be either positive or negative. A detailed discussion of this cross phase relation and of the parallel Reynolds stress is deferred to a later section. The dissipation term $-\int[\partial_z(\tilde{\Phi}-\tilde{n})]^2dz$ is associated with the phase difference between the density fluctuations $\tilde{n}$ and the electric potential fluctuations $\tilde{\phi}$. This term is always negative. In the frequently encountered case of weakly non-adiabatic electrons, this term is always smaller than the energy input source term: $-\int[\partial_z(\tilde{\Phi}-\tilde{n})]^2dz \ll -\langle\tilde{n}\tilde{v}_x\rangle\nabla\bar{n}$ [SDSK13]. Indeed, for $\tilde{n} = (1-i\Delta)\tilde{\phi}$ with $\Delta \ll 1$ and $\omega \simeq |\omega^\star|/(1+k_\perp^2\rho_s^2)$, the estimates of the dissipation and the energy input terms are: $\omega^2(|\omega^\star|-\omega)^2$ and $\omega|\omega^\star|(|\omega^\star|-\omega)^2$ respectively. With $\omega < |\omega^\star|$, the dissipation term can be neglected from eq.(2.3). The $\langle\tilde{n}\tilde{v}_z\rangle$ term represents parallel particle flux. Since such flux can be experimentally zeroed, it will be omitted from the energy equation. Terms that are proportional to D_0, μ_0 and ν_0, represent collisional energy dissipation by direct energy cascade. These terms damp the fluctuation energy at small scales at a rate $\sqrt{\varepsilon}/l_{mix}$. We write the energy dissipation as $\varepsilon^{3/2}/l_{mix}$, and leave the discussion of the expression for the turbulent mixing length l_{mix} to a subsequent section. In addition to collisional dissipation, ion-neutral collisions represent a nonlinear energy damping to larger scales. Both collisional dissipation and neutral energy damping represent a sink of turbulent energy ε. Finally, the nonlinear terms in eqs. (2.1) are related to the $E\times B$ drift, the polarization drift, and the axial drift respectively. These terms represent the spreading of turbulence. This spreading is mesoscopic, and involves two aspects. The first aspect is a perturbation in the local intensity gradient $\partial_x\varepsilon$,

i.e., a diffusion of the energy envelope to a more stable region away from its source. The second aspect includes nonlinear interaction of the local fluctuations via inverse cascade. Based in the three wave coupling, zonal flows created through inverse cascade shear the fluctuations and regulate turbulence spreading [GDH06, GDH07]. We write this energy spreading as a Fickian energy flux: $\Gamma_\varepsilon = -D_\varepsilon \partial_x \varepsilon = -l_{mix} \varepsilon^{1/2} \partial_x \varepsilon$. An energy source P representing drift wave turbulent energy production is added to eq.(2.3). The generation of these fluctuations results from the relaxation of the mean profiles and represents the excitation in the linear phase. The energy production term is linear in ε and proportional to γ_ε, the characteristic growth rate of the DW instabilities: $P = \gamma_\varepsilon \varepsilon$. The final form of eq.(2.3) then becomes:

$$\frac{\partial \varepsilon}{\partial t} + \partial_x \Gamma_\varepsilon = -\langle \tilde{n} \tilde{v}_x \rangle \frac{d\bar{n}}{dx} - \langle \tilde{v}_x \tilde{v}_z \rangle \frac{d\bar{v}_z}{dx} - \langle \tilde{v}_x \tilde{v}_y \rangle \frac{d\bar{v}_y}{dx} - \frac{\varepsilon^{3/2}}{l_{mix}} + P \tag{2.4}$$

In addition to eq.(2.4), the equations for $\bar{n}$, $\bar{v}_y$ and $\bar{v}_z$, which form the reduced model of turbulence intensity for the modified Hasegawa-Wakatani model are:

$$\frac{\partial \bar{n}}{\partial t} = -\frac{\partial}{\partial x} \langle \tilde{v}_x \tilde{n} \rangle + D_c \frac{\partial^2 \bar{n}}{\partial x^2} + S_n \tag{2.5}$$

$$\frac{\partial \bar{v}_z}{\partial t} = -\frac{\partial}{\partial x} \langle \tilde{v}_x \tilde{v}_z \rangle + \nu_{c,\parallel} \frac{\partial^2 \bar{v}_z}{\partial x^2} - \nu_{in} \bar{v}_z - \nu_{ii} \bar{v}_z + S_{v_z} \tag{2.6}$$

$$\frac{\partial \bar{v}_y}{\partial t} = -\frac{\partial}{\partial x} \langle \tilde{v}_x \tilde{v}_y \rangle + \nu_{c,\perp} \frac{\partial^2 \bar{v}_y}{\partial x^2} - \nu_{in} \bar{v}_y - \nu_{ii} \bar{v}_y + S_{v_y} \tag{2.7}$$

Here we assumed that the electron pressure gradient does not vary neither in the axial nor in the azimuthal direction. Note however that this assumption remains valid only in the case of an attached plasma. When the pressure of the injected neutral gas is high enough, a detached plasma is obtained, and axial and azimuthal variations of ∇p_e are no longer equal to zero. The first terms on the RHS of eqs.(4.8a-2.7) represent particle and momentum transport, while those proportional to D_c, $\nu_{c,\perp}$ and $\nu_{c,\parallel}$ represent collisional diffusivity and viscosity respectively. A

particle source S_n representing the ionization of the injected neutrals is added to the density equation. Similarly, axial and azimuthal momentum sources S_{v_z} and S_{v_y} representing external input of momentum into the plasma are added to $\bar{v}_y$ and $\bar{v}_z$ equations. In CSDX however, no external momentum is injected and $S_{v_z} = S_{v_y} = 0$, in contrast to refs. [IKI+16, KIK+16, KII17] where external axial momentum is injected into the plasma. In eq.(2.7), the term proportional to the ion-neutral collision frequency ν_{in} represents momentum transfer between ions and neutrals, and is significant only in the boundary layer close to the plasma wall. The last term proportional to ν_{ii} represents viscous damping via ion-ion collisions. The expressions for viscous and diffusive coefficients are [LL94]:

$$D_c = \frac{D}{1+\omega_{ci}^2\tau_i^2} \simeq \frac{D_e}{(\omega_{ci}\tau_i)^2} \sim \frac{4\sqrt{2\pi}n_0 \ln\Lambda e^2\sqrt{m_e}}{3\sqrt{T_e}} \tag{2.8a}$$

$$\nu_{c,\perp} = \nu_{i,\perp} = \frac{3}{10}\frac{n_i T_i}{\omega_{ci}^2\tau_i} \sim \frac{2\sqrt{\pi}n_0^2 \ln\Lambda e^2 m_i^{3/2}}{T_i^{1/2}} \tag{2.8b}$$

$$\nu_{c,\parallel} = \nu_{e,\parallel} = 0.73 n_e T_e \tau_e \sim \frac{3\sqrt{m_e}T_e^{5/2}}{4\sqrt{2\pi}\ln\Lambda e^4} \tag{2.8c}$$

The system formed by eqs.(2.4-2.7) conserve the total energy E_{tot} in time, up to dissipation and production. Here E_{tot} is equal to the sum of the turbulent energy ε and the mean energy $E_{mean} = \left(\bar{n}^2 + \bar{v}_z^2 + (\nabla_\perp\bar{\phi})^2\right)/2$. For zero energy flux conditions at the boundaries ($\partial_x\varepsilon = 0$), energy conservation (up to dissipation and production) is demonstrated as:

$$\begin{aligned}
\frac{d\langle E_{tot}\rangle}{dt} &= \frac{d\langle\varepsilon\rangle}{dt} + \frac{d\langle E_{mean}\rangle}{dt} \\
&= \frac{d\langle\varepsilon\rangle}{dt} + \frac{1}{2}\frac{\partial}{\partial t}\int\left[\bar{n}^2 + \bar{v}_z^2 + (\nabla_\perp\bar{\phi})^2\right]dzdy \\
&= -\langle\tilde{n}\tilde{v}_x\rangle\frac{d\bar{n}}{dx} - \langle\tilde{v}_x\tilde{v}_z\rangle\frac{d\bar{v}_z}{dx} - \langle\tilde{v}_x\tilde{v}_y\rangle\frac{d\bar{v}_y}{dx} + P - \frac{\varepsilon^{3/2}}{l_{mix}} \\
&\qquad + \langle\tilde{n}\tilde{v}_x\rangle\frac{d\bar{n}}{dx} + \langle\tilde{v}_x\tilde{v}_z\rangle\frac{d\bar{v}_z}{dx} + \langle\tilde{v}_x\tilde{v}_y\rangle\frac{d\bar{v}_y}{dx} \\
&= -\frac{\varepsilon^{3/2}}{l_{mix}} + P
\end{aligned} \tag{2.9}$$

where the order of operations $\bar{..}$ and $\langle..\rangle$ have been interchanged. Eqs.(2.4-2.7) thus constitute a model that describes profile evolution for both parallel and perpendicular flows, in addition to the plasma density, by self-consistently evolving turbulence as well as the mean profiles. This model offers the possibility to explain the generation and acceleration of intrinsic axial flows as a result of changes in the turbulence spectrum, governed by conservation of total energy E_{tot}.

2.3 CALCULATING THE TURBULENT FLUXES

Eqs.(2.4-2.7) describe time and space evolution of the three mean fields: $\bar{n}$, $\bar{v}_y$ and $\bar{v}_z$, in addition to the mean fluctuating energy ε. The solution of this system of equations requires calculating the expressions for the different turbulent fluxes in terms of ε and the mean field gradients. In this section, we determine the expressions for the various turbulent fluxes, with the provision that these expressions are valid only in the case of nearly adiabatic electrons, that is when $k_z^2 v_{th}^2/(\nu_{ei}|\omega|) \gg 1$. In this limit, quasi-linear theory is used to calculate the expressions for the transport fluxes by Fourier decomposing each field as: $\tilde{f}_m = \delta f_m(x) e^{i[k_m y + k_z z - \omega t]}$ where $\omega = \omega^r + i|\gamma_m|$, with $|\gamma_m| \ll \omega_m^r = \omega^\star(1+k_\perp^2\rho_s^2)^{-1}$. Here $\omega^\star = k_m v_d$, where the electron diamagnetic velocity is $v_d = -\rho_s c_s \nabla\bar{n} = \rho_s c_s/L_n$,

2.3.1 The Turbulent Particle Flux

The particle flux $\langle\tilde{n}\tilde{v}_x\rangle$ is calculated after linearizing the density equation:

$$\frac{\partial\tilde{n}}{\partial t} - \tilde{v}_x v_d + \nabla_z\tilde{v}_z = -\frac{v_{th}^2}{\nu_{ei}}\nabla_z^2(\tilde{\phi}-\tilde{n}) + D_0\nabla_\perp^2\tilde{n} + \{\tilde{n},\tilde{\phi}\} \tag{2.10}$$

The expression for the particle flux is then:

$$\Gamma = \langle\tilde{n}\tilde{v}_x\rangle = \sum_m \frac{v_d(\alpha+|\gamma_m|) - \alpha\omega^r/k_m}{|\omega/k_m + i\alpha/k_m|^2}|\delta\phi^2| \tag{2.11}$$

In the case of classic resistive drift waves, $|\gamma_m| \ll 1$ and the particle flux is:

$$\Gamma = \sum_m \alpha \frac{v_d - \omega^r/k_m}{|\omega/k_m + i\alpha/k_m|^2} |\delta\phi^2| \tag{2.12}$$

where $\alpha = k_z^2 v_{th}^2/\nu_{ei}$ is the plasma adiabaticity parameter. The first term of the numerator represents diffusive relaxation of the density gradient, while the second is due to pumping by waves. The competition between these two terms is what ultimately sets the sign of Γ, i.e., the direction of the particle flux. For adiabatic electrons: $k_z^2 v_{th}^2/\nu_{ei} \gg |\omega|$, and $\alpha \gg (\omega^r, |\gamma_m|)$. The particle flux then becomes:

$$\begin{aligned} \Gamma = \langle \tilde{n}\tilde{v}_x \rangle &= \sum_m -\frac{k_m^2 \rho_s^2 c_s^2}{\alpha} . \frac{k_\perp^2 \rho_s^2}{1 + k_\perp^2 \rho_s^2} . \frac{1}{n_0} \frac{d\bar{n}}{dx} . |\delta\phi^2| \\ &= -D . \frac{1}{n_0} \frac{d\bar{n}}{dx} > 0 \end{aligned} \tag{2.13}$$

where the particle diffusion coefficient D is:

$$D = \sum_m \frac{k_m^2 \rho_s^2 c_s^2}{\alpha} . \frac{k_\perp^2 \rho_s^2}{1 + k_\perp^2 \rho_s^2} |\delta\phi^2| = \frac{k_\perp^2 \rho_s^2}{1 + k_\perp^2 \rho_s^2} . \frac{\langle \delta v_x^2 \rangle}{\alpha} \approx \frac{f\varepsilon}{\alpha} \tag{2.14}$$

The factor f introduced in eq.(2.14) represents the fraction of the fluctuation energy ε which is kinetic energy of radial motion, i.e., $f = \langle \delta v_x^2 \rangle / \varepsilon$.

Expression for the energy fraction f

Since the fluctuation energy ε is composed of internal energy as well as kinetic energy for both radial and axial motion, we write the following expression for the fraction of ε allocated to kinetic energy in the radial motion as:

$$f = \frac{\langle \delta v_x^2 \rangle}{\varepsilon} = \frac{\langle \delta v_x^2 \rangle}{\langle \delta n^2 \rangle + \langle \delta v_x^2 \rangle + \langle \delta v_z^2 \rangle}$$

Writing the density and radial velocity fluctuations as $\delta n = (1 - i\Delta)\delta\phi$ and $\delta v_x = -ik_\perp \rho_s c_s \delta\phi$ respectively, straightforward linearization of the axial velocity equation gives:

$$\langle \delta v_z^2 \rangle = \frac{(k_m \rho_s c_s \nabla \bar{v}_z - k_z c_s^2 (1+\Delta^2))}{\omega^2 + 1/\tau_c^2} \langle \delta\phi^2 \rangle$$

With $\tau_c = l_{mix}/\langle \tilde{v}_x^2 \rangle^{1/2} = l_{mix}/\sqrt{f\varepsilon}$, the denominator is equal to:

$$\frac{1}{\omega^2 + 1/\tau_c^2} = \frac{l_{mix}^2 (1 + k_\perp^2 \rho_s^2)^2}{\left(l_{mix}^2 \omega^{\star 2} + f\varepsilon (1 + k_\perp^2 \rho_s^2)^2 \right)}$$

The final expression for f is:

$$f = \frac{k_\perp^2 \rho_s^2}{(1+\Delta^2) + k_\perp^2 \rho_s^2 + \dfrac{|k_m \rho_s \nabla \bar{v}_z - k_z c_s (1 - i\Delta)|^2}{\omega^2 + 1/\tau_c^2}} \tag{2.15}$$

For adiabatic electrons and in the absence of mean axial shear ($\bar{v}_z' = 0$), f is:

$$f = \frac{k_\perp^2 \rho_s^2}{1 + k_\perp^2 \rho_s^2 + k_z^2 c_s^2 / (\omega^2 + 1/\tau_c^2)} \tag{2.16}$$

with $\omega = |\omega^r| = k_m \rho_s c_s / [L_n (1 + k_\perp^2 \rho_s^2)]$ and $1/\tau_c^2 = \varepsilon / l_{mix}^2$. In the limit of small k_z and pure DWs, eq.(2.16) gives: $f = k_\perp^2 \rho_s^2 / (1 + k_\perp^2 \rho_s^2) \simeq k_\perp^2 \rho_s^2$ and $\langle \delta v_x^2 \rangle \simeq k_\perp^2 \rho_s^2 \varepsilon$, as expected for adiabatic electrons. Eq.(2.15) includes the correlator $\langle k_m k_z \rangle$, which expresses the cross phase relation between the velocity fluctuations in the radial direction ($\tilde{v}_x \sim k_m \tilde{\phi}$) and those in the axial direction ($\tilde{v}_z \sim k_z \tilde{p} \sim k_z T_e \tilde{n}$). Here we assumed adiabatic response with constant temperature T_e. In CSDX, the parallel to perpendicular coupling is small in comparison to $k_\perp^2 \rho_s^2$, as indicated by measurements of modest axial flow velocities [HLT$^+$17, HLH$^+$17]. The $\langle k_m k_z \rangle$ correlator can thus be neglected in f. However, in the parallel Reynolds stress, $\langle k_m k_z \rangle$ appears as zeroth order and so cannot be dropped. Here it will be expressed in terms of an empirical constant σ_{VT} that will be introduced in a subsequent section.

2.3.2 The Vorticity Flux, the Perpendicular Reynolds Stress and the Reynolds Work

The expression for the Reynolds force needed in eq.(2.7) is obtained from Taylor's identity: $-\partial_x\langle\tilde{v}_x\tilde{v}_y\rangle = \langle\tilde{v}_x\nabla_\perp^2\tilde{\phi}\rangle$, which relates the Reynolds force to the vorticity flux, and links the eddy fluxes of momentum and potential vorticity [Tay15]. When neutrals are negligible and in the presence of an externally imposed azimuthal flow V_0, the quasi-linear expression for the vorticity flux Π_{xy} is obtained after linearizing the vorticity equation [ADG16]:

$$\begin{aligned}\Pi_{xy} &= \sum_m \Bigg\{ -|\gamma_m|\frac{v_d + d\langle\nabla_\perp^2\phi\rangle/dx + V_0''}{|V_0' - \omega|^2} \\ &\qquad + \frac{|\gamma_m| v_d + \alpha\Big(v_d + V_0 - \omega^r/k_m\Big)}{|\omega + i\alpha - V_0'|^2}\Bigg\} k_m^2\rho_s^2c_s^2|\delta\phi^2| \qquad (2.17)\\ &= -\chi_y^{non-resonant} d(\langle\nabla_\perp^2\phi\rangle + V_0')/dx + \Pi_{xy}^{res} \\ &= -\chi_y^{non-resonant} d^2(\bar{v}_y + V_0)/dx^2 + \Pi_{xy}^{res}\end{aligned}$$

Here $\langle\nabla_\perp^2\phi\rangle$ is a self generated flow driven by the DW interaction. The expression for the vorticity flux thus consists of a residual flux Π_{xy}^{res} and a diffusive part proportional to $\chi_y^{non-resonant}$:

$$\chi_y^{non-resonant} = \sum_m \frac{|\gamma_m|}{|V_0' - \omega|^2} k_m^2\rho_s^2c_s^2|\delta\phi^2| \qquad (2.18)$$

The denominator of $\chi_y^{non-resonant}$ is a competition between the wave frequency ω and the flow shear V_0'. In CSDX, a comparison between the shearing rate V_0' and the drift wave frequency ω shows that $V_0' \ll \omega$ [CAT$^+$16]. Thus we neglect the flow shear from the expression for $\chi_y^{non-resonant}$:

$$\chi_y^{non-resonant} = \sum_m \frac{|\gamma_m|}{|\omega|^2} k_m^2\rho_s^2c_s^2|\delta\phi^2|$$

We also mention that the total turbulent viscosity is: $\chi_y^{tot} = \chi_y^{resonant} + \chi_y^{non-resonant}$, where

$\chi_y^{resonant}$ and $\chi_y^{non-resonant}$ are the resonant and the nonresonant turbulent viscosities respectively. Here $\chi_y^{resonant} = \sum_m k_m^2 \rho_s^2 c_s^2 \pi \delta(\omega - k_m \bar{v}_y - k_z \bar{v}_z)$ results from the resonance between the plasma flows and the unstable mode of frequency ω [MD10]. Hereafter, we drop the *resonant* and $non-resonant$ superscripts to simplify the notation. The residual vorticity stress Π_{xy}^{res} is:

$$\Pi_{xy}^{res} = \sum_m \left\{ \frac{|\gamma_m| v_d + \alpha(v_d - \omega^r/k_m)}{|\omega + i\alpha|^2} \right\} k_m^2 \rho_s^2 c_s^2 |\delta\phi^2| - \chi_y v_d \tag{2.19}$$

Note that it is through Π_{xy}^{res} that the free energy in the density gradient is converted into positive Reynolds work, resulting in the generation of flow shear. The residual stress Π_{xy}^{res} is the only term in the vorticity flux that survives when both $\bar{v}_y$ and $\bar{v}_y'$ vanish. Thus, it must be the case that the density gradient $\nabla \bar{n}$ accelerates the azimuthal flow from rest through Π_{xy}^{res}. For pure Kelvin-Helmholtz modes, $k_z = \alpha = 0$ and the total stress is:

$$\Pi_{xy} = -\chi_y d \langle \nabla_\perp^2 \phi \rangle / dx \tag{2.20}$$

The residual vorticity of the pure KH modes is zero and the density gradient alone cannot drive these instabilities. KH modes simply relax the $E \times B$ flow profile via viscous diffusion. Using the expression for the particle flux, Π_{xy}^{res} is rewritten as [ADG16]:

$$\Pi_{xy}^{res} = \Gamma - \chi_y v_d \tag{2.21}$$

In the near adiabatic limit, the particle flux $\Gamma \propto 1/\alpha \ll 1$ as $\alpha \gg |\omega|$ and the residual stress is: $\Pi_{xy}^{res} = -\chi_y v_d = -\chi_y \rho_s c_s \nabla \bar{n}$. The expressions for χ_y and Π_{xy}^{res} in this limit are:

$$\begin{aligned} \chi_y &= \sum_m \frac{|\gamma_m|}{|\omega|^2} k_m^2 \rho_s^2 c_s^2 |\delta\phi^2| = \tau_c \langle \delta v_x^2 \rangle = l_{mix} \sqrt{f\varepsilon} \\ \Pi_{xy}^{res} &= -\sum_m \frac{|\gamma_m| \omega^\star k_m^2 \rho_s c_s^2}{|\omega|^2} |\delta\phi^2| = -\frac{\langle \delta v_x^2 \rangle \tau_c c_s}{\rho_s L_n} = -\frac{l_{mix} \sqrt{f\varepsilon} \omega_{ci}}{L_n} \end{aligned} \tag{2.22}$$

where the fluctuation correlation time is $\tau_c = l_{mix}/\sqrt{f\varepsilon}$.

In addition to the Reynolds force, the expression for the local Reynolds power is needed in eq.(2.4). For this, we write the Reynolds stress as:

$$\langle \tilde{v}_x \tilde{v}_y \rangle = -\chi_y \frac{d\bar{v}_y}{dx} + \langle \tilde{v}_x \tilde{v}_y \rangle^{res}$$

The total Reynolds power $P_{Re} = \int (d\bar{v}_y/dx)\langle \tilde{v}_x \tilde{v}_y \rangle dV$ where $dV = dxdydz$ can then be written as:

$$\begin{aligned} P_{Re} &= \int \frac{d\bar{v}_y}{dx}\Big(-\chi_y \frac{d\bar{v}_y}{dx} + \langle \tilde{v}_x \tilde{v}_y \rangle^{res} \Big) dV \\ &= \int -\chi_y \Big(\frac{d\bar{v}_y}{dx} \Big)^2 dV + \int \frac{d\bar{v}_y}{dx} \langle \tilde{v}_x \tilde{v}_y \rangle^{res} dV \\ &= \int \Big\{ -\chi_y \Big(\frac{d\bar{v}_y}{dx} \Big)^2 - \bar{v}_y \partial_x \Big[\langle \tilde{v}_x \tilde{v}_y \rangle^{res} \Big] \Big\} dV + \bar{v}_y \langle \tilde{v}_x \tilde{v}_y \rangle^{res} \Big|_{bound} \\ &= \int -\chi_y (\frac{d\bar{v}_y}{dx})^2 dV + \int \bar{v}_y \Pi_{xy}^{res} dV \end{aligned} \tag{2.23}$$

Here we drop the boundary term $\bar{v}_y \langle \tilde{v}_x \tilde{v}_y \rangle^{res} \Big|_{bound}$ that results from integration by parts. We justify this by the strong neutral drag (close to the plasma boundary), so the perpendicular flow $\bar{v}_y$ must vanish at the boundary due to no-slip condition. The local Reynolds power density is thus:

$$\langle \tilde{v}_x \tilde{v}_y \rangle \frac{d\bar{v}_y}{dx} = -\chi_y \Big(\frac{d\bar{v}_y}{dx} \Big)^2 + \bar{v}_y \Pi_{xy}^{res} \tag{2.24}$$

2.4 THE PARALLEL REYNOLDS STRESS $\langle \tilde{v}_x \tilde{v}_z \rangle$

Adding axial flow to the Hasegawa-Wakatani equations breaks conservation of PV, and thus that of potential enstrophy. Moreover, it introduces an energy transfer channel between the parallel and perpendicular directions, via acoustic coupling. Experimental results show that when drift waves dominate, the turbulence production due to the release of free energy in $\nabla \bar{n}$, can excite secondary parallel flows [IKI$^+$16, KIK$^+$16, KII17, TGM$^+$16]. Theoretical studies also show

that both axial and zonal flows are driven by turbulence, particularly by the non-diffusive residual stress in both expressions for $\langle \tilde{v}_x \tilde{v}_y \rangle$ and $\langle \tilde{v}_x \tilde{v}_z \rangle$ [HLT$^+$17, LD17, KII16, KDG10, DKG$^+$13]. Ref.[WDH12] investigates the relation between the axial and azimuthal flows and turbulence, and formulates a new zonal momentum balance theorem for the coupled drift-ion acoustic waves. Due to acoustic coupling, a dynamical mechanism for ZF generation is established. This mechanism does not require any potential vorticity flux. The sheared $E \times B$ layers so formed, break parallel symmetry (in a sheared magnetic field), generate a non-zero parallel residual stress Π_{xz}^{res}, and accelerate the axial flow $\bar{v}_z$, according to the mechanism of ref. [GDHS07]. We note, however, that strong $E \times B$ shear eventually will damp the PSFI (Fig.4.4). As an aside, we mention that the acceleration of zonal flows does not require external breaking of azimuthal symmetry. Zonal flows are generated by modulational instability of drift waves to a seed shear. This does not require a geometrically broken azimuthal symmetry. Axial flows on the other hand require a non-zero parallel residual stress, which can develop from a broken parallel spectral symmetry. This is one reason why zonal flows are much easier to accelerate than parallel flows. These parallel symmetry breaking mechanisms usually require the presence of a magnetic shear.

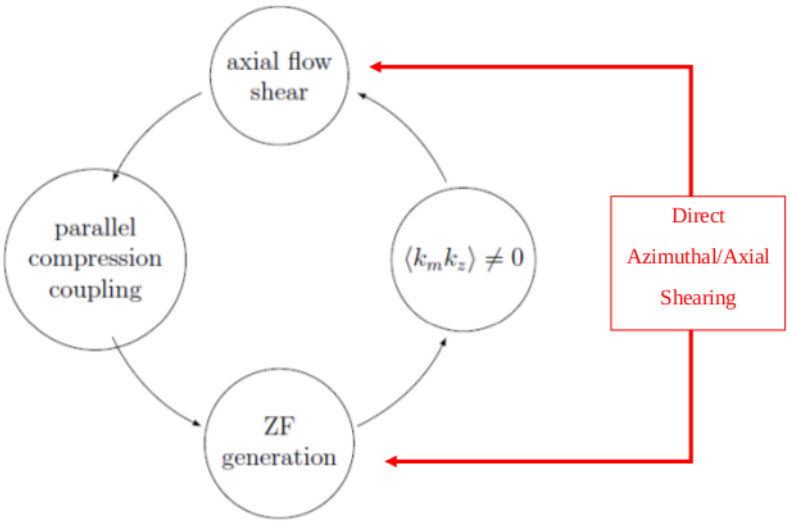

Figure 2.2: Feedback loop between axial and zonal flows via $\langle k_m k_z \rangle$. A strong zonal flow shear can affect the axial flow.

However, such mechanisms are not relevant to CSDX, since **B** is constant and magnetic shear is absent. Symmetry breaking is then provided by a dynamical mechanism, based on DWs and momentum evolution [LDXT16]. The growth rate of the DWs in CSDX is determined by the frequency shift: $|\gamma| \sim \omega^\star - \omega$. A test flow shear $\bar{v}_z'$ changes this frequency shift, setting modes with $k_m k_z |\bar{v}_z'| > 0$ to grow faster than those with $k_m k_z |\bar{v}_z'| < 0$, and causing a spectral imbalance in the $k_m - k_z$ space to develop. This creates a parallel residual stress $\Pi_{xz}^{res} = -|\chi_z^{res}| \nabla \bar{v}_z$. The latter reinforces the test shear, and amplifies the parallel flow through a process of 'negative viscosity'. If $\bar{v}_z'$ keeps increasing, the parallel shear flow instability (PSFI) will occur [KIIe5, KIK$^+$16]. When the PSFI is turned on, $\nabla \bar{v}_z$ saturates at the PSFI linear threshold and the total viscosity remains positive: $\chi_z^{tot} = \chi_z^{DW} + \chi_z^{PSFI} - |\chi_z^{res}| > 0$. In CSDX, no external axial momentum is injected into the plasma, and $\nabla \bar{v}_z$ never exceeds the critical value necessary to destabilize the PSFI [LD17]. Turbulence production thus primarily accelerates the axial flow in CSDX without destabilizing it.

2.4.1 Calculating the Expression for $\langle \tilde{v}_x \tilde{v}_z \rangle$

In the near adiabatic limit, the expression for the parallel stress $\langle \tilde{v}_x \tilde{v}_z \rangle$ is obtained by writing $\tilde{v}_x = -ik_m \rho_s c_s \tilde{\phi}$ and using eq.(2.1c) to get:

$$\langle \tilde{v}_x \tilde{v}_z \rangle = -\frac{|\gamma_m| \langle \delta v_x^2 \rangle}{|\omega|^2} \frac{d\bar{v}_z}{dx} + \langle k_m k_z \rangle \rho_s c_s^3 \Big[\frac{|\gamma_m|}{|\omega|^2} + \frac{(\omega^\star - \omega^r)}{|\omega| \alpha} \Big] \tag{2.25}$$

In obtaining the expression for $\langle \tilde{v}_x \tilde{v}_z \rangle$, we neglected the contribution of the flow shear V_0' with respect to the wave frequency ω, as we did in the expression for $\langle \tilde{v}_x \tilde{v}_y \rangle$. Just like χ_y, the total parallel diffusivity χ_z is equal to the sum of the resonant and the non-resonant part. The first component of eq.(2.25) is a diffusive term that is written as $-\chi_z d\bar{v}_z/dx$, where the turbulent diffusivity is:

$$\chi_z = \frac{|\gamma_m| \langle \delta v_x^2 \rangle}{|\omega|^2} = \tau_c \langle \delta v_x^2 \rangle = l_{mix} \sqrt{f \varepsilon} \tag{2.26}$$

We note that the turbulent parallel diffusivity χ_z given in eq.(2.26) is the same as the perpendicular diffusivity χ_y given in eq.(2.3.2). The remaining part of eq.(2.25), involving the correlator $\langle k_m k_z \rangle = \sum k_m k_z |\delta\phi^2|$, constitutes the parallel residual stress, Π_{xz}^{res}. This term is responsible for generating the intrinsic axial flow. The expression for the parallel residual stress is:

$$\begin{aligned}
\Pi_{xz}^{res} &= \sum_m \frac{|\gamma_m| k_m k_z \rho_s c_s^3}{|\omega|^2} |\delta\phi^2| + \frac{k_m k_z \rho_s c_s^3 (\omega^\star - \omega^r)}{|\omega| \alpha} |\delta\phi^2| \\
&= \sum_m \frac{|\gamma_m| k_m k_z \rho_s c_s^3}{|\omega|^2} |\delta\phi^2| + \frac{k_m k_z \rho_s^3 c_s^3 k_\perp^2}{\alpha} |\delta\phi^2| \\
&= \langle k_m k_z \rangle \rho_s c_s^3 \left[\tau_c + \frac{\rho_s^2 k_\perp^2}{\alpha} \right]
\end{aligned} \tag{2.27}$$

2.4.2 Analogy to Pipe Flow: A Simple Approach to the Physics of the $\langle k_m k_z \rangle$ Correlator

In order to calculate the parallel residual stress Π_{xz}^{res}, an expression for the correlator $\langle k_m k_z \rangle = \sum k_m k_z |\delta\phi^2|$ is needed. More importantly, in order to model the axial flow generation in CSDX, $\langle k_m k_z \rangle$ needs to be expressed in terms of a simple coefficient that can be used in numerical results. We thus draw an analogy with turbulence in a pipe flow and write $\tilde{v}_z$ as:

$$\begin{aligned}
\tilde{v}_z &= -\tilde{v}_x \tau_c \nabla \bar{v}_z + \tilde{v}^{res} \\
&= -l_{mix} \nabla \bar{v}_z + R \nabla \bar{n}
\end{aligned} \tag{2.28}$$

The first term (proportional to $\nabla \bar{v}_z$) results from turbulent mixing on a scale l_{mix}. The second term (proportional to $\nabla \bar{n}$) relates to DWs and represents the acoustic coupling from turbulent mixing of $\nabla \bar{n}$. The latter shows how the free energy creates a residual velocity $\tilde{v}_z^{res}$,

(i.e., a parallel residual stress). The parallel velocity equation reads:

$$\frac{d\tilde{v}_z}{dt} = -\tilde{v}_x \frac{d\bar{v}_z}{dx} - c_s^2 \nabla_z \Big[\frac{e\tilde{\phi}}{T_e} + \frac{\tilde{p}_e}{p_e} \Big] \tag{2.29}$$

In the CSDX plasma which is nearly adiabatic and where variations of the electron temperature are negligible, we have $e\tilde{\phi}/T_e \sim \tilde{n}/\bar{n}$ and $\tilde{p}_e/p_e \sim \tilde{n}/\bar{n}$. Proceeding as for Prandtl mixing length theory, we write $\tilde{n}/\bar{n} \sim l_{mix}|\nabla\bar{n}|/\bar{n}$, and obtain:

$$\tilde{v}_z^{res} = \frac{\sigma_{VT} c_s^2 \tau_c}{L_\parallel} . \Big(\frac{-l_{mix}}{\bar{n}} \frac{d\bar{n}}{dx} \Big)$$

where $L_\parallel = L_z$ is the axial plasma length, $\bar{n}$ is the average plasma density and $\tau_c = l_{mix}/\tilde{v}_x$ is the fluctuation correlation time. The constant σ_{VT} is introduced as a dimensionless scaling factor between variations of $\tilde{v}_z$ and variations of the density gradient $\nabla\bar{n}$. The final expression for $\tilde{v}_z$ is then:

$$\tilde{v}_z = -l_{mix} \frac{d\bar{v}_z}{dx} + \frac{\sigma_{VT} c_s^2 \tau_c}{L_\parallel} . \Big(- \frac{l_{mix}}{\bar{n}} \frac{dn}{dx} \Big),$$

The parallel Reynolds stress $\langle \tilde{v}_x \tilde{v}_z \rangle$ then becomes:

$$\langle \tilde{v}_x \tilde{v}_z \rangle = -\chi_z \frac{d\bar{v}_z}{dx} - \frac{\sigma_{VT} c_s^2 \langle l_{mix}^2 \rangle}{L_\parallel} . \frac{\nabla\bar{n}}{\bar{n}} \tag{2.30}$$

The first term in eq.(2.30) is the diagonal stress and is proportional to $\chi_z = \langle l_{mix}^2 \rangle / \tau_c$. The second term represents the parallel residual stress:

$$\Pi_{xz}^{res} = -\frac{\sigma_{VT} c_s^2 \langle l_{mix}^2 \rangle}{L_\parallel} . \frac{\nabla\bar{n}}{\bar{n}} \tag{2.31}$$

The parallel Reynolds stress can then be written as:

$$\langle \tilde{v}_x \tilde{v}_z \rangle = -\chi_z \Big[\frac{d\bar{v}_z}{dx} + \frac{\sigma_{VT} c_s^2 l_{mix}}{\tilde{v}_x L_\parallel \bar{n}} . \frac{d\bar{n}}{dx} \Big] \tag{2.32}$$

A comparison of eq.(2.27) and eq.(2.30) shows that the correlator $\langle k_m k_z \rangle$ is equal to:

$$\langle k_m k_z \rangle \Big[\frac{l_{mix}}{\sqrt{f\varepsilon}} + \frac{\rho_s^2 k_\perp^2}{\alpha} \Big] = -\frac{\sigma_{VT} \nabla \bar{n}}{\bar{n}} . \frac{\langle l_{mix}^2 \rangle}{L_\parallel \rho_s c_s} \tag{2.33}$$

Eq.(2.33) shows that σ_{VT} is the counterpart of the correlator $\langle k_m k_z \rangle$. This constant σ_{VT} can be written as:

$$\sigma_{VT} = \frac{\langle k_m k_z \rangle}{\langle k_\perp^2 \rangle^{1/2} / L_\parallel} \tag{2.34}$$

where both $L_\parallel$ and the radial wavenumber $\langle k_\perp^2 \rangle^{1/2}$ can be determined empirically. σ_{VT} captures the cross-phase information between $\tilde{v}_x$ and $\tilde{v}_z$, and determines whether the parallel Reynolds power density $-\langle \tilde{v}_x \tilde{v}_z \rangle \nabla \bar{v}_z$ is an energy source or sink in eq.(2.4). σ_{VT} also represents the degree of symmetry breaking in the correlator $\langle k_m k_z \rangle$, and quantifies the efficiency of $\nabla \bar{n}$ in driving an axial flow. For turbulence-driven axial flows, with no axial momentum input, the parallel Reynolds stress vanishes, and the net axial flux is equal to zero: $\langle \tilde{v}_x \tilde{v}_z \rangle = 0$. The relation between the axial velocity shear and the density gradient must be:

$$\nabla \bar{v}_z = -\frac{\sigma_{VT} c_s^2 \tau_c}{L_\parallel \bar{n}} \nabla \bar{n} \tag{2.35}$$

Eq.(2.35) can be used to determine empirically the value for σ_{VT}, as τ_c is experimentally measurable.

One can also relate the variations in $\nabla \bar{v}_z$ to those in the azimuthal shear $\nabla \bar{v}_y$ via σ_{VT}. For a zero net vorticity flux: $\langle \tilde{v}_x \nabla_\perp^2 \phi \rangle = 0$, and the diffusive and the residual components of the vorticity flux are at balance:

$$\chi_y \frac{d^2 \bar{v}_y}{dx^2} = \Pi_{xy}^{res} \propto \nabla \bar{n}$$

Using eqs.(2.22) for χ_y and Π_{xy}^{res} in the near adiabatic limit, as well as the scaling of eq.(4.36),

we obtain the following relation:

$$\frac{d}{dx}\nabla\bar{v}_y = \frac{\omega_{ci}L_{\parallel}}{\sigma_{VT}c_s^2\tau_c}\nabla\bar{v}_z \tag{2.36}$$

Eq.(2.36) shows then how parallel and perpendicular flow dynamics are coupled. It also explains how the azimuthal shearing $\nabla\bar{v}_y$ limits the axial plasma response to the parallel residual stress Π_{xz}^{res}. As $\nabla\bar{v}_y$ increases, turbulence is suppressed, and $\bar{v}_z$ decreases. This in turn causes σ_{VT} to decrease, thus reducing the acoustic coupling.

2.5 THE RADIAL MIXING LENGTH l_{mix}

A solution of the coupled drift-ion acoustic wave system requires an expression for the radial turbulent mixing length l_{mix}. In 2-D turbulent systems, the Rhines' scale, l_{Rh}, defined as the scale beyond which the inverse energy cascade terminates, emerges as an appropriate mixing length [HDAT17]. Turbulence simply changes character for $l > l_{Rh}$, and the plasma dynamics evolve from a turbulence cascade regime to wave like behavior. In CSDX, the plasma system does not exhibit a sufficiently large dynamical range of energy transfer to observe this transition in turbulence dynamics [MXTT11, CAT$^+$16]. Therefore, the significance of the Rhines' scale is unclear in this experiment. As mixing is regulated primarily by shearing in CSDX, a scale length that accounts for turbulence suppression due to coupling between radial fluctuations and sheared azimuthal and axial flows is suggested.

2.5.1 Case of a purely azimuthal shear

In the case of mean azimuthal shears, the following form of mixing length is suggested [BDT90]:

$$l_{mix}^2 = \frac{l_0^2}{\left[1+(\bar{v}_y')^2\tau_c^2\right]^{\delta}} \tag{2.37}$$

Here δ is the suppression parameter, τ_c is the fluctuation correlation time, and l_0 is the mixing scale for turbulence in CSDX in the absence of shear flow. When the azimuthal shearing rate is greater than the fluctuations growth rate: $\bar{v}_y' > |\gamma_m|$, turbulent eddies are decorrelated and turbulence is suppressed. Coupling between the azimuthal shearing and the turbulent radial scattering of fluctuations can quench turbulence and decrease l_{mix}. An empirical relation for the scale length of turbulence $l_0 = [(\bar{k}_r^2)^{1/2}]^{-1}$ is found by expressing the inverse radial wave number k_r^{-1} as a function of the density fluctuations $\tilde{n}$ normalized by the average plasma density $\bar{n}$ [HDAT17]:

$$l_0 \simeq 2.3\rho_s^{0.6} L_n^{0.3} \tag{2.38}$$

This suggests that the CSDX turbulent plasma diffusion coefficient scales like:

$$D_{CSDX} \simeq D_B \rho_\star^{0.6} \tag{2.39}$$

where D_B is the Bohm diffusive coefficient, and $\rho_\star$ is the ion gyroradius normalized by the inverse density gradient scale length: $\rho_\star = \rho/L_n$. Eq.(2.39) suggests that the scalings of diffusion in CSDX fall in between the Bohm and gyroBohm diffusion scalings. For τ_c, we write:

$$1/\tau_c = \left(k_m^2 (v_y')^2 \chi_y\right)^{1/3} \tag{2.40}$$

where the wavenumber is $k_m \simeq 1/l_0$ and the turbulent diffusivity is $\chi_y = \tau_c \langle \delta v_x^2 \rangle = \tau_c f \varepsilon$. The correlation time is then:

$$\tau_c = \left[\frac{(v_y')^2 f\varepsilon}{l_0^2}\right]^{-1/4}$$

and the mixing length becomes:

$$l_{mix}^2 = l_0^2 \left[1 + \frac{|v_y'| l_0}{\sqrt{f\varepsilon}}\right]^{-1} \tag{2.41}$$

The structure of eq.(2.41) shows an intuitively plausible inverse relation between the shear and the mixing length.

2.5.2 Case of azimuthal and axial shear

When both axial and azimuthal shear are present in the system, and when the azimuthal shear rate is greater than the radial correlation rate: $\vec{v}'_y > \sqrt{f\varepsilon}/l_0$, the expression for the mixing length becomes:

$$l_{mix}^2 = \frac{l_0^2}{\left[1 + \left(k_m \vec{v}'_y + k_z \vec{v}'_z\right)^2 \tau_c^2\right]} \tag{2.42}$$

Here the wavenumbers can be chosen as: $k_m = 1/l_0$ and $k_z = 1/L_\parallel$. The expression for the mixing length is:

$$l_{mix}^2 = l_0^2 \left[1 + \left(\frac{\vec{v}'_y}{l_0} + \frac{\vec{v}'_z}{L_\parallel}\right)^2 \frac{l_0^2}{f\varepsilon}\right]^{-1} \tag{2.43}$$

The structure of eq.(2.43) is not significantly different from that of eq.(2.41). Both expressions show that l_{mix} is inversely proportional to $\vec{v}'_y/\vec{v}'_z$: as the shear grows, the mixing length l_{mix} shrinks. This in turn reduces the turbulent energy ε, and increases the mean energy because of total energy conservation. In CSDX, the effective mean azimuthal shear $\vec{v}'_y$ dominates the mean axial shear $\vec{v}'_z$.

2.6 SUMMARY AND DISCUSSION OF THE MODEL

In summary, the model consists of the equations:

$$\frac{\partial \bar{n}}{\partial t} = -\frac{\partial}{\partial x}\langle \tilde{v}_x \tilde{n} \rangle + D_c \frac{\partial^2 \bar{n}}{\partial x^2} + S_n \tag{2.44a}$$

$$\frac{\partial \bar{v}_z}{\partial t} = -\frac{\partial}{\partial x}\langle \tilde{v}_x \tilde{v}_z \rangle + \nu_{c,\parallel} \frac{\partial^2 \bar{v}_z}{\partial x^2} + S_{v_z} \tag{2.44b}$$

$$\frac{\partial \bar{v}_y}{\partial t} = -\frac{\partial}{\partial x}\langle \tilde{v}_x \tilde{v}_y \rangle + \nu_{c,\perp} \frac{\partial^2 \bar{v}_y}{\partial x^2} - \nu_{in}(\bar{v}_y - \bar{v}_n) - \nu_{ii}\bar{v}_y + S_{v_y} \tag{2.44c}$$

$$\frac{\partial \varepsilon}{\partial t} - \partial_x(l_{mix}\varepsilon^{1/2}\partial_x \varepsilon) = -\langle \tilde{n}\tilde{v}_x \rangle \frac{d\bar{n}}{dx} - \langle \tilde{v}_x \tilde{v}_z \rangle \frac{d\bar{v}_z}{dx} - \langle \tilde{v}_x \tilde{v}_y \rangle \frac{d\bar{v}_y}{dx} - \frac{\varepsilon^{3/2}}{l_{mix}} + P \tag{2.44d}$$

The expressions for the turbulent fluxes and the Reynolds power density are:

$$\langle \tilde{n}\tilde{v}_x \rangle = -\frac{f\varepsilon}{\alpha} \cdot \frac{k_\perp^2 \rho_s^2}{1 + k_\perp^2 \rho_s^2} \cdot \frac{1}{n_0} \frac{d\bar{n}}{dx} \tag{2.45a}$$

$$-\frac{\partial \langle \tilde{v}_x \tilde{v}_y \rangle}{\partial x} = -l_{mix}\sqrt{f\varepsilon} \frac{d^2 \bar{v}_y}{dx^2} - \frac{l_{mix}\sqrt{f\varepsilon}\omega_{ci}}{L_n} \tag{2.45b}$$

$$-\langle \tilde{v}_x \tilde{v}_y \rangle \frac{d\bar{v}_y}{dx} = -l_{mix}\sqrt{f\varepsilon}\left(\frac{d\bar{v}_y}{dx}\right)^2 - \bar{v}_y \frac{l_{mix}\sqrt{f\varepsilon}\omega_{ci}}{L_n} \tag{2.45c}$$

$$\langle \tilde{v}_x \tilde{v}_z \rangle = -l_{mix}\sqrt{f\varepsilon} \frac{d\bar{v}_z}{dx} + \langle k_m k_z \rangle \rho_s c_s^3 \left[\frac{l_{mix}}{\sqrt{f\varepsilon}} + \frac{\rho_s^2 k_\perp^2}{\alpha} \right] \tag{2.45d}$$

$$= -l_{mix}\sqrt{f\varepsilon} \frac{d\bar{v}_z}{dx} - \frac{\sigma_{VT} c_s^2 \langle l_{mix}^2 \rangle}{L_\parallel L_n} \tag{2.45e}$$

Here l_{mix} and f are given by eq.(2.43) and eq.(2.15) respectively. The model evolves the fields $\bar{n}$, $\bar{v}_y$, $\bar{v}_z$ and ε in space and time (x,t) using a slowly varying envelope approximation. In addition, the model self consistently relates the evolution of turbulence to that of the parallel and perpendicular flow dynamics. The coupling terms associating the turbulent energy to variations

of the mean profiles $\bar{n}$, $\bar{v}_y$ and $\bar{v}_z$, are expressed in terms of a mixing length l_{mix}, the expression for which depends on both axial and azimuthal shear (eq.(2.43)). The particle flux is purely diffusive: $\langle \tilde{n}\tilde{v}_x \rangle = -D\nabla\bar{n}$. Both parallel and perpendicular Reynolds stresses consist of a diffusive part ($-\chi_z \nabla \bar{v}_z$ and $-\chi_y \nabla \bar{v}_y$), as well as a residual component proportional to $\nabla\bar{n}$ that generates an axial and an azimuthal flow.

The generated axial flow is associated with the correlator $\langle k_m k_z \rangle \neq 0$ that measures the acoustic coupling. A version of this model introduces the empirical constant σ_{VT} in the expression for $\langle k_m k_z \rangle$ (eq.(2.31)). This experimentally measurable constant relates the variations of the axial shear to those of the density gradient, via eq.(4.36). It also shows how free energy released from the density gradient can accelerate $\bar{v}_z$, even in the case of no axial momentum input. In addition, this constant accounts for the strength of the parallel to perpendicular flow coupling as: $\sigma_{VT} \sim \langle \tilde{v}_x \tilde{v}_z \rangle \sim \langle k_m k_z \rangle$. This coupling is stated in eq.(2.36), which relates $\bar{v}_z'$ to $\bar{v}_y'$ since both shears are dependent on the density gradient $\nabla\bar{n}$. Finally, we note that this model manifests the well known relation between turbulence and azimuthal flows via the Reynolds stress $\langle \tilde{v}_x \tilde{v}_y \rangle$ and also manifests a similar relation between fluctuations and axial flows via the parallel Reynolds stress $\langle \tilde{v}_x \tilde{v}_z \rangle$. Numerical solutions of this model will be published in a future work.

2.7 REDUCING THE MODEL

When the eddy turnover time $\tau_c = l_{mix}/\tilde{v}_x$ is smaller than the confinement time $\tau_{conf} = [\bar{n}^{-1} D \nabla^2 \bar{n}]^{-1}$, the model can then be reduced to a 3 field model by slaving the expression for ε to the mean profiles, and solving the equations for $\bar{n}$, $\bar{v}_y$ and $\bar{v}_z$. Experimental results from CSDX show that the energy transfer to the axial flow via the parallel Reynolds power density: $\int -\partial_x \langle \tilde{v}_x \tilde{v}_z \rangle \bar{v}_z dx$, i.e., the power exerted by turbulence on the axial flow, is less than that exerted on the azimuthal profile via: $\int -\partial_x \langle \tilde{v}_x \tilde{v}_y \rangle \bar{v}_y dx$, by a factor of five [HLT$^+$17, HLH$^+$17]. The axial

flow then can be considered as parasitic to the system of $\nabla\bar{v}_y$ and $\nabla\bar{n}$. The model can be reduced even further, to 2 fields, by neglecting the axial flow equation $\bar{v}_z$, and solving the density and azimuthal flow equations using the stationary slaved expression for ε obtained from the equation for the mean fluctuating energy.

2.7.1 Equations and Fluxes

In this reduced model, one would still use the equations:

$$\frac{\partial\bar{n}}{\partial t} = -\frac{\partial}{\partial x}\langle\tilde{v}_x\tilde{n}\rangle + D_c\frac{\partial^2\bar{n}}{\partial x^2} + S_n \tag{2.46a}$$

$$\frac{\partial\bar{v}_y}{\partial t} = -\frac{\partial}{\partial x}\langle\tilde{v}_x\tilde{v}_y\rangle + \nu_{c,\perp}\frac{\partial^2\bar{v}_y}{\partial x^2} - \nu_{in}(\bar{v}_y - \bar{v}_n) - \nu_{ii}\bar{v}_y \tag{2.46b}$$

We note here that, unlike tokamaks where there is a clear scale separation: $a \geq L_n \geq l_{mix} > \rho_s$, the scale ordering in CSDX is compressed: $a > L_n \simeq l_{mix} \geq \rho_s$. Here a is the radus of the plasma. In addition, when $\sqrt{\varepsilon}/l_{mix} < (D\nabla^2\bar{n})/\bar{n}$, a steady state solution of the energy equation generates an expression for ε, which can be used in both $\bar{n}$ and $\bar{v}_y$ equations. The predator-prey model thus obtained describes turbulence suppression and azimuthal flow evolution, where the flow $\bar{v}_y$ feeds on the density gradient $\nabla\bar{n}$. An interesting feature of this model is that, unlike the model of ref. [HS93], the fluctuations intensity is not treated as an *ad hoc* constant, but rather evolves self consistently, albeit adiabatically (i.e. slaved to $\bar{n}$ and $\bar{v}_y$). The shear $\nabla\bar{v}_y$ and $\nabla\bar{n}$ evolve in time, allowing for the level of fluctuation intensity to vary as well. In the near adiabatic electron limit, the expressions for the particle and vorticity fluxes are:

$$\Gamma = -\frac{\varepsilon f^2}{\alpha}\frac{d\ln n}{dx} = -D\frac{d\ln n}{dx} \tag{2.47a}$$

$$\Pi = -\sqrt{f\varepsilon}\,l_{mix}\frac{d^2\bar{v}_y}{dx^2} + \frac{l_{mix}\sqrt{f\varepsilon}\omega_{ci}}{L_n} = -\chi_y\frac{d^2\bar{v}_y}{dx^2} + \Pi^{res} \tag{2.47b}$$

Here $f = k_\perp^2\rho_s^2/(1+k_\perp^2\rho_s^2)$ and l_{mix} is given by eq.(2.41).

2.7.2 Closure by Slaving

For slaved turbulence, both the energy spreading and the energy production terms are neglected, because the eddy turnover time is shorter than the confinement time. Using eq.(2.24) for the Reynolds power, the fluctuation turbulent energy equation is:

$$-\Gamma_n \frac{d\bar{n}}{dx} + \chi_y (\frac{d\bar{v}_y}{dx})^2 - \bar{v}_y \Pi^{res} - \frac{\varepsilon^{3/2}}{l_{mix}} = 0 \tag{2.48}$$

with χ_y and Π^{res} given above. Solution of this equation gives:

$$\varepsilon = -\rho_s^2 \Big(\frac{d\bar{v}_y}{dx}\Big)^2 + \frac{l_0^2}{4}\left[\frac{f^2}{\alpha}\Big(\frac{dn}{dx}\Big)^2 + \sqrt{\Theta}\right]^2 \tag{2.49}$$

where

$$\Theta = \left[\frac{f^2}{\alpha}\Big(\frac{d\bar{n}}{dx}\Big)^2\right]^2 + 4f\left[\Big(\frac{d\bar{v}_y}{dx}\Big)^2 - \bar{v}_y \omega_{ci} \frac{d\bar{n}}{dx}\right] \tag{2.50}$$

One can thus use eq.(2.49) in the expressions for Γ and Π to close this reduced 2-field model. We note here that, in contrast to the model of ref. [HS93], the fluctuation level evolves in time. The reduced model then presents a coherent description of turbulence and mean profiles, without imposing a fixed level of turbulence. Solutions of this reduced model can be found by numerically solving the equations for $\bar{n}$ and $\bar{v}_y$, while taking into account the corresponding expressions for l_{mix}.

2.8 CONCLUSION

This paper presents a 4-field reduced model that describes the evolution of turbulence and mean profiles in the cylindrical drift-ion acoustic plasma of CSDX. The model studies the spatiotemporal evolution of the parallel and perpendicular flow dynamics, as well as the

variations of the fluctuation intensity ε. Also, the model fills the gap in approach between a 0-D 2-field reduced model ($\bar{n}$ and $\bar{v}_y$), and a DNS of the three primitive equations. Moreover, this reduced model yields a better physical interpretation for the mesoscopic results observed in CSDX, while avoiding the computational cost of a full 4-field DNS.

A self-consistent description of the variations of three mean fields: density $\bar{n}$, azimuthal flow $\bar{v}_y$, and axial flow $\bar{v}_z$, in addition to the fluctuation intensity ε is presented here. Conservation of the total (mean + turbulent) energy, including dissipation and internal energy production, is a key element. Due to acoustic coupling, $\langle \tilde{n}^2 + (\nabla_\perp \tilde{\phi})^2 + \tilde{v}_z^2 \rangle$ is the conserved energy field. Because mixing occurs primarily by shearing in CSDX, the model employs a mixing length that is inversely proportional to both axial and azimuthal flow shear (eq.(2.43)). However, we note that in CSDX, $\bar{v}_y' > \bar{v}_z'$. The choice of a mixing length that is inversely proportional to the shear closes the loop on the total energy, and allows development of improved confinement in CSDX. Key elements of the model and its predications of experimental findings are:

1. Evolution of the profiles, including mean flows and turbulent stresses, in a cylindrical plasma characterized by a constant magnetic field. The model explains how an increase in the magnitude of **B** decreases the scale of turbulent transport and steepens the density profile. Free energy released from $\nabla\bar{n}$ accelerates then the azimuthal plasma flow $\bar{v}_y$, as verified experimentally [CAT$^+$16]. The current model is an extension of that presented in ref.[HDAT17], where the predator/prey relation between DWs and ZFs was derived and validated.

2. In the DW dominated plasma of CSDX, a test axial flow shear breaks the parallel symmetry, which results in a residual stress $\Pi_{xz}^{res} \propto \nabla\bar{n}$ and an axial flow $\bar{v}_z$. Energy released from $\nabla\bar{n}$ also accelerates $\bar{v}_z$ via the parallel Reynolds stress $\langle \tilde{v}_x \tilde{v}_z \rangle$. This trend is in agreement with the experimental results [HLT$^+$17, HLH$^+$17], and supports the analogy between the plasma and an engine [KDG10]. The model thus unfolds a coupling relation between $\bar{v}_z$ and $\bar{v}_y$, as both flows are accelerated by the same free energy source.

3. The model reduces the evolution of plasma profiles to three fluxes: a particle diffusive flux, as well as a parallel and perpendicular Reynolds stress with residual components Π_{xz}^{res} and Π_{xy}^{res}. These fluxes regulate the transfer of energy between fluctuations and mean flows and governs the ecology of flows and drift wave turbulence.

4. The model introduces an empirical constant σ_{VT} that measures the correlator $\langle k_m k_z \rangle = \sum_m k_m k_z |\tilde{\phi}|^2$. This correlator encodes the broken symmetry of turbulence, and quantifies the efficiency of drift waves in driving Π_{xz}^{res} and $\bar{v}_z$ through eq.(4.36). Because σ_{VT} measures the cross phase relation between $\tilde{v}_x$ and $\tilde{v}_z$, it determines the direction of energy transfer between turbulence and axial flow.

5. Eq.(4.36) provides an expression for the critical density gradient necessary for onset of an axial flow shear $\nabla \bar{v}_z$. By balancing the residual and the diffusive components of the parallel Reynolds stress, we obtain:

$$\left| \frac{\nabla \bar{n}_{crit}}{\bar{n}} \right| = \frac{k_z^2 v_{th}^2}{\nu_{ei}} \frac{\omega^\star L_\parallel}{\langle k_m k_z \rangle \rho_s c_s^3 \tau_c}$$

   where τ_c is the correlation time. The model thus explains why a sheared $\bar{v}_z$ flow was observed only above a critical **B** value in CSDX, i.e., beyond a critical density gradient.

6. Through eq.(2.36), the model provides a direct expression for the parallel to perpendicular flow coupling that is reported experimentally in refs.[HLT$^+$17, HLH$^+$17]. Because $\chi_y = \chi_z$, and since both Π_{xy}^{res} and Π_{xz}^{res} are proportional to $\nabla \bar{n}$, the relation:

$$\frac{d(\nabla \bar{v}_y)/dx}{\nabla \bar{v}_z} = \frac{\Pi_{xy}^{res}}{\Pi_{xz}^{res}} = \frac{\omega_{ci} L_\parallel}{\sigma_{VT} c_s^2 \tau_c}$$

   is established, and σ_{VT} is interpreted as a measure of the magnitude of coupling between $\nabla \bar{v}_y$ and $\nabla \bar{v}_z$.

7. According to eq.(2.39), turbulent diffusion in CSDX does not follow Bohm scaling. Scalings of turbulent diffusion in both CSDX and larger devices characterized by higher temperature follow the same trend [TBI$^+$04, GKP$^+$03]

When the axial to azimuthal flow coupling is weak, the axial flow is mainly driven by the turbulent Reynolds stress, particularly by the parallel residual part. The reduced 4-field model can thus be simplified to a 2-field predator-prey model which evolves $\bar{v}_y$ and $\bar{n}$. In CSDX, probe measurements show that the magnitude of $\bar{v}_z$ is moderate, and that the parallel Reynolds power is much less than that in the perpendicular direction. Measurements also indicate a weak coupling between $\bar{v}_y$ and $\bar{v}_z$ [HLT$^+$17, HLH$^+$17]. This is consistent with the observation that $\nabla\bar{v}_y \ll |\omega|$ (i.e. moderate azimuthal flow) and the absence of transport barriers, because of a decoupled $\bar{v}_z$ from $\bar{v}_y$. Analytically, in order to simplify the model, a slaved expression for ε is replaced in the equations for density and azimuthal flow. In contrast to the model in ref.[HS93] which treats the fluctuations as an *ad hoc* constant, both the fluctuations and the shear evolve in this new predator-prey model. An investigation of the numerical results obtained from such a 2-field reduced model is planned as a future work. The theory suggests the formation of zonal flows is the key part of turbulence regulation, with axial flows as parasitic. $\langle\tilde{v}_x^2$ fluctuations can be determined using eq.(2.49), and then used to obtain $\bar{v}_z(x)$ via eq.(2.44b).

Future work also includes an investigation of the numerical results obtained by simulation of the reduced 4-field model, while using appropriate boundary conditions and initial profiles. These results will elucidate the details of the acceleration of axial flow, and the coupling between $\bar{v}_y$ and $\bar{v}_z$. Numerical results will also confirm the existence of a critical density gradient $\nabla\bar{n}|_{crit}$ necessary for the onset of the axial flow shear $\nabla\bar{v}_z$. The possibility of the emergence of a staircase in this 4-field model can be examined. Such crucial step is essential to understand the evolution of mesoscale structures that condense to form macroscopic barriers in the density profile.

Finally, future work in CSDX includes adding both a particle source as well as an external axial momentum source. These two sources enhance the interactions between the flows and

turbulence in the plasma, leading thereby to further coupling between $\bar{v}_y$ and $\bar{v}_z$ according to the mechanism illustrated in fig.2.3. However, the azimuthal Reynolds power is much larger than

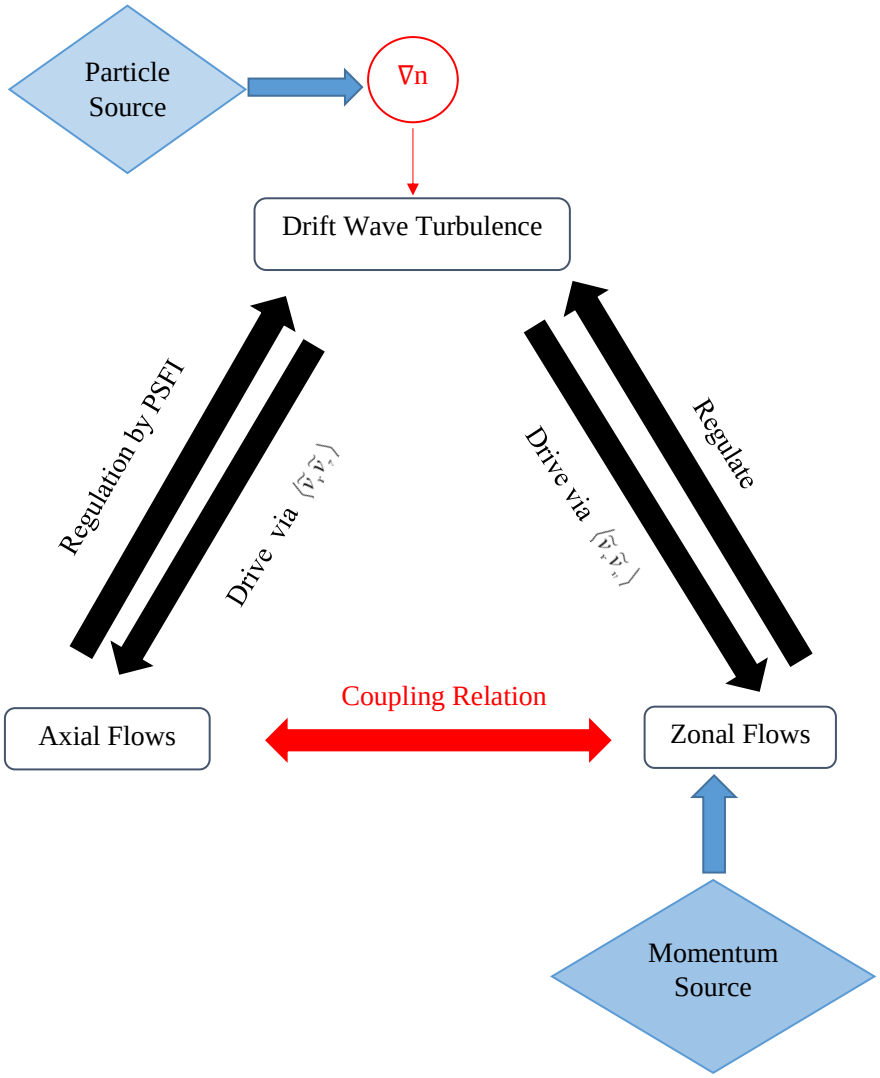

Figure 2.3: The future of CSDX: particle and axial momentum sources enhance the interactions between flows and turbulence, and generate further coupling between the axial and perpendicular flow dynamics.

the axial Reynolds power, so one may regard the axial flow evolution as parasitic to the drift wavezonal flow system. This is consistent with the observation that V moderate azimuthal flow shear) and thus there is no transport barrier.

2.9 Acknowledgments

The text and data in chapter 2 is a reprint of the material as it appears in ” The Ecology of Flows and Drift Wave Turbulence in CSDX: a Model” in the Journal of Physics of Plasmas **25**, 022301 (2018). Hajjar R. J., Diamond P.H., Tynan G.R., American Institute of Physics, 2018. The dissertation author was the primary investigator and author of this article.

Chapter 3

MODELING ENHANCED CONFINEMENT IN DRIFT WAVE TURBULENCE

3.1 Introduction

Turbulent phenomena and their evolving properties in fluids are topics of both classical and current significance. Of particular interest are the spectral features and transport properties of turbulence in magnetized plasmas. Density and temperature gradients, typically present near the edges of large scale magnetically confined devices, generate fluctuations that give rise to fully developed drift wave (DW) instabilities. Such instabilities carry fluxes via cross-field transport and limit the energy confinement time τ_E [Hor99, Gar01]. Suppression of these instabilities and reduction of the cross-field transport rates are therefore essential requirements for achieving enhanced confinement, in ITER and future tokamaks.

One way the plasma itself mitigates cross-field transport rates is via fluctuation driven zonal flows (ZF). In laboratory plasmas, zonal flows are strongly sheared $E \times B$ layers. Generated

via Reynolds stresses and particle transport, zonal flows arise when low-frequency drift modes interact by modulational instability or via an inverse cascade, to form a large scale anisotropic structure. The direct relation between microscale drift waves and macroscale zonal flows has been already well established both theoretically [MDM$^+$15] and experimentally [SZR$^+$12, TXD$^+$13], so much so that the system is now referred to as "drift wave-zonal flow turbulence" (see ref.[DIIH05] for a detailed review).

Interaction between separate components of the DW-ZF turbulence is found to affect the turbulent transport dynamics. Experimental studies in both linear and toroidal devices show that the state of turbulence changes with on the magnetic field (CSDX)[BTA$^+$05, AYT07], the filling gas pressure (LMDU)[AKI$^+$09] and the radial electric field (KIWI)[KLP$^+$97]. Shearing of the DW structures leads to an energy transfer between low frequency fluctuations and vortices with finite azimuthal mode numbers, including $m \sim 0$ zonal flows. This coupling initiates a process of depletion of the fluctuations energy, which may continue to the point of the collapse of the turbulence intensity. When sufficient heat source, torque and fueling are available, a thermally insulation layer, supported by a strongly sheared $E \times B$ flow is formed. A transport barrier is thus created and an enhanced confinement regime occurs [DGH$^+$08, CLGD93, Hin91]. The concept of shear enhanced turbulence decorrelation was proposed nearly three decades ago [BDT90, HB95]. Since then, several variations on the theme of predator-prey model describing the interplay between turbulent fluctuations and $E \times B$ sheared flows have been suggested to explain the plasma evolution towards an enhanced confinement state in fusion devices like TJ-II [EHH$^+$10], NSTX [ZMH$^+$10] and EAST [XWW$^+$11]. Moreover, net inward fluxes would often accompany this transition, as it was observed in various toroidal [MBB$^+$11, SGK$^+$99] and small scale linear devices [KIK$^+$16, ZHB$^+$10, THY$^+$06].

In CSDX, early observations showed a controlled transition from nonlinearly coupled eigenmodes to fully developed broadband turbulence in the plasma, as the magnitude of B is increased [TBC$^+$14]. Recent studies revealed the existence of an enhanced regime at $B = 1200G$,

associated with a steepening of the mean density profile, the development of a strong velocity shearing and turbulent kinetic energy coupling to the flow. An inward particle flux as well as a change in the global and local turbulence features were also observed [CTD$^+$15, CAT$^+$16].

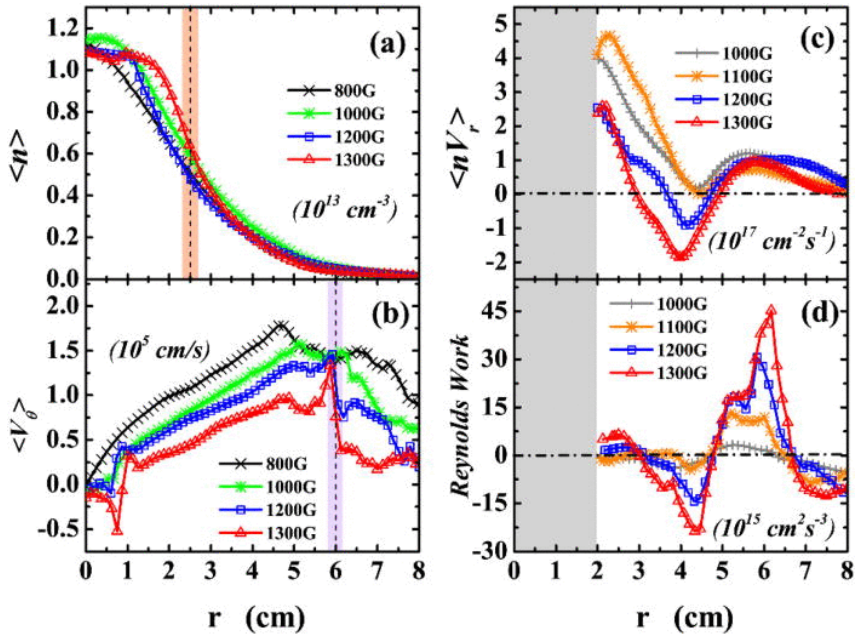

Figure 3.1: Experimental plasma profiles at different magnetic field values. Reprinted with permission from Cui *et al.*, Physics of Plasmas, **22**, 050704 (2015). Copyright 2015 AIP Publishing. [CTD$^+$15]

We present a reduced 1D transport model that describes the space-time evolution of turbulence and mean fields in the turbulent plasma conditions of CSDX. The model is formulated in terms of potential vorticity dynamics, and conserves total potential enstrophy [AD16]. All evolution is expressed in terms of the particle and vorticity fluxes. Flux nonlinearity enters via a gradient dependent mixing length, and the vorticity flux includes both a diffusive and a residual component. The model recovers profile evolution in CSDX with increasing B, without the need to include an explicit inward particle pinch in the expression for the particle flux. This evolution corresponds to: i) steepening of the mean density profile as a signature of a enhanced confinement ii) the development of a radially sheared azimuthal flow velocity that triggers the transition to an improved energy confinement state and iii) negative Reynolds work values indicating that energy is transfered to flow as the system self-organizes. We mention here that the Reynolds

work sign convention used in ref.[CTD$^+$15, CAT$^+$16] is opposite to the one adopted here; a positive Reynolds work in ref.[CTD$^+$15, CAT$^+$16] indicates a turbulence decay and a zonal flow drive. The model can also be used to study the effects of other factors on the dynamics of this global transition. These factors include: presence of a thin layer of neutrals around the plasma, variations of the plasma ion fueling intensity S and of the macroscopic turbulent mixing length l_0 to be defined in a subsequent section. The model is used to investigate the relevant case of a plasma with a high collisional Prandtl number: $Pr = \nu_c/D_c$.

The remainder of this paper is organized as follows: Section (II) presents the model, with a discussion of the corresponding physics and assumptions. This requires an explanation of the expression for the mixing length l_{mix}, and a review of the physics behind the Rhines' scale. Expressions for the density, vorticity and potential enstrophy fluxes and coefficients are also presented in this section, along with the three spatio-temporal equations of the model. Section (III) reports on the numerical results obtained when varying the magnitude of the magnetic field. A diffusive vorticity flux: $\Pi = -\chi\nabla u$, where the vorticity $u = \nabla^2\phi$, is first used in section (III). A residual stress Π_{res} is then included in the vorticity flux expression: $\Pi = \Pi_{res} - \chi\nabla u$ to assess its potential role. A set of local and global validation metrics are then presented in Section(IV) in order to verify that the model truly describes the plasma evolution as it occurs in CSDX. Section (V) explores the energy exchange between fluctuations and the mean flow and studies time variations of two parameters; R_T already introduced in a previous work [MDG$^+$12] and a new parameter R_{DT}, derived from this model. Both parameters provide quantitative and qualitative measurements of this exchange, and serve as turbulence collapse indicators. Conclusions are presented in section (VI).

3.2 Structure of the 3-Field Reduced Model.

The proposed model investigates space and time variations of the following three fields: the mean density $\langle n \rangle$, the mean vorticity $\langle u \rangle = \langle \nabla^2 \phi \rangle$ and the turbulent potential enstrophy $\varepsilon = \langle \frac{(\tilde{n}-\tilde{u})^2}{2} \rangle$. It is derived from the collisional Hasegawa-Wakatani equations [HW83, HW87]:

$$(\partial_t - \nabla\phi \times \hat{z}.\nabla)\nabla_\perp^2 \tilde{\phi} = -c_1 \nabla_\parallel^2 (\tilde{\phi} - \tilde{n}) + c_2 \nabla^2 (\nabla_\perp^2 \tilde{\phi}) \tag{3.1a}$$

$$(\partial_t - \nabla\phi \times \hat{z}.\nabla)(\tilde{n} + \ln n_0) = -c_1 \nabla_\parallel^2 (\tilde{\phi} - \tilde{n}) \tag{3.1b}$$

Here $c_1 = T_e / e^2 n_0 \eta \omega_{ci}$ and $c_2 = \mu / \rho_s^2 \omega_{ci}$. μ and η are the ion viscosity and plasma resistivity, n_0 is the average plasma density, and n and ϕ are the normalized fluctuating density and potential. CSDX plasma being collisional, a modified Hasegawa-Wakatani model can be used to describe turbulent transport in this device. In addition, LIF measurements in CSDX show that the axial flow is well within the subsonic limit [TGM$^+$16]. Thus, the radial gradient of the parallel velocity reported as contributing to an inward particle flux in ref.([IKI$^+$16]), does not contribute to such a flux here, as a parallel shear flow instability simply cannot be triggered [LD17]. This fact is taken into account while formulating the model. Our reduced model relies on two related points: conservation of the total potential enstrophy PE (mean and turbulent) up to dissipation and external forcing, and inhomogeneous potential vorticity (PV) mixing via vorticity diffusion. This mixing occurs on a scale l_{mix} that is an interpolation between an excitation scale l_0 and the Rhines' scale of turbulence l_{Rh}. Dynamic dependence of l_{mix} on l_{Rh} results from the interaction between the mean fields and the turbulence structures, and allows the model to capture the internal energy exchange during this interaction. The Rhines' scale is inversely proportional to the potential vorticity gradient $\nabla q = \nabla n - \nabla u$, hence l_{mix} has also an inverse dependence on ∇q and shrinks as ∇u and ∇n steepen. The model uses purely diffusive expressions for the turbulent field fluxes *without* an explicit pinch velocity contribution to the

particle flux. In fact, local expressions for the fluxes of n, u and ε as derived using the quasi-linear theory are [ADG16]: $\Gamma_n = -D_n \nabla n$, $\Gamma_\varepsilon = -D_\varepsilon \nabla \varepsilon$ and $\Pi = \Pi_{res} - \chi \nabla u$. A discussion of the diffusion coefficients and the residual vorticity stress is deferred to a later section.

A full derivation of the model is available in ref.[AD16]. We mention here only the relevant equations:

$$\partial_t u = -\partial_x \Pi + \mu_c \nabla^2 u \tag{3.2a}$$

$$\partial_t n = -\partial_x \Gamma_n + D_c \nabla^2 n \tag{3.2b}$$

$$\partial_t \varepsilon = -\partial_x \Gamma_\varepsilon + P - \varepsilon^{3/2} - (\Gamma_n - \Pi)(\partial_x n - \partial_x u) \tag{3.2c}$$

for mean density n and mean vorticity fields u, as well as for fluctuating potential enstrophy $\varepsilon = (\tilde{n}/n_0 - \rho_s^2 \nabla^2 e\tilde{\phi}/T_e)^2/2$. Here, the fields are expanded into a mean and a fluctuating part: $n = \langle n \rangle + \tilde{n}$, $\mathbf{v}_E = \langle v \rangle \hat{y} + \delta\mathbf{v}$, $u = \langle u \rangle + \tilde{u} = \partial_x \langle v \rangle + \tilde{u}$. Fluxes of turbulent vorticity, density and potential enstrophy fluxes are: $\Pi = \langle \tilde{v}_x \tilde{u} \rangle$, $\Gamma_n = \langle \tilde{v}_x \tilde{n} \rangle$ and $\Gamma_\varepsilon = \langle \tilde{v}_x \tilde{q}^2 \rangle$ respectively. Turbulent enstrophy is related to the fluctuating potential vorticity $\tilde{q} = \tilde{n} - \tilde{u}$ via: $\varepsilon = \langle \tilde{q}^2 \rangle/2$. μ_c and D_c are plasma collisional viscosity and diffusivity, $\tilde{n}$ and $\tilde{\phi}$ are normalized to n_0 and T_e/e, space and times scales are normalized to $\rho_s = \sqrt{m_i T_e}/eB$ and $1/\omega_{ci} = m_i c/eB$.

The first terms of the RHS of eqs.(3.2a-3.2c) represent a turbulent diffusive flux or spreading of the corresponding field. In eq.(3.2c), P represents the enstrophy production due to an external stirring, and replaces explicit linear instability which is not treated in this model. Note that in this model formulation, the forcing serves only to initialize a background turbulence level. It does not represent the turbulence drive in the steady state. Drive is due to ∇n relaxation, i.e., $\Gamma_n \nabla n$ term in eq.(3.2c). The turbulence and transport results are insensitive to the initializing forcing, and we write it as: $P = \sqrt{\varepsilon}(u_0^2 - \varepsilon)$. This form of P reflects generation of enstrophy via external stirring. Other forms of $P \propto \varepsilon$ are equally valid and generate similar results. Enstrophy dissipation, proportional to $\varepsilon^{3/2}$, is a direct outcome of the forward enstrophy cascade associated

with nonlinear dissipation of ε at smaller scales. The last term of eq.(3.2c) is a direct coupling between the vorticity and density fluctuations, and is interpreted as an internal production of potential enstrophy. As PV mixing occurs, mean PE values are converted into turbulent ones and vice versa, while total PE is conserved. Eqs.(3.2a-3.2c) constitute a closed system that can be solved numerically once expressions for the field fluxes are known. Since the model is diffusive, expressions for the diffusion coefficients and the corresponding mixing length are thus needed. Although CSDX is a cylindrical plasma, the previous equations are written in a 1D form. This results from taking the axial and azimuthal average of the density, vorticity and enstrophy fields in order to obtain the corresponding mean quantities: $\langle n(r)\rangle$, $\langle u(r)\rangle = \langle \nabla^2\phi\rangle$ and $\langle \varepsilon(r)\rangle$.

3.2.1 The Mixing Length

Central to the formulation of a Fickian flux is the use of a mixing length l_{mix}. In this model l_{mix} is an interpolation between the external excitation dimension l_0 and the Rhines' scale of turbulence l_{Rh} [Rhi75]. The dimension l_0 is known from experiment, and thus an investigation of l_{mix} requires a study of the physics behind the Rhines' scale. In 3D turbulence, vortex stretching leads to enstrophy production that drives the fluid energy to smaller scales until it is removed from the system by viscous dissipation. However, in quasi 2D turbulence, vortex stretching is by definition inhibited and other nonlinear processes, such as vortex merging, play the prominent role. In the 2D case, energy undergoes an *inverse energy cascade* towards larger scales, which explains the emergence of large scale jets from small scale turbulent structures. As eddies become bigger, their size increases and their overturning slows, which makes their dynamics much more wave-like. The Rhines' scale l_{Rh} can be interpreted as a transition length scale between a turbulence dominated regime and wave-like dynamics [Rhi75], and is obtained by balancing the turbulence characteristic rate, i.e., the eddy turnover rate, with the wave frequency. In a DW system, an estimate of the eddy turnover rate is: $1/\tau_c \approx \delta v/l_{Rh} \approx \sqrt{\varepsilon}$, while the drift wave frequency is: $\omega \approx -k_y v_{De}/(1+k_\perp^2\rho_s^2) \approx l_{Rh}\nabla q$ where v_{De} is the electron diamagnetic drift

velocity. Balancing these two scales then gives: $l_{Rh} \approx \sqrt{\varepsilon}/\nabla q = \sqrt{\varepsilon}/\nabla(n-u)$.

In our model, l_0 and l_{Rh} are the two significant length scales of the system. When $l_0 \ll l_{Rh}$, the vorticity gradient is weak, and the natural estimate of the mixing length is simply the external dimension: $l_{mix} \sim l_0$. This prescription however is not accurate in the case of a strong vorticity gradient, where ∇q can no longer be neglected. In this case, when the Rhines' scale is much smaller than the stirring dimension ($l_{Rh} \ll l_0$), coupling between different scales is stimulated. A reasonable estimate of the mixing length is then obtained by balancing the mean kinetic energy dissipation rate and the mean PV gradient frequency [SM00]. The Rhines' scale is then the governing spatial structure for turbulence mixing in these cases of steep PV gradients, generating $l_{mix} \sim l_{Rh}$. In between these two limiting cases, one should include the effect of finite drift-Rossby frequency in l_{mix}. This is achieved by writing l_{mix} as an interpolation between l_0 and l_{Rh}:

$$l_{mix}^2 = \frac{l_0^2}{1+(l_0/l_{Rh})^2} = \frac{l_0^2}{1+l_0^2(\partial_x(n-u))^2/\varepsilon} \tag{3.3}$$

3.2.2 Expressions for the Turbulent Fluxes

Expressions for the turbulent density and vorticity fluxes were previously derived using quasi-linear theory [ADG16]. In the near adiabatic regime in which parallel diffusion timescale is the smallest characteristic time scale of the system, and in the absence of any shear, the drift wave frequency is $\omega^\star = \omega^r = v_d k_m/(1+k_\perp^2)$ where $k_\perp^2 = -\nabla_\perp^2\phi/\phi$. Expressions for the fluxes

and the diffusion coefficients are:

$$\Gamma_n = -D_n \partial_x \langle n \rangle \tag{3.4a}$$

$$\Pi = (\chi - D_n)\partial_x \langle n \rangle - \chi \partial_x^2 \langle v \rangle = \Pi_{res} - \chi \partial_x \langle u \rangle \tag{3.4b}$$

$$D_n = \sum_m \frac{k_\perp^2}{1+k_\perp^2} \frac{k_m^2}{\alpha} \langle \delta\phi_m^2 \rangle \tag{3.4c}$$

$$\chi = \sum_m \frac{|\gamma_m|}{|V_0 - \omega/k_m|^2} \langle \delta\phi_m^2 \rangle \tag{3.4d}$$

Here the dimensionless electron drift velocity is $v_d(x) = -d \ln n_0(x)/dx = \chi \nabla n$ and the plasma flow velocity is $V_0 = \langle v \rangle$. The mode number is $\mathbf{m} = (m,n,l)$ with m, n and l being the azimuthal, axial and radial mode numbers respectively. $\omega = \omega^r + i|\gamma_m|$ is the mode eigenfrequency, k_m and $k_\parallel$ are the azimuthal and parallel wave numbers and $\alpha = \eta k_\parallel^2$ is the parallel diffusion rate.

The residual stress Π_{res} in eq.(4.16) originates from a decomposition of the Reynolds stress into a diffusive and non-diffusive components, and appears when the off-diagonal terms of the poloidal Reynolds stress does not vanish. This results as a consequence of a symmetry breaking mechanism in $\langle k_r k_\theta \rangle$ where $\langle \dots \rangle$ is a spectral average [DMG$^+$09, GDH08]. Physically, Π_{res} converts parts of the diving particle flux to an azimuthal flow. Π_{res} is responsible of generation of plasma flows through the density gradient, even in the absence of any magnetic shear [LDXT16]. Using quasi-linear theory, the residual stress $\Pi_{res} = \Gamma_n/n - \chi v_d$ [ADG16]. In the adiabatic regime, the first term in the expression of Π_{res} is negligible with respect to the second one, simply because it is proportional to $1/\alpha$ and $\alpha \gg 1$. One can thus label it as the non-adiabatic term. When no flow is present, or when the flow velocity V_0 is constant, the vorticity flux reduces to Π_{res}. Writing $\Gamma_\varepsilon = -D_\varepsilon \partial_x \varepsilon$ and plugging in the model equations, we

obtain the final form for the three field equations:

$$\partial_t n = \partial_x[D_n \partial_x n] + D_c \partial_x^2 n \tag{3.5a}$$

$$\partial_t u = \partial_x[\chi \partial_x u] + \mu_c \partial_x^2 u - \partial_x[\Pi_{res}] \tag{3.5b}$$

$$\partial_t \varepsilon = \partial_x[D_\varepsilon \partial_x \varepsilon] + \Pi_{res}(\partial_x n - \partial_x u) - (\chi \partial_x u - D_n \partial_x n)(\partial_x n - \partial_x u) - \varepsilon^{3/2} + \sqrt{\varepsilon}(u_0^2 - \varepsilon) \tag{3.5c}$$

Eqs.(3.5a-3.5c) are rearranged and integrated to give:

$$\begin{aligned}\int_0^L \partial_t(\varepsilon + \frac{(n-u)^2}{2})dx &= \int_0^L (P - \varepsilon^{3/2} - \partial_x \Gamma_\varepsilon - (\Gamma_n - \Pi)(\partial_x n - \partial_x u) + (n-u)(\partial_t n - \partial_t u))dx \\ &= \int_0^L (P - \varepsilon^{3/2})dx\end{aligned} \tag{3.6}$$

after neglecting the terms proportional to D_c and μ_c. This shows that the system conserves total PE up to forcing and dissipation, as a result of enstrophy exchange between mean fields and fluctuations. The internal turbulent PE production term is canceled by the corresponding loss term in the evolution equation for the mean PE as a part of this enstrophy exchange. In view of the total PE conservation elucidated above, we go back to eq.(3.3) to emphasize how crucial the expression for l_{mix} is in closing the feedback loop between the PV gradient and the corresponding diffusion coefficient: as $\nabla q = \nabla n - \nabla u$ steepens, the mean potential enstrophy $\frac{(n-u)^2}{2}$ increases, causing a drop in turbulent potential enstrophy ε as a result of total PE conservation. When ε decreases, the mixing length and thus the corresponding PV diffusion coefficient shrink, leading to a further increase in the PV gradient. Hence a closed feedback loop is generated.

3.2.3 Viscosity and Diffusion Coefficients

In the near adiabatic regime, the timescale ordering is: $\eta k_{\parallel}^2 \gg \omega \gg V_0'$. Using $|k_m^2\langle\delta\phi_m^2\rangle| = |\langle\delta v_m^2\rangle| \approx l_{mix}^2\varepsilon$, the particle diffusion coefficient D_n is:

$$D_n = \varepsilon l_{mix}^2/\alpha \tag{3.7}$$

where the resistive parallel diffusion rate has been rescaled as: $\alpha = (1+k_\perp^2)\alpha/k_\perp^2$. From dimensional analysis, α is proportional to $\sqrt{\varepsilon}$ and the particle diffusion coefficient is: $D_n = l_{mix}^2\sqrt{\varepsilon}$. As for the vorticity diffusion coefficient, χ is not dominated by a large resistive parallel diffusion rate. Unlike the expression for D_n, the denominator of eq.(3.4d) represents the competition between the flow shear V_0' and the wave frequency ω. In the absence of shear, instabilities are density gradient driven collisional DWs, that are damped by viscous dissipation. Their growth rate is then that of a drift wave: $|\gamma_{DW}| = \omega^2/\alpha$, reduced by the dissipation rate $|\gamma_\mu|$. The vorticity diffusion coefficient is then:

$$\chi = \sum_{\mathbf{m}} \frac{(|\gamma_{DW}| - |\gamma_\mu|)|k_m^2\langle\delta\phi_m^2\rangle|}{\omega^2} = \sum_m \frac{\frac{\omega^2}{\alpha}|k_m^2\langle\delta\phi_m^2\rangle|}{\omega^2} \sim \frac{\varepsilon l_{mix}^2}{\alpha}$$

When a flow shear V_0' is present, the vorticity diffusion coefficient χ is reduced, as the net turbulence correlation time decreases. When incorporating the shear effect into the turbulence correlation time, $1/\alpha$ becomes: $1/\alpha \simeq 1/\sqrt{(k_\perp\delta v)^2 + (V_0')^2} \simeq 1/\sqrt{\varepsilon + q^2}$, reflecting enstrophy generation and presence of flow shear respectively. The vorticity diffusion coefficient χ then becomes:

$$\chi = \varepsilon l_{mix}^2/\sqrt{\varepsilon + q^2} = l_{mix}^2\varepsilon/\sqrt{\alpha^2 + c_u u^2} \tag{3.8}$$

Here a coefficient c_u reflecting the strength of the shear flow has been added to the expression of χ. We will show later on that the numerical solutions for this model are insensitive to the parameter c_u. In a stationary regime, $\sqrt{\varepsilon} > q$ and the vorticity coefficient $\chi = \sqrt{\varepsilon} l_{mix}^2$

found previously [BLSY98] is recovered. In a strong shear regime where $q > \sqrt{\varepsilon}$, the vorticity coefficient is $\chi = \varepsilon l_{mix}^2/|q|$. Finally, we use the following expression for D_ε: $D_\varepsilon = l_{mix}^2 \varepsilon/\alpha$. We mention here that the model includes three different time scales: the wave frequency and growth rate inverse time scales ω_m^{-1} and $|\gamma|^{-1}$ appearing in the spectral sums of the diffusion coefficients expressions, the correlation or eddy turnover time $\varepsilon^{-1/2}$ appearing in the enstrophy equation, and a diffusive time scale which characterizes the evolution of the mean field quantities as a result of turbulent fluxes evolution. While the first two are fast time scales, the last one is a slow (diffusive) one.

3.3 Model Predictions of Plasma Profiles.

In order to compare the model predictions to the experimental results obtained from CSDX, we present in this section the density and vorticity profiles numerically predicted by the model for different B values. Two forms of vorticity fluxes are considered. First, a diffusive vorticity form: $\Pi = -\partial_x u$. Then, a residual stress Π_{res} is added to the vorticity flux. The two cases are then compared to evaluate any potential role of Π_{res}. Before proceeding, we lay out the experimental parameters of CSDX cylindrical magnetized helicon plasma: the plasma column has a total length $L = 2.8m$ and a radius $a = 10cm$. Argon plasma with the following characteristics is produced: $n_e = 10^{13} cm^{-3}$, $T_e = 4eV$ and $T_i = 0.3 - 0.7eV$. The magnitude of the magnetic field B ranges between $800G$ and $1300G$, giving $\omega_{ci}^{-1} \approx 30\mu s$ and $\rho_s = C_s/\omega_{ci} \approx 1cm$ where $C_s = \sqrt{T_e/m_i}$ is the plasma sound speed. Argon neutrals are radially injected at a constant flow rate of 25 sccm, and the corresponding neutral gas pressure $P_{gas} = 3.2mTorr$ is equivalent to a neutral density $n_n = 10^{14} cm^{-3}$ [CTD$^+$15, CAT$^+$16]. Plasma neutral ionization rate at $T_e = 5eV$ is $S = n_e n_n \langle \sigma_{ion} v_e \rangle = 10^{17} cm^{-3} s^{-1}$, where $\langle \sigma_{ion} v_e \rangle = 10^{-10} cm^3/s$ is the ionization rate coefficient at 5eV. These values will be used in our calculations, in order to benchmark our model predictions to the experimental results.

3.3.1 Diffusive Vorticity Flux: $\Pi = -\chi\partial_x u$

Model Equations

For a shear strength parameter $c_u = 0$ and $\alpha = \sqrt{\varepsilon}$, the diffusion coefficients are equal: $D_n = \chi = D_\varepsilon = l_{mix}^2 \varepsilon^{1/2}$ and $\Pi_{res} = 0$. The vorticity flux is then: $\Pi = -\chi\partial_x u$. Eqs.(3.5a-3.5c) are rescaled using: $x \equiv Lx$, $\varepsilon \equiv u_0^2\varepsilon$, $n \equiv Lu_0 n$, $u \equiv Lu_0 u$, $t \equiv L^2 t/u_0$, $\mu_c \equiv u_0\mu_c$ and $D_c \equiv u_0 D_c$:

$$\partial_t n = \partial_x[\frac{l_0^2\varepsilon^{3/2}\partial_x n}{\varepsilon + l_0^2(\partial_x(n-u))^2} + D_c\partial_x n] + S \tag{3.9a}$$

$$\partial_t u = \partial_x[\frac{l_0^2\varepsilon^{3/2}\partial_x u}{\varepsilon + l_0^2(\partial_x(n-u))^2} + \mu_c\partial_x u] \tag{3.9b}$$

$$\partial_t \varepsilon = \partial_x[\frac{l_0^2\varepsilon^{3/2}\partial_x \varepsilon}{\varepsilon + l_0^2(\partial_x(n-u))^2}\frac{\partial\varepsilon}{\partial x}] + L^2[\frac{l_0^2\varepsilon^{3/2}(\partial_x(n-u))^2}{\varepsilon + l_0^2(\partial_x(n-u))^2} - 2\varepsilon^{3/2} + \sqrt{\varepsilon}] \tag{3.9c}$$

Here L is the total plasma column length and S (normalized to $n_0 = 10^{13}cm^{-3}$) is the external fueling source for ion density. The latter represents the combination of continuous neutral injection and the ionization energy provided by the external source of heat, i.e. CSDX external antenna. Parameters of eqs.(3.9a-3.9c) are rescaled to their dimensional form to express the B dependence: $t \equiv t/\omega_{ci}$ and $u \equiv \nabla_\perp^2(T_e\phi/e)/\rho_s^2$. In addition, $length \equiv length \times \rho_s$. As a matter of fact, we report the following scale for turbulence in CSDX. Here we use normalized density fluctuations $\tilde{n}/n_0$ to calculate $\bar{k}_r$:

Table 3.1: Scaling of $\bar{k}_r$ with B

$B(G)$	800	900	1000	1200	1300
$\rho_s(cm)$	1.40	1.24	1.12	0.93	0.86
$L_n^{-1}(cm^{-1})$	0.53	0.55	0.6	0.62	0.5
$\bar{k}_r(cm^{-1})$	0.33	0.33	0.37	0.32	0.34
$1/[2.3\rho_s^{0.6}L_n^{0.3}]$	0.29	0.32	0.34	0.39	0.37

Thus:

$$l_0 = \bar{k}_r^{-1} = 2.3\rho_s^{0.6} L_n^{0.3} \sim \rho_s$$

as L_n and ρ_s are of the same order before the transition occurs. Similarly, the Rhines' scale $l_{Rh} \sim \rho_s$, as it involves a radial derivative proportional in turn to ρ_s. We mention here that these results are clearly affected by the low values of $\rho^* = \rho_s/a$ in CSDX. Further studies at lower ρ^* are clearly needed. The potential enstrophy $\varepsilon = (n - \rho_s^2 \nabla_\perp^2 \phi)^2/2 = (n - \rho_s^2 k_\perp^2 \phi)^2/2 = (n - (\rho_s/l_{mix})^2 \phi)^2/2$ does not depend explicitly on B, as both n and $\rho_s k_\perp = \rho_s/l_{mix}$ are explicitly B-independent. With both the perpendicular ion diffusivity D_c and viscosity μ_c proportional to $1/B^2$, we obtain the following B-dependent equations:

$$\omega_{ci}\partial_t n = \partial_x[\frac{\varepsilon^{3/2} l_0^2 \partial_x n}{\varepsilon + l_0^2(\partial_x(n - u/\rho_s^2))^2} + D_c \partial_x n] + S \tag{3.10a}$$

$$\omega_{ci}\partial_t u = \partial_x[\frac{\varepsilon^{3/2} l_0^2 \partial_x u}{\varepsilon + l_0^2(\partial_x(n - u/\rho_s^2))^2} + \mu_c \partial_x u] \tag{3.10b}$$

$$\omega_{ci}\partial_t \varepsilon = \partial_x[\frac{\varepsilon^{3/2} l_0^2 \partial_x \varepsilon}{\varepsilon + l_0^2(\partial_x(n - u/\rho_s^2))^2}] + L^2[\frac{l_0^2 \varepsilon^{3/2}(\partial_x(n - u/\rho_s^2))^2}{\varepsilon + l_0^2(\partial_x(n - u/\rho_s^2))^2} - 2\varepsilon^{3/2} + \sqrt{\varepsilon}] \tag{3.10c}$$

Numerical Techniques and Model Calculation.

A finite difference method with a fixed space step size and adaptive time step sizes is used. The boundary conditions used here are: $n|_{x=1} = u|_{x=1} = \partial_x n|_{x=0} = \partial_x \varepsilon|_{x=0} = \partial_x \varepsilon|_{x=1} = \partial_x u|_{x=0} = 0$. Note that Neumann boundary conditions are imposed on ε at both ends of the domain to prevent energy inflow/outflow from or to the system. As a trial case, we use the following initial profiles: $n(x,0) = (1-x)\exp[-ax^2 + b]$, $u(x,0) = cx^2 + dx^3$ and $\varepsilon(x,0) = (n(x,0) - u(x,0))^2/2$ with $a = -5$, $b = 0.125$, $c = 1$ and $d = -1$. The initial density profile corresponds to a fitting of CSDX experimental data at $B = 800G$. Initial vorticity and enstrophy profiles are arbitrary. Collisional Prandtl number $Pr = \mu_c/D_c = 650 \gg 1$ and a normalized mode scale length $l_0 = 1/5$ are used. We write the ion density source $S(x)$ as a shifted Gaussian:

$S(x) = S(1-x)\exp[-(x-x_0)^2/e]$, where $x_0 = 0.7$, $e = 0.05$ and S is the source amplitude. This form of density source is justified by the fact that radially injected neutrals become ionized at a normalized radial position $x_0 = 0.7$, as revealed by the decreasing (increasing) radial profile measurements of neutrals (ions). These radial variations are insensitive to any change in the axial location of the probe along the magnetic field axis. As for the amplitude S, the ionization rate corresponding to the conditions of CSDX experiments implies a normalized value of $S = 10^4$.

In addition to calculating the plasma profiles at different B values to relate to CSDX experiments, we perform a scan of the external ion density fueling source and calculate the profiles at different S values. The latter corresponds to a change in the heating power of CSDX. Unless stated otherwise, we will use the following code colors throughout the paper: $B_{blue} < B_{red} < B_{green} < B_{black}$. Fig.3.2 shows radial variations of the density profiles for an increasing magnetic field B and two ion source amplitudes $S = 10$ and $S = 10^4$. The latter corresponds to a CSDX experiment. Similar to experimental results, a steepening trend in the mean density profiles is observed in both cases, as B increases. This steepening is clearly noticeable in the range $0.2 < x < 0.5$ for the $S = 10^4$ case.

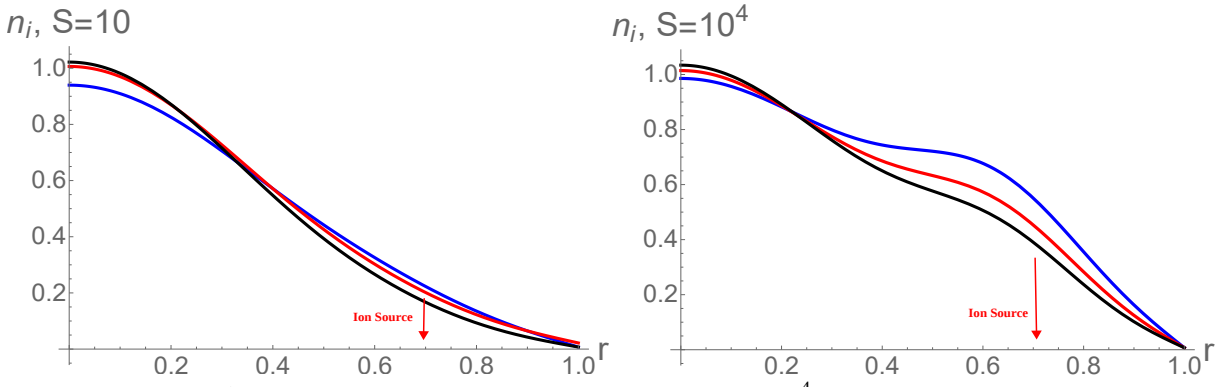

Figure 3.2: Density profiles for $S = 10$ and $S = 10^4$ for increasing B.

A closer look at the $S = 10^4$ density profiles shows that a density peak initially observed at the injection location $x_0 = 0.7$, appears to shift inward as B increases. Moreover, the peaking of density profiles close to the center as B increases suggests the existence of an inward flux. This begs then the following questions: what is this apparent inward particle flux due to? Does

it develop as a response to an increasing B? Is it inherent to the dynamics? To answer these questions, we investigate variations of the radial particle flux as a function of an increasing B. Fig.3.3 shows reduction in the particle transport, i.e., a reduction in Γ_n, as B is increased, for an

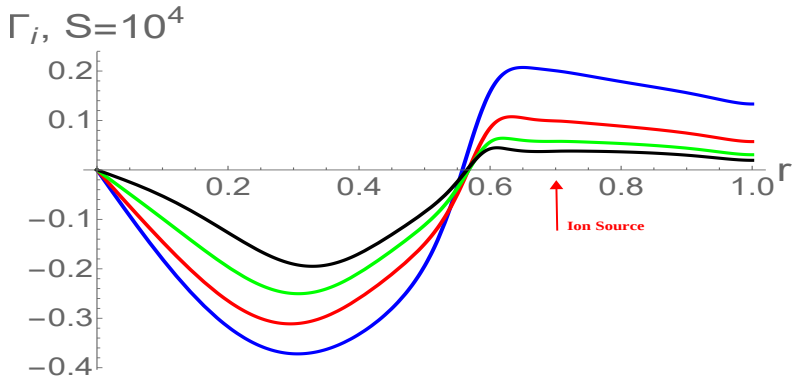

Figure 3.3: Fluxes for $S = 10^4$ for increasing B.

ion density source $S = 10^4$. This occurs as a result of the decrease of the diffusion coefficient $D_n = l_{mix}^2 \varepsilon^{1/2}$ with B (see fig.3.4). The calculated profiles in fig.3.3 also imply an inward Γ_n for $0 < x < 0.5$. Experimentally, the apparent inward particle flux was reported to increase in response to an increasing B. This feature however, does not appear in the model. We emphasize here though that for a helicon plasma source, the RF input power into the source varies with B. This leads to a variation in the amplitude of the ion density source S. Typically, one would manually adjust this power in order to keep the ion density source constant. However, this step was not implemented in CSDX experiments. One might therefore indirectly relate a change in B to a corresponding change in the particle flux profiles via variations of the density source S. This option is not considered here, as S magnitude is kept constant throughout the simulations.

Examining fig.3.5a, the particle flux corresponding to $S = 10$ is always outward (positive). This suggests that the experimental apparent inward flux is rather the result of the increasing amplitude of the off-axis density source S, and not a direct consequence of an increasing magnetic field B. We test this conjecture by holding B constant and increasing S. We find that Γ_n starts to go negative in the device core for increasing S values, at constant B, as shown in fig.3.5b. Here $S_{blue} = 10$, $S_{red} = 30$, $S_{green} = 50$ and $S_{black} = 10^4$. Moreover, at sufficiently long times,

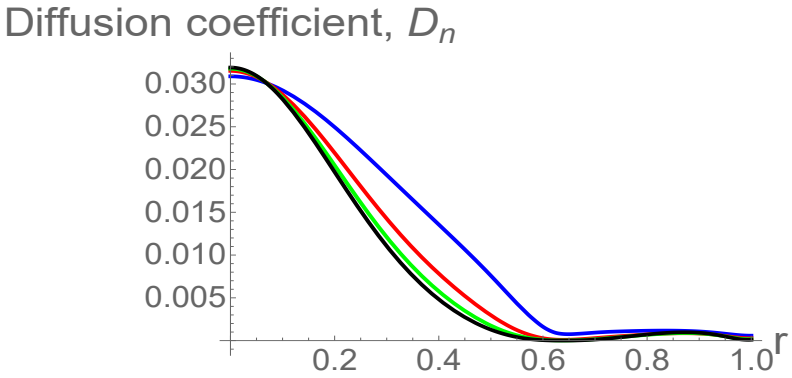

Figure 3.4: Diffusion coefficient for increasing B.

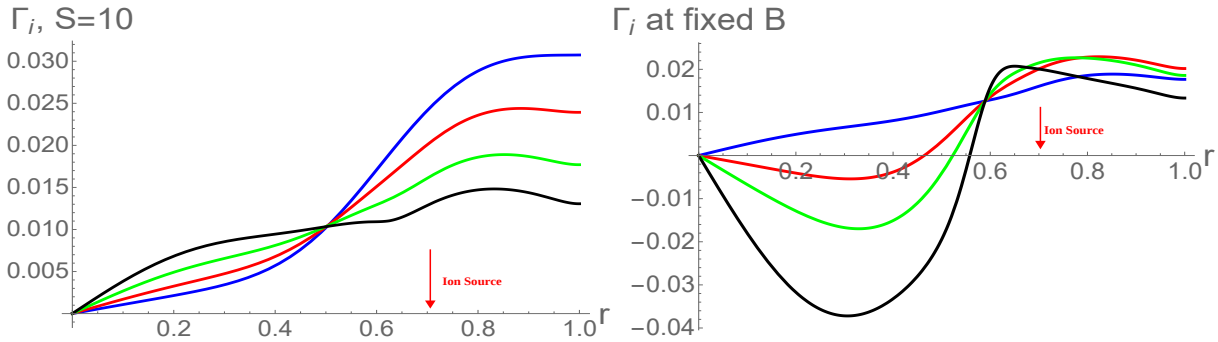

Figure 3.5: Particle flux at $S = 10$ for increasing B and particle flux at constant B and increasing $S : S_{blue} < S_{red} < S_{green} < S_{black}$.

the calculated particle flux saturates, and Γ_n profiles are positive and show no indication of inward flux (fig.3.6). We conclude then that the experimentally reported apparent inward flux appears to be a consequence of a change in the source amplitude and its position. Thus, we recover the apparent inward flux *semi-qualitatively*, using a diffusive model for $\Gamma_n = -\partial_x n$ (no particle pinch V_{pinch}, i.e., no off-diagonal term in Γ_n). It is essential to note here that experiments corresponding to different heating powers have been performed in CSDX. Data collected from these experiments show a dependence of both the direction and the amplitude of the particle flux Γ_n on the input heating power. Further investigation of this data is of crucial importance to fully understand the nature of this apparent inward flux.

In order to determine if the model captures the DW-ZF interactions in CSDX, we examine variations of the shear flow and of the Reynolds work with B. Fig.3.7a shows the existence of an azimuthal velocity shear layer in the radial direction, that gradually becomes stronger

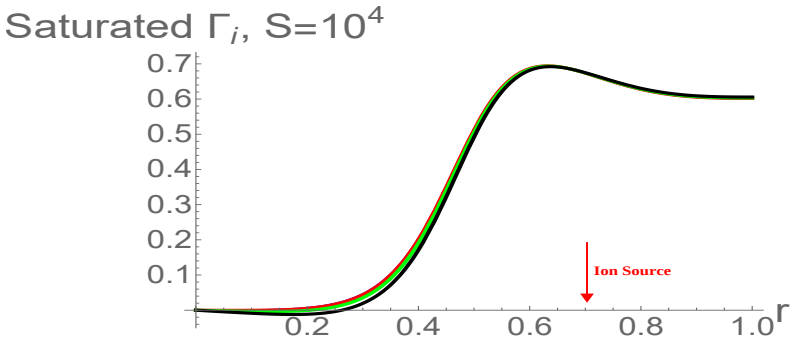

Figure 3.6: Purely outward particle flux at sufficiently long time

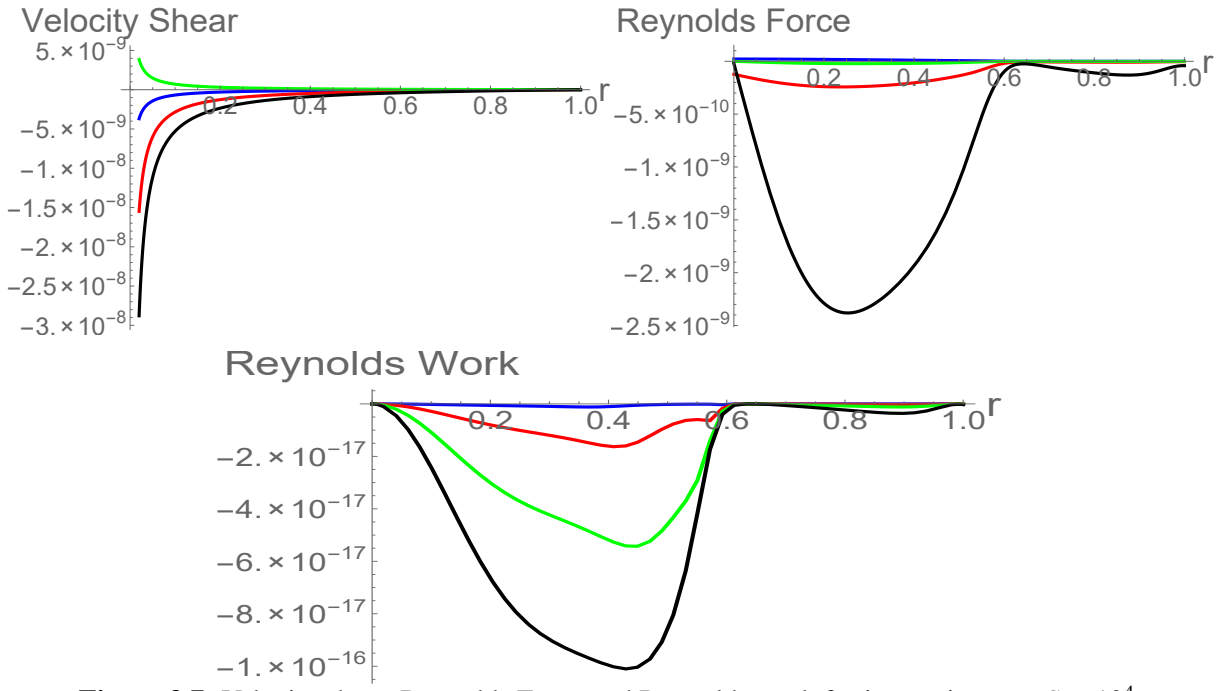

Figure 3.7: Velocity shear, Reynolds Force and Reynolds work for increasing B at $S = 10^4$.

as B increases. This shear does not depend on the ion source intensity S. The Reynolds force $-\partial_x\langle\tilde{V}_x\tilde{V}_y\rangle$ applied by turbulence on the flow increases in absolute value with B (fig.3.7b). Variation rates of the Reynolds work P_{Re} done by the turbulence on the flow, i.e., the net shear flow production rates, also increase in absolute value (fig.3.7c). This indicates an enhanced turbulence suppression as B increases. We note that the same values are obtained either by direct numerical computations or by multiplication of the Reynolds force by the absolute values of the azimuthal velocity. In summary, steepening of the density profiles, amplification of the

azimuthal velocity shear and negative Reynolds work values are all indications of turbulence reduction that intensifies, as B increases. As B rises, Reynolds force increases and reinforces the plasma flow. At the same time, the corresponding cross-field ion turbulence scale length ρ_s decreases, allowing for more energy transfer from the microscopic scales to the mesoscopic ones. These observations were reported experimentally in ref.[MXTT11, XTH$^+$09, YTH$^+$10], when applying cross-bispectral analysis to density and potential fluctuations data retrieved from CSDX.

3.3.2 Vorticity Flux with Residual Stress: $\Pi = \Pi_{res} - \chi\partial_x u$

Next we study the system dynamics when a residual $\Pi_{res} = (\chi - D_n)\partial_x n$ is included in the vorticity flux expression. The 3-fields equations become:

$$\partial_t n = \partial_x[D_n\partial_x n] + D_c\partial_x^2 n + S(x) \tag{3.11a}$$

$$\partial_t u = \partial_x[(D_n - \chi)\partial_x n] + \partial_x[\chi\partial_x u] + \mu_c\partial_x^2 u \tag{3.11b}$$

$$\partial_t \varepsilon = \partial_x[D_\varepsilon\partial_x\varepsilon] + \Pi_{res}(\partial_x n - \partial_x u) - (\chi\partial_x u - D_n\partial_x n)(\partial_x n - \partial_x u) - \varepsilon^{3/2} + \sqrt{\varepsilon}(u_0^2 - \varepsilon) \tag{3.11c}$$

Here we use the following diffusion coefficients: $D_n = l_{mix}^2\varepsilon/\alpha$, $D_\varepsilon = l_{mix}^2\varepsilon^{1/2}$ and $\chi = l_{mix}^2\varepsilon/\sqrt{\alpha^2 + c_u u^2}$. Using the same scaling factors of the last section in addition to: $\alpha \equiv u_0\alpha$ and

$c_u \equiv c_u/L^2$, we obtain the following B-dependent equations:

$$\omega_{ci}\partial_t n = \partial_x\Big[\frac{l_0^2\varepsilon^2\partial_x n}{\varepsilon + l_0^2(\partial_x(n-u/\rho_s^2))^2}\frac{1}{\alpha} + D_c\partial_x n\Big] + S \tag{3.12a}$$

$$\omega_{ci}\partial_t u = \rho_s^2\partial_x\Big[\frac{l_0^2\varepsilon^2}{\varepsilon + l_0^2(\partial_x(n-u/\rho_s^2))^2}\Big[(\frac{1}{\alpha} - \frac{1}{\sqrt{\alpha^2 + c_u(u/\rho_s^2)^2}})\partial_x n + (\frac{1}{\sqrt{\alpha^2 + c_u(u/\rho_s^2)^2}} + \mu_c)\partial_x u\Big]\Big] \tag{3.12b}$$

$$\omega_{ci}\partial_t \varepsilon = \partial_x\Big[\frac{l_0^2\varepsilon^{3/2}\partial_x\varepsilon}{\varepsilon + l_0^2(\partial_x(n-u/\rho_s^2))^2}\Big] + L^2\Big[\frac{l_0^2\varepsilon^2\rho_s(\partial_x n - \partial_x u/\rho_s^2)}{\varepsilon + l_0^2(\partial_x(n-u/\rho_s^2))^2)}(-\frac{1}{\alpha} + \frac{1}{\sqrt{\alpha^2 + c_u(u/\rho_s^2)^2}}) - \frac{l_0^2\varepsilon^2}{\varepsilon + l_0^2(\partial_x(n-u/\rho_s^2))^2}(-\frac{\partial_x}{\alpha} + \frac{1}{\sqrt{\alpha^2 + c_u(u/\rho_s^2)^2}}\frac{\partial_x u}{\rho_s^2})(\partial_x n - \frac{\partial_x u}{\rho_s^2}) - 2\varepsilon^{3/2} + \sqrt{\varepsilon}\Big] \tag{3.12c}$$

We show here numerical results that correspond to both Dirichlet and Neumann vorticity boundary condition at $x = 1$. Starting with a Dirichlet condition $u|_{x=1} = 0$, for an arbitrary case $\alpha = 3$ and $c_u = 6$ trial case, numerical results are similar to those obtained when no residual stress is included in the expression of Π. The steepening of the density profiles, the sheared azimuthal velocity layer and the negative Reynolds work values in the three left figures of fig.3.8 are all consistent with a global transition that occurs in the plasma as B increases. Variation of the shearing coefficient c_u, which reflects a change in the strength of the flow shear, does not seem to affect qualitatively the numerical results (right three figures of fig.3.8); the results are simply insensitive to a change in c_u. Therefore we conclude that, while Π^{res} is needed to account for intrinsic rotation in tokamaks and axial flow generation in linear devices [LDXT16], a state of enhanced confinement can be recovered using a simple diffusive form of the vorticity flux, without the need to include a residual stress in the expression for Π.

The scenario of a plasma column surrounded by a layer of fixed neutrals next to the walls corresponds to a Neumann vorticity boundary condition: $\frac{\partial u}{\partial x}|_{x=1} = 0$. Viscous effects are

negligible in this case. We mention here though that the usual experimental case corresponds to a Dirichlet boundary condition. Steepening of the density profiles, as well as negative Reynolds work values are recovered as a sign of turbulence suppression, as B increases. The velocity shear, although present and prominent at the density steepening location, is B independent (top three figures of fig.3.9). Higher magnetic field values are required for this B-dependence to appear. The Reynolds work becomes then positive (bottom three figures of fig.3.9). The latter suggests turbulence production by the flow at high B values, i.e., an instability that might be triggered by the vorticity gradient at high B instead of being suppressed by the velocity shear.

A change in the mode scale length from $l_0 = \rho_s/5$ to $l_0 = 10^{-3}\rho_s$ leads to the same previously mentioned trends of turbulence suppression as indicated by density profile steepening, negative Reynolds work values and a B dependent sheared azimuthal velocity (see fig.3.10).

More interesting is the relevant case of a higher Prandtl number $Pr = \mu_c/D_c = 65000$. In this case, momentum diffusivity dominates the behavior of the plasma characterized by a low diffusion coefficient D_c. Fig.3.11 shows time evolution of the plasma profiles at consecutive times t_1 and t_2. The plasma density builds up at the injection location and the inward flux develops as a result of density localized concentration, regardless of the magnitude of B. Evidence of a turbulence suppression such as negative Reynolds work rates and sheared azimuthal velocity are also recovered.

3.4 Validation Metrics for Model Comparison with Experiment.

Going beyond the simple qualitative comparisons between numerical and experimental profiles, we propose here a set of quantitative metrics which aim to test whether the adopted model equations are indeed capable of explaining the experimental observations. Quoting Oberkampf and Trucano (2002), "an important issue concerns how comparisons of computational results

and experimental data could be quantified" (p.216) [OT]. A set of validation metrics is therefore needed to check the consistency of the model with the experimental data [Hol16]. We start first by checking the relative variation of the inverse density gradient scale length $1/L_n = |\nabla \ln n|$ and recover a value close the experimental one obtained from profiles of fig.(2) in ref.[CAT$^+$16]:

$$\frac{\Delta(1/L_n)}{L_{n_i}} = \frac{1/L_{n_f} - 1/L_{n_i}}{1/L_{n_i}} = \begin{cases} 0.70 & \text{numerically} \\ 0.55 & \text{experimemtally} \end{cases}$$

Here $1/L_{n_i}$ ($1/L_{n_f}$) is the inverse gradient scale length of the initial (final) density profile, i.e., before (after) the plasma transition occurs. Similarly, we calculate the corresponding relative variation of the inverse gradient scale length of the velocity profiles and find:

$$\frac{\Delta(1/L_v)}{L_{v_i}} = \frac{1/L_{v_f} - 1/L_{v_i}}{1/L_{v_i}} = \begin{cases} 0.73 & \text{numerically} \\ 0.57 & \text{experimentally} \end{cases}$$

While the previous validation metrics constitute *local* assessment quantities, we also propose two *global* validation metric. Fig.3.12 is a plot of the radially integrated Reynolds work, $P_{Re-tot} = \int_0^1 P_{Re} dr$ which denotes the total work done by turbulence on the flow over the plasma cross section as a function of the density gradient. $1/L_n$ and P_{Re-tot} are proportional to each other; as B increases, density profiles steepen, the ion gradient scale length L_n shrinks and the total Reynolds work rate increases, indicating a transfer of energy from fluctuations to flow.

Further validation of turbulence suppression is obtained by examining the particle loss rate $1/\tau_{turb-loss}$, due to turbulent radial transport. This rate is expected to drop as B increases. Integration of the particle flux along r gives values of the loss rates: $1/\tau_{turb-loss} \propto \int_0^r r\Gamma_n dr$. Data reported in table (3.2) show a declining trend as B increases. This suggests a change in the global particle balance, i.e., a change in the nature of the turbulence in the system.

Table 3.2: Particle loss rate $1/\tau$ for increasing B.

$1/\tau_{loss}(\times 10^{-2})$	$S=10$	$S=50$	$S=10^4$
B_{blue}	1.4	3	1.1
B_{red}	1.2	2.6	0.5
B_{black}	0.9	1.8	0.2

3.5 What is the Criterion for Turbulence Suppression?

A conceptual question in modeling drift wave-zonal flow turbulence is the prediction of when transport barriers are triggered. A variety of proposals are on record. Most are equivalent to a comparison of linear growth rate to $E\times B$ shearing rate (i.e., $|\gamma_L|$ vs. $|\gamma_{E\times B}|$). The relevance of this type of criterion to fully developed turbulence is, at best, unclear. A somewhat non-trivial criterion [MDG$^+$12], is $R_T > 1$ where:

$$R_T = \frac{\langle \tilde{v}_x \tilde{v}_y \rangle' v_{E\times B}}{|\gamma_{eff}| \langle \tilde{v}_\perp^2 \rangle} \tag{3.13}$$

is the local ratio of the Reynolds power density, to the effective increase in turbulent kinetic energy. Here $|\gamma_{eff}|(\nabla n, \nabla T, V_{ZF})$ is the turbulence effective growth rate. The idea here is that when $R_T > R_{T_{crit}}$ (usually $R_{T_{crit}} \sim 1$), the energy transfer to the shear flow exceeds the effective increase in turbulent kinetic energy, suggesting a collapse of the $k_\theta \neq 0$ portion of the turbulence spectrum, i.e., the part which causes transport. For the model under study here, the instantaneous potential enstrophy growth rate is $|\gamma_{eff}| = (1/\varepsilon).(\partial\varepsilon/\partial t)$ and $\langle \tilde{v}_\perp^2 \rangle = \varepsilon l_{mix}^2 = l_0^2\varepsilon^2/(\varepsilon + (l_0\nabla(n-u))^2)$. Fig.3.13 shows variations of R_T with B for this system. Here, R_T values are calculated at the density steepening location and at the turbulent energy saturation time. The proportionality between B and R_T is recovered as anticipated, since an increase in B triggers the formation of transport barriers.

While the $R_T > R_{T_{crit}}$ criterion is attractive for its extreme simplicity, it suffers from the facts that: i) $|\gamma_{eff}|$ is ill-defined, and difficult to calculate, ii) contributions from energy other than

the kinetic are ignored. Thus we propose here an alternate criterion, $R_{DT} \geq R_{DT_{crit}}$, where the global parameter $R_{DT} = \tau_{relax}/\tau_{transfer}$. Here $1/\tau_{relax} = -\int dx \Gamma_n \nabla n/n_0$, where $\Gamma_n = \langle \tilde{v}_x \tilde{n}/n_0 \rangle$ is the normalized particle flux, $1/\tau_{relax}$ is the rate of relaxation of the free energy source, which is ∇n in this model. Of course, ∇n relaxes by exciting drift wave turbulence, so $1/\tau_{relax}$ is effectively the turbulent enstrophy production rate and would have a connection to the energy input rate, $|\gamma_{eff}|$, used in the R_T criterion. Logically then, that should be compared to the rate of transfer of enstrophy to the mean flow vorticity profile. This may be thought of a turbulent enstrophy destruction rate, and is closely related to the Reynolds work which appears in R_T. We have then: $1/\tau_{transfer} = -\int dx \langle \tilde{v}_x \tilde{u} \rangle \nabla u$ where $u = \rho_s^2 \nabla_\perp^2 (e\phi/T_e)$. Integrating by parts gives: $1/\tau_{transfer} = \int dx \partial_x \langle \tilde{v}_x \tilde{u} \rangle u$ so:

$$R_{DT} = \frac{\int \partial_x \langle \tilde{v}_x \tilde{u} \rangle u dx}{-\int \Gamma_n \nabla n/n_0 dx} \tag{3.14}$$

R_{DT} is manifestly dimensionless and the integrals are calculated along the radius. Noting the Taylor identity and the fact that $u \sim \nabla_\perp (\nabla_\perp \phi) \sim \nabla_\perp V_y$, the correspondence of the numerator of R_{DT} to that of R_T is evident. Finally, given that the potential vorticity is conserved on fluid particle trajectories, it is not difficult to see the correspondence between fluctuating entropy ($\sim -\int dv (\delta f)^2/\langle f \rangle$) and fluctuating enstrophy. Thus, R_{DT} may be thought of as the ratio of fluctuation entropy destruction via coupling to the mean flow, to fluctuating entropy production via relaxation of ∇n. Both numerator and denominator reflect flux-gradient interaction and both emerge naturally from the formulation of the model, i.e. from expanding the production term $P_{prod} = (\Gamma_n - \Pi).(\nabla n - \nabla u) = \underline{\Gamma_n \nabla n} + \underline{\Pi \nabla u} - \Pi \nabla n - \Gamma_n \nabla u$ in eq.3.2c. Neglecting the last two cross terms in P_{prod}, the numerator and denominator of R_{DT} simply represent the product of Π and ∇u, and Γ_n and ∇n respectively. Thus R_{DT} exceeding unity may be thought of as the simplification of the more general criterion that $\int P_{prod}$ passes through zero, i.e., $\int P_{prod} > 0 \rightarrow \int P_{prod} < 0$, as the indicator of turbulence collapses. Fig.3.14 shows variations of R_{DT} with B at the same time and location as for R_T. The close relation between R_{DT} and B can also be interpreted in terms of enstrophy exchange of fluctuations to flow, as B increases. However,

the $R_{DT} > R_{DT_{crit}}$ criterion has a broader and more solid theoretical foundation then $R_T > R_{T_{crit}}$, and easily may be generalized (to more complex models) by expanding the consideration of potential enstrophy balance. When either R_{DT} or R_T exceeds unity, the turbulence levels will drop and a barrier is likely to be formed. We do not have a proof of either though - particularly given the ambiguity in just exactly what a barrier is.

3.6 Discussion ans Conclusions.

Features of a CSDX improved confinement are reproduced here using a 1D time-dependent reduced model. The model recovers the profile evolution in CSDX with an increasing B, and includes both a slow and a fast time scale: the former corresponding to the time evolution of the mean fields, and the later corresponding to turbulence production and fast dissipation. Potential enstrophy is conserved up to dissipation and initial forcing. Inhomogeneous PV mixing is a central feature here, and occurs on a mixing length that is inversely proportional to the PV gradient. The use of a mixing length that shrinks as ∇n and ∇u steepen, closes the positive feedback loop on PV. The model novelty relies in the fact that it reduces the profiles evolution to only two fluxes: a vorticity and a density flux.

Numerical solutions agree with the experimental findings, and show: a steepening of the density profile, a reinforced $E \times B$ sheared layer, an increased Reynolds work and a reduction in the turbulence and particle transport, as B increases. Numerical solutions also show that the steepening of ∇n is recovered without the use of an off-diagonal term nV_{pinch} in the expression of the particle flux Γ_n. The experimentally apparent inward flux is simply of diffusive nature at high B. Moreover, the model predicts qualitatively similar results, with or without the inclusion a residual stress Π_{res} in the vorticity flux expression Π. We conclude then the following: both density and vorticity fluxes have purely diffusive forms: $\Gamma_n = -\partial_x n$ and $\Pi = -\partial_x u$, where u is the vorticity. The inward pinch V_{pinch} and residual stress Π_{res} necessary to drive axial flows

in linear devices are not required to recover the experimental results. As a matter of fact, the validation metrics presented above show a consistent level of agreement between computation and experiment, using purely diffusive expressions for Γ_n and Π.

The only experimental feature not recovered is the apparent inward particle flux. The apparent inward flux, experimentally believed to be related to increasing B, is a direct consequence of the amplitude and location of the ion source. Additional investigation of the influence the fueling intensity might have on the particle flux, is crucial to determine the nature of this inward flux.

The energy parameter R_{DT}, defined in eq.(4.33), emerges as a better global turbulence collapse indicator to be used in the future. It rests on a broader and more solid theoretical foundation than R_T, and can be obtained both in computations and experiments. In addition, R_{DT} includes the basic physics behind R_T, but transcends it. Finally, modeling of the parallel flow dynamics is planned for future work. This will be pursued by adding an equation for $v_{\|}$ to the model.

3.7 Acknowledgments

The text and data in chapter 3 is a reprint of the material as it appears in "Modeling Enhanced Confinement in Drift-Wave Turbulence" in the Journal of Physics of Plasmas **24**, 062106 (2017). Hajjar R. J., Diamond P. H., Ashourvan A., Tynan G.R, American Institute of Physics, 2017.Hajjar. R. J., Diamond P. H., Ashourvan A., Tynan G. R. (2017). The dissertation author was the primary investigator and author of this paper.

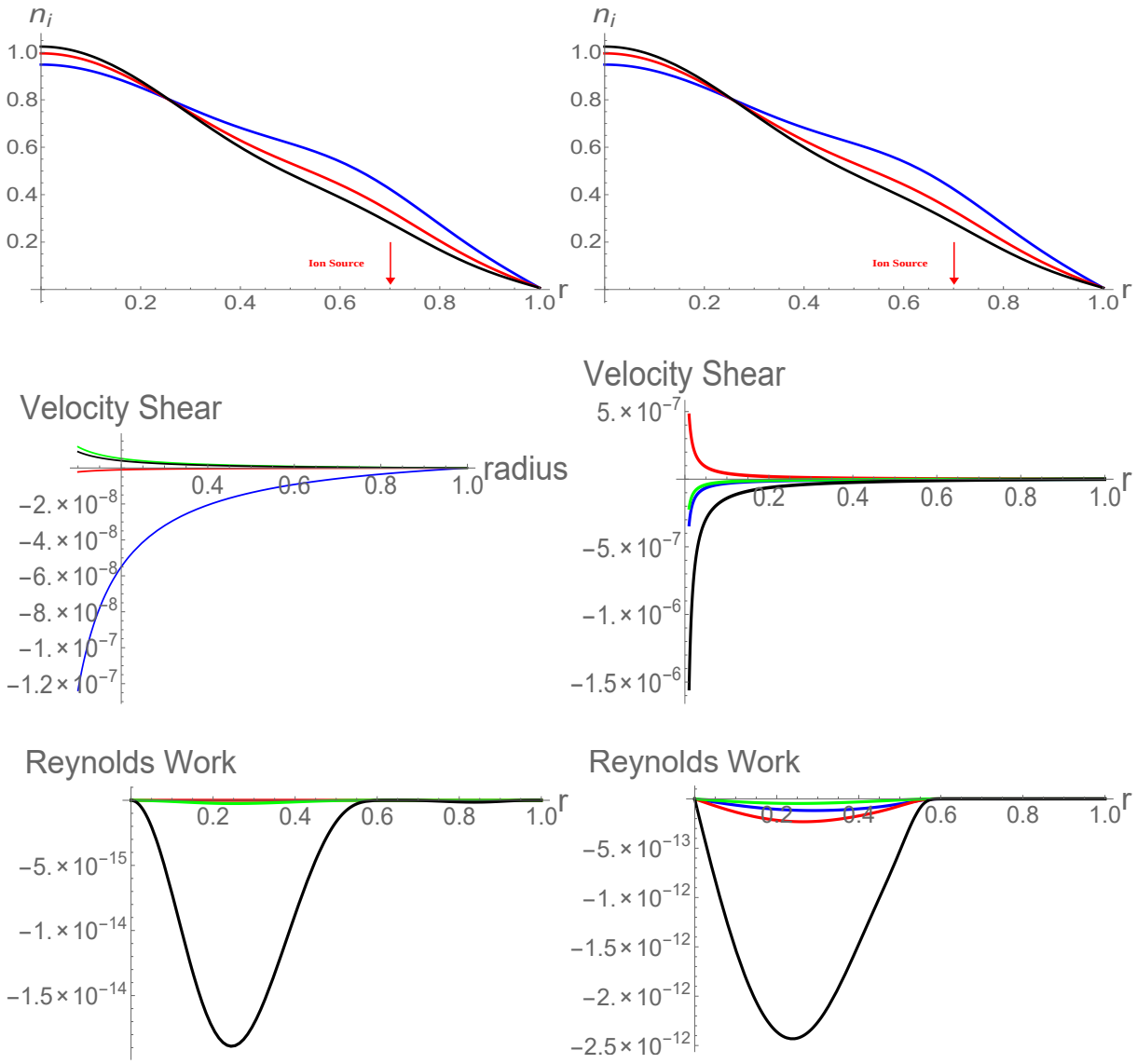

Figure 3.8: Profiles with Π_{res} and Dirichlet boundary conditions for $c_u = 6$ and $c_u = 600$.

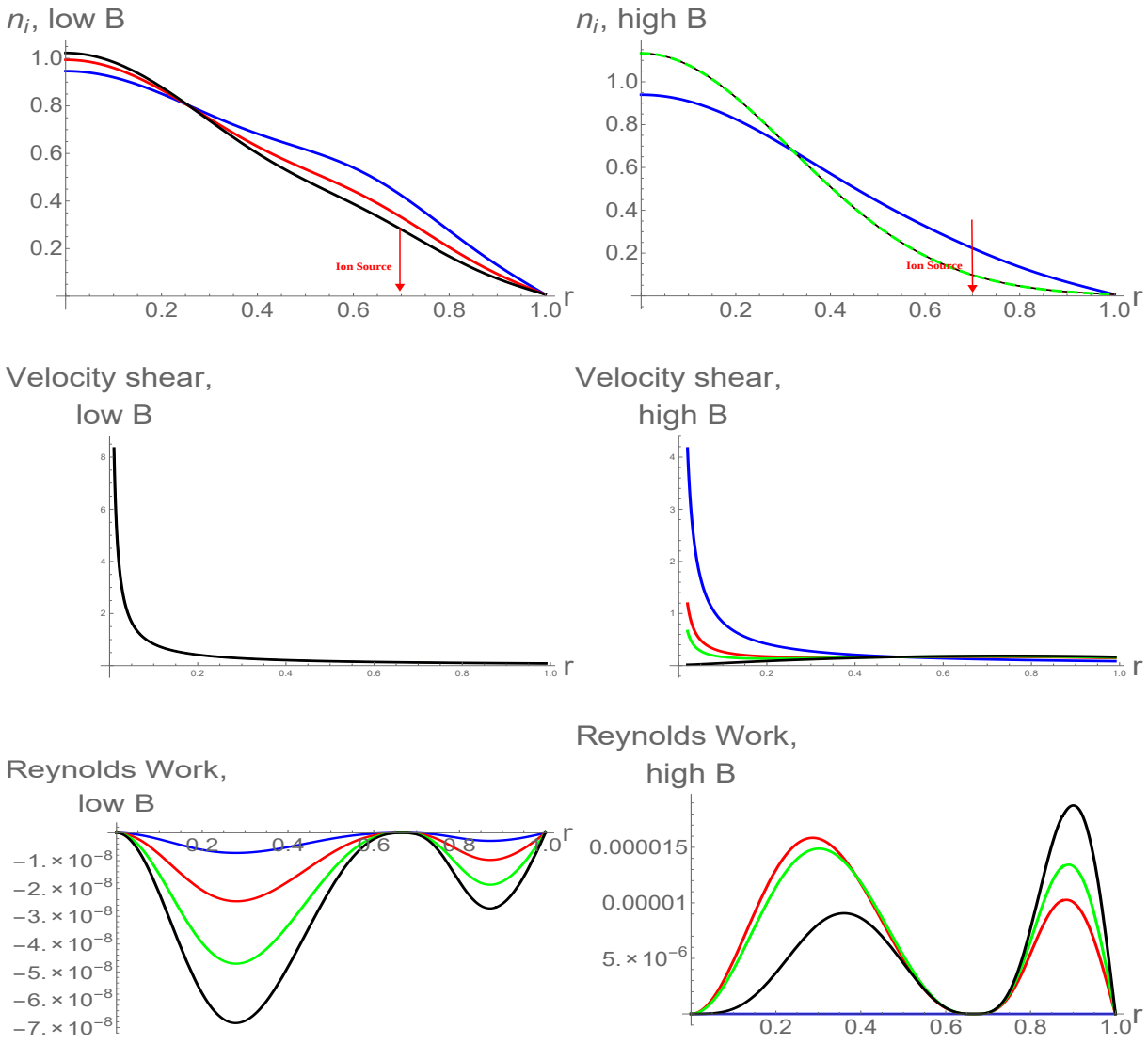

Figure 3.9: Profiles with Π_{res} and Neumann boundary conditions for increasing B.

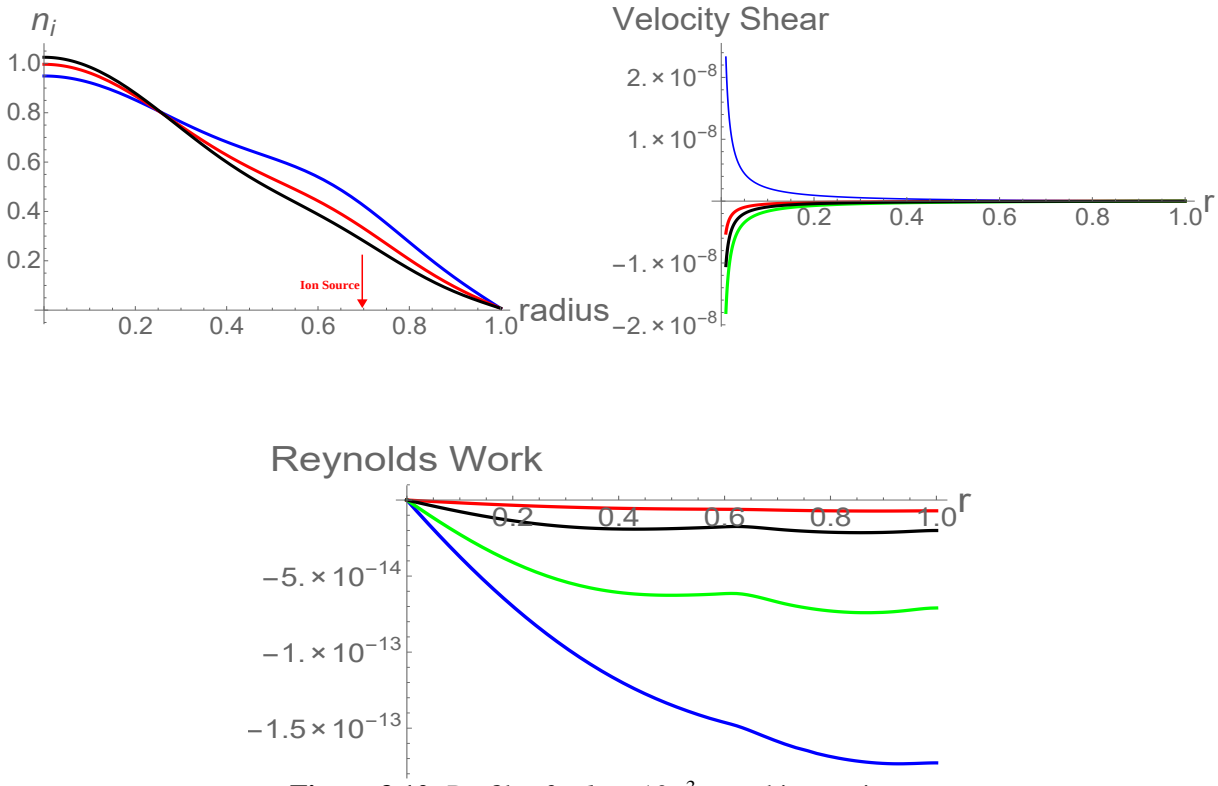

Figure 3.10: Profiles for $l_0 = 10^{-3}\rho_s$ and increasing B.

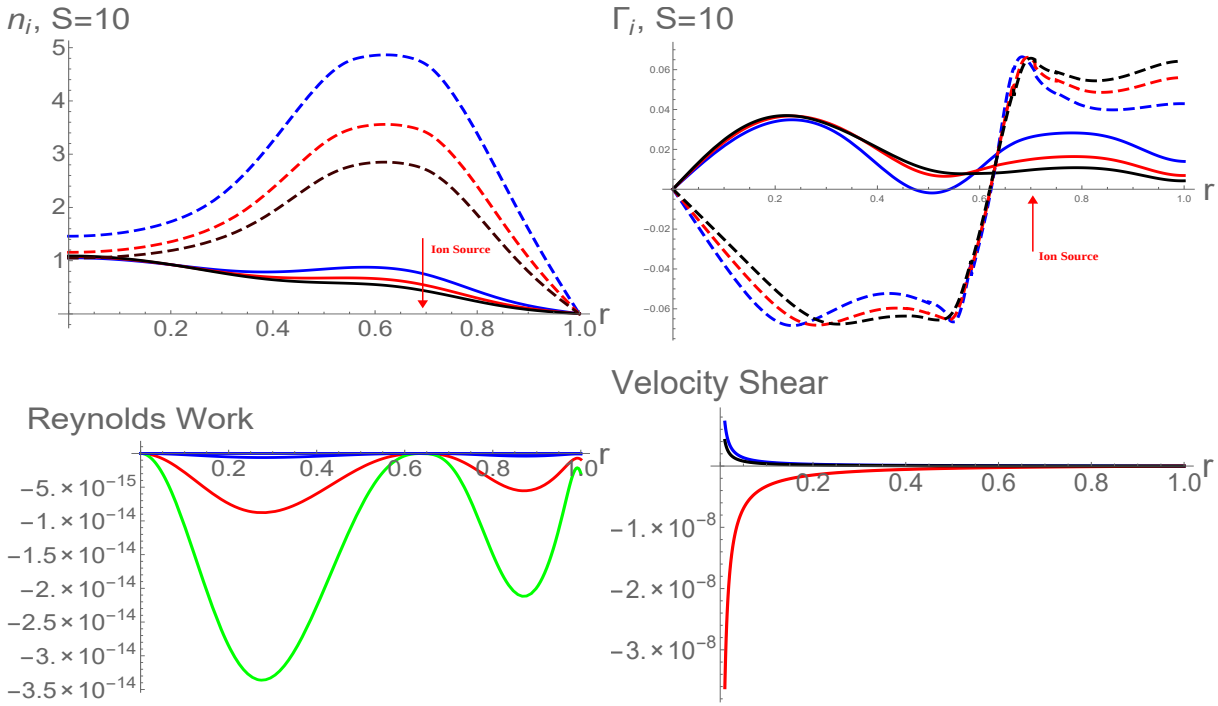

Figure 3.11: Profiles for $Pr = 65000$ and increasing B. Solid and dashed plots correspond to data at t_1 and t_2 respectively.

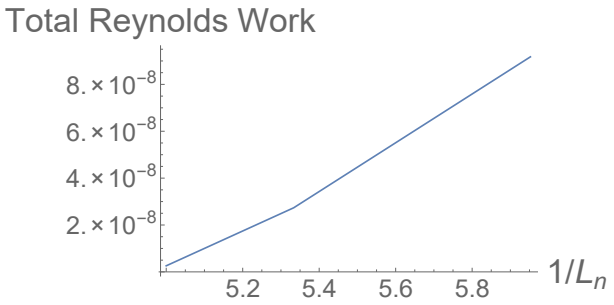

Figure 3.12: P_{Re-tot} as function of $1/L_n$ for increasing B.

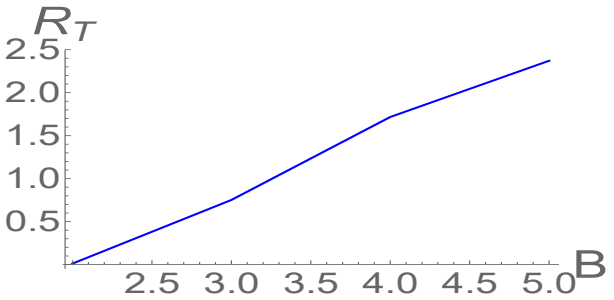

Figure 3.13: R_T time variations at $x = 0.1$, 0.6 and 0.8 (Blue, Green, Brown) for $S = 40$.

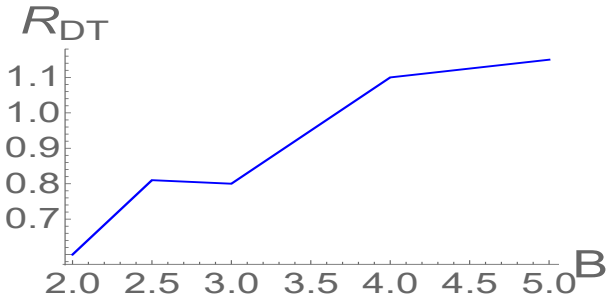

Figure 3.14: R_{DT} variations for $S = 10$ and increasing B .

Chapter 4

DYNAMICS OF ZONAL SHEAR COLLAPSE FOR HYDRODYNAMIC ELECTRONS

4.1 Introduction

Drift wave (DW) turbulence is one of the fundamental issues in magnetically confined plasmas, and continues to be a subject of interest for many experimental, theoretical and numerical studies [DIIH05, Ter00]. Driven by radial density gradients, drift wave turbulence enhances particle and thermal transport, and increases the loss of particles and heat from fusion devices. One mechanism that regulates DW fluctuations is the self-generation of sheared zonal flows (ZFs) by turbulent Reynolds stresses. These flows decorrelate turbulent eddies by shearing, thus allowing for energy transfer between the disparate scales of the plasma [Hor99, Sco05]. ZFs are therefore often linked to $L-H$ transition and internal transport barrier (ITB) formation [KD03]. Many models describing the regulations of DWs by ZFs have been proposed, so much so that the problem is now referred to as DW/ZF turbulence.

In another vein, there is evidence to suggest that ZFs collapse when the plasma density approaches the Greenwald density limit n_G. This limit is an operational bound on the plasma density, and represents the maximum attainable density before the plasma develops strong MHD activity [GTW$^+$88]. Increasing the density above n_G leads ultimately to degradation of particle confinement and disruption. A series of symptoms are frequently manifested at the density limit. These include, but are not limited to: edge cooling, multifaceted asymmetric radiation from edge (MARFE), current shrinkage and weakening of the edge shear $E \times B$ layers. In particular, a recent experiment in the HL-2A tokamak [HTD$^+$18] showed that as $\bar{n}$ approaches n_G, the edge shear flow collapses. This is accompanied by an enhancement of the turbulent particle flux near the separatrix as the plasma density increases in these ohmic L-mode discharges. Cooling of the edge plasma and decrease in the Reynolds force responsible for driving the zonal flow were also observed as $\bar{n}/n_G$ increased. Also, there was a significant decrease in the adiabaticity parameter $\alpha = k_z^2 v_{th}^2/(\nu_{ei}|\omega|)$ from 3 to 0.5, as $\bar{n}$ was increased. Here $|\omega|$ represents the frequency of the DW unstable mode. Note the low β values in this HL-2A experiment, where $0.01 < \beta < 0.02$.

A conventional approach is to attribute these observations to an increase in the plasma collisionality with $\bar{n}$, and an increase in the damping of the ZFs[Gre02, GTW$^+$88]. Increasing the plasma density boosts the collisional damping of zonal flows, thus inhibiting the self-regulation of turbulence [MRS09, XTD$^+$12]. As a result, transport of particle and heat is enhanced, and plasma confinement degrades. Alternatively, another approach links these observations to the development of additional linear instabilities, such as resistive ballooning modes, in the edge of the tokamak [RDZ98, Tok03, TKL05]. The onset of resistive ballooning modes is linked to $k_z^2 v_{th}^2/(\nu_{ei}|\omega|)$ dropping below one. These additional instabilities are thought to enhance transport and lead to further deterioration of the plasma confinement.

Motivated by these observations, we present a model that investigates turbulence and the collapse of the plasma edge shear layer in the hydrodynamic electron limit. Specifically, we present a theory for the evolution of turbulence and mean profiles (including flows) as the

adiabaticity parameter α decreases below unity that is, as the plasma response passes from the adiabatic limit ($\alpha \gg 1$) to the hydrodynamic limit ($\alpha \ll 1$). Interestingly enough, findings of this paper are easily applicable to the density limit experiments since $\alpha \propto 1/\bar{n}$. A particularly simple model proposed by Hasegawa and Wakatani describes the dynamics of two-dimensional (2D) edge drift wave turbulence in a collisional plasma in the presence of a constant magnetic field. This generic system of equations describes the excitation and damping of unstable modes in terms of a few collisionality parameters, leading to a stationary turbulence level without external drive. In particular, the Hasegawa-Wakatani system of equations remains a valid model for edge turbulence dynamics, regardless of the magnitude of the plasma β. Although multiple studies investigating the characteristics of turbulence in the hydrodynamic limit have been published, no explanation of why the shear flow collapses and/or why drift wave turbulence is enhanced for $\alpha < 1$ was presented. In fact, most studies of ZF behavior in the hydrodynamic electron regime simply repeat numerical results that show strong turbulence and weak zonal flows in the hydrodynamic limit [KT13, NBD07, CBS95, PBN13], and verify the usual power laws of turbulent energies in this limit [GG15]. Note that for the parameters of the HL-2A experiments, it is quite unlikely that resistive ballooning modes are excited.

This paper addresses these questions by presenting a simple reduced model for transport enhancement and weakening of the edge shear layer in the hydrodynamic electron limit. The model is derived from the Hasegawa-Wakatani (HW) equations for collisional drift waves, and self-consistently studies space and time evolution of the mean density $\bar{n}$, mean azimuthal flow $\bar{v}_y$ and turbulent potential enstrophy ε. The model determines the role of the Reynolds stress $\langle \tilde{v}_x \tilde{v}_y \rangle$ in the feedback loop between flows and turbulence, and gives additional insight into the DW/ZF relation in the hydrodynamic electron limit. Quasi-linear analysis shows that both the particle flux Γ_n and the turbulent viscosity χ_y are enhanced as α decreases. However, the residual vorticity stress Π^{res}, which accelerates the flow, is reduced with α. The mean vorticity gradient equal to Π^{res}/χ_y is then reduced, and the edge shear layer collapses. As a result, transport

of particles and heat increases. These findings are relevant to the density limit experiment, as $\alpha \propto 1/\bar{n}$. When $\bar{n}$ increases, α decreases, and Π^{res}/χ_y is reduced. The plasma production of zonal flows declines and turbulence and transport increase. Thermal and particle transport increase, thereby triggering cooling of the edge plasma, in part because of inward turbulence spreading. For constant pressure, a drop in plasma temperature T_e leads to further increase in the density and feedback loop between T_e and $\bar{n}$ forms.

The rest of the paper is organized as follows: Section (4.2) gives the linear response analysis of the basic Hasegawa-Wakatani system, as well as solution of the DW dispersion relation in both the adiabatic and hydrodynamic limits. Section (4.3) introduces the reduced model used to describe the evolution of the three fields: $\bar{n}$, $\bar{v}_y$ and ε. In Section (4.4), we calculate the expressions for the particle flux, the vorticity flux and the Reynolds work in both adiabatic and hydrodynamic limits. The latter reflects the potential enstrophy exchange between fluctuations and mean flow. The model is then simplified to a predator/prey model by slaving the expression for ε in the equations for $\bar{n}$ and $\bar{v}_y$ in Section (4.5). Section (4.6) gives a physical argument as to why zonal flow formation is weak in the hydrodynamic limit. Variations of the mean vorticity gradient Π^{res}/χ_y, as well as changes in the scaling of the vorticity flux $\langle \tilde{v}_x \nabla_\perp^2 \phi \rangle$ are examined, in order to characterize the mesoscopic plasma response as α decreases. The drop in zonal flow drive is reconciled with the persistence of potential vorticity mixing in the hydrodynamic limit. Section (4.7) interprets the experimental observations obtained in the density limit experiment from the perspective of the collapse of ZFs in the hydrodynamic electron limit. A scenario linking shear layer collapse to the density limit is proposed. Finally, conclusions and future work are discussed in Section (4.8).

4.2 Basic System and Linear Stability Analysis

In a box of dimensions: $0 \leq x \leq L_x$, $0 \leq y \leq L_y$, $0 \leq z \leq L_z$, the equations for the density n and vorticity $\nabla^2\phi$ in a nonuniform plasma with density $n_0(x)$ and constant magnetic field $\mathbf{B} = B\hat{z}$ are [HW83]:

$$\frac{dn}{dt} = -\frac{v_{th}^2}{\nu_{ei}}\nabla_\parallel^2(\phi - n) + D_0\nabla^2 n \tag{4.1a}$$

$$\frac{d\nabla^2\phi}{dt} = -\frac{v_{th}^2}{\nu_{ei}}\nabla_\parallel^2(\phi - n) + \mu_0\nabla^2(\nabla^2\phi) \tag{4.1b}$$

Here the fields are normalized as: $n \equiv n/n_0$, $\phi \equiv e\phi/T_e$, $t \equiv \omega_{ci}t$, $length \equiv length/\rho_s$, $v_{th} \equiv v_{th}/c_s$ and $\nu_{ei} \equiv \nu_{ei}/\omega_{ci}$. The average plasma density, the electron temperature and thermal velocity, as well as the plasma sound speed are n_0, T_e, v_{th} and c_s respectively. ω_{ci} is the ion cyclotron frequency, and $\rho_s = c_s/\omega_{ci}$ is the ion Larmor radius with temperature T_e. The collisional diffusion coefficients D_0 and μ_0 dissipate energy at small scales by frictional drag through forward energy cascade. The electron parallel diffusion rate $\hat{\alpha} = -v_{th}^2\nabla_\parallel^2/\nu_{ei} = k_z^2 v_{th}^2/\nu_{ei}$ couples the vorticity fluctuations to those in the density profile. The convective derivative is equal to: $d/dt = \partial_t + (\hat{z}\times\nabla\phi).\nabla = \partial_t + v_E.\nabla$ where v_E is the $E\times B$ drift. The fields are decomposed into a perturbation and a zonally averaged part: $f = \bar{f}(x,t) + \tilde{f}(x,y,z,t)$, where the averaging is preformed over the directions of symmetry y and z:

$$\langle f\rangle = \bar{f} = \frac{1}{L_y L_z}\int_0^{L_y}\int_0^{L_z} f\,dydz$$

Equations for the density and vorticity fluctuations are written as:

$$\partial_t \tilde{n} + \tilde{v}_x.\nabla \bar{n} = -\frac{v_{th}^2}{\nu_{ei}} \nabla_\parallel^2 (\tilde{\phi} - \tilde{n}) - \{\tilde{\phi}, \tilde{n}\} + D_0 \nabla^2 \tilde{n} \tag{4.2a}$$

$$\partial_t \nabla^2 \tilde{\phi} + \tilde{v}_x.\nabla \overline{\nabla^2 \phi} = -\frac{v_{th}^2}{\nu_{ei}} \nabla_\parallel^2 (\tilde{\phi} - \tilde{n}) - \{\tilde{\phi}, \nabla^2 \tilde{\phi}\} + \mu_0 \nabla^2 (\nabla^2 \tilde{\phi}) \tag{4.2b}$$

Here the mean flow shear $\overline{\nabla^2 \phi}$ in eq.(4.2b) is self-generated by the Reynolds stress $\langle \tilde{v}_x \tilde{v}_y \rangle$, and is driven by the DW interactions. Based in the triad coupling, this internal shear results from nonlinear energy transfer related, but not identical to, the inverse energy cascade in a 2D fluid. The nonlinear advection terms are expressed as Poisson brackets: $\{f, g\} = \partial_x f \partial_y g - \partial_y f \partial_x g$ and represent spatial scattering of the fluctuation energy.

In the Hasegawa-Wakatani (HW) system, the plasma response and the character of the flow are mainly determined by three parameters: the collisional diffusion coefficients D_0 and μ_0, and the adiabaticity parameter $\alpha = k_z^2 v_{th}^2 / (\nu_{ei} |\omega|)$. While D_0 and μ_0 regulate the dissipation of energy at small scales, α determines the efficiency of zonal flow production, and controls its mescocopic response. Defined as the ratio between the parallel diffusion rate and the drift frequency, α controls the phase difference between $\tilde{\phi}$ and $\tilde{n}$, and thus the transport. When $\alpha > 1$, the plasma response is near adiabatic, $\tilde{\phi}$ and $\tilde{n}$ are closely coupled, and $\tilde{n} \simeq \tilde{\phi}$. The Hasegawa-Wakatani system effectively reduces then to the Hasegawa-Mima equation [HM77], with a phase shift between $\tilde{n}$ and $\tilde{\phi}$. In the opposite limit however, $\alpha < 1$, the plasma response is said to be hydrodynamic. Eqs.(4.2a-4.2b) are then weakly coupled, and the $\tilde{n}$ dynamics resemble that of a passive scalar. Moreover, the vorticity equation tends toward that for a 2D Navier-Stokes fluid [CBS95].

For a linear stability analysis of the HW equations, we write the fluctuation fields as: $\tilde{f}_m = \delta f_m(x) e^{i[k_m y + k_z z - \omega t]}$ with $\omega = \omega^r + i|\gamma_m|$. Here ω^r, $|\gamma_m|$, k_m and k_z are the linear eigenfrequency, the growth rate, the azimuthal and the parallel wavenumbers of the unstable

mode respectively. The drift wave dispersion relation is then:

$$\omega^2 + i\frac{\hat{\alpha}}{k_\perp^2\rho_s^2}\Big[\omega(1+k_\perp^2\rho_s^2) - \omega^\star\Big] = 0 \tag{4.3}$$

where $\omega^\star = k_m|v_d| = -k_m\rho_s c_s\nabla\bar{n} > 0$ is the electron drift frequency, and $v_d = \rho_s c_s\nabla\bar{n} < 0$ is the electron diamagnetic drift velocity. The solution of eq.(4.3) is given by:

$$\omega = \frac{1}{2}\left(-i\frac{\hat{\alpha}(1+k_\perp^2\rho_s^2)}{k_\perp^2\rho_s^2} + \sqrt{\frac{4i\omega^\star\hat{\alpha}}{k_\perp^2\rho_s^2} - \Big(\frac{\hat{\alpha}(1+k_\perp^2\rho_s^2)}{k_\perp^2\rho_s^2}\Big)^2}\right) \tag{4.4}$$

This expression is simplified, according to the magnitude of $\hat{\alpha}/|\omega|$, i.e., the magnitude of α.

In the adiabatic limit: ($\alpha \gg 1$ and $\hat{\alpha} \gg |\omega|$)

When the parallel diffusion rate $k_z^2 v_{th}^2/\nu_{ei}$ is larger than both the drift frequency $|\omega|$ and the electron diamagnetic frequency $|\omega^\star|$, eq.(4.4) reduces to:

$$\omega_{adiabatic} = \frac{\omega^\star}{1+k_\perp^2\rho_s^2} + i\frac{\omega^{\star 2}k_\perp^2\rho_s^2}{\hat{\alpha}} \tag{4.5}$$

In the adiabatic limit, ω^r does not depend on $\hat{\alpha}$. However, the growth rate $|\gamma_m|$ is proportional to $1/\hat{\alpha}$. For large $\hat{\alpha}$, the growth rate is $|\gamma_m| \ll 1$, and the drift wave eigenfrequency is simply written as:

$$\omega_{adiabatic} \simeq \omega^r = \omega^\star(1+k_\perp^2\rho_s^2)^{-1} \tag{4.6}$$

In the hydrodynamic limit: ($\alpha \ll 1$ and $\hat{\alpha} \ll |\omega|$)

When the parallel diffusion rate $k_z^2 v_{th}^2/\nu_{ei}$ is much smaller than $|\omega|$, the expression for the frequency reads:

$$\omega_{hydrodynamic} \simeq \frac{1}{2}\left(-i\frac{\hat{\alpha}(1+k_\perp^2\rho_s^2)}{k_\perp^2\rho_s^2} + \sqrt{\frac{4i\hat{\alpha}\omega^\star}{k_\perp^2\rho_s^2}}\right) \simeq \sqrt{\frac{\omega^\star\hat{\alpha}}{2k_\perp^2\rho_s^2}}(1+i) \tag{4.7}$$

In this limit, the growth rate and the real part are both equal to: $\omega^r = |\gamma_m| = \sqrt{\omega^\star \hat{\alpha}/2k_\perp^2 \rho_s^2}$. In contrast to the adiabatic limit, the contribution of $|\gamma_m|$ cannot be neglected in the expression for $\omega_{hydrodynamic}$.

A comparison of eq.(4.6) and eq.(4.7) shows that $\omega_{adiabatic}$ is dominantly real, while $\omega_{hydrodynamic}$ involves a comparable real and imaginary part. While the motion of the drift waves is purely oscillatory in the adiabatic limit, in the hydrodynamic limit, the dynamics of the perturbation resembles that of a convective cell. This feature dictates the behavior of the flow in the two plasma regimes.

4.3 Reduced Model

4.3.1 The equations

In this section, a 1D reduced model that self-consistently describes the evolution of turbulence and plasma profiles is presented. The equations relating the time and space evolution of the plasma mean density $\bar{n}$, and mean vorticity $\overline{\nabla^2\phi}$ are obtained by averaging eqs.(4.1a-4.1b) over the directions of symmetry:

$$\partial_t \bar{n} = -\partial_x \langle \tilde{v}_x \tilde{n} \rangle + D_0 \nabla^2 \bar{n} \tag{4.8a}$$

$$\partial_t \overline{\nabla^2\phi} = -\partial_x \langle \tilde{v}_x \nabla^2 \tilde{\phi} \rangle - \nu_{in}(\bar{v}_y - \bar{v}_n) + \mu_0 \nabla^2 \overline{\nabla^2\phi} \tag{4.8b}$$

A neutral damping term proportional to the ion-neutral collision frequency $\nu_{in} \propto n_n$, is added to the mean vorticity equation. This term can be significant at the plasma edge. It is a sink of energy transfered to larger scales, and so damps the zonal flows. The neutral friction can be dropped from the mean vorticity equation if $\nu_{in} \to 0$, i.e., for low neutral density n_n.

In addition to eqs.(4.8a-4.8b), we formulate an equation for the fluctuation potential enstrophy $\varepsilon = \langle (\tilde{n} - \nabla^2\tilde{\phi})^2/2 \rangle$. The HW system locally conserves the potential vorticity defined

as $q = n - \nabla^2\phi$, up to viscosity and particle diffusivity. A linearized equation describing the time evolution of the turbulent potential vorticity $\tilde{q} = \tilde{n} - \nabla^2\tilde{\phi}$ is obtained by subtracting eq.(4.2b) from eq.(4.2a):

$$\frac{\partial \tilde{q}}{\partial t} + \tilde{v}_x.\nabla\bar{q} = -\{\tilde{\phi}, \tilde{q}\} + \mu_0\nabla^2 q \Longrightarrow \frac{dq}{dt} = \mu_0\nabla^2 q \tag{4.9}$$

where $q = \bar{q} + \tilde{q}$, and μ_0 and D_0 are assumed to be of the same order. Eq.(4.9) represents a conservation of the total potential vorticity up to viscous dissipation. Therefore, the potential enstrophy $\varepsilon = \langle\tilde{q}^2\rangle/2 = \langle(\tilde{n} - \nabla^2\tilde{\phi})^2\rangle/2$ is also conserved up to collisional diffusion. This can be shown by multiplying eq.(4.9) by $\tilde{q} = \tilde{n} - \nabla^2\tilde{\phi}$, and performing a zonal integral. Detailed calculations can be found in ref. [HDAT17, ADG16, AD16]. Here we simply write the time evolution equation for the potential enstrophy ε:

$$\partial_t\varepsilon + \partial_x\Gamma_\varepsilon = -(\Gamma_n - \Pi)(\partial_x\bar{n} - \partial_{xx}\bar{v}_y) - \varepsilon^{3/2} + P \tag{4.10}$$

In eq.(4.10), Γ_n and Π are the particle and vorticity flux respectively, while $\partial_x\bar{n}$ and $\partial_{xx}\bar{v}_y$ are the mean density and mean vorticity gradients respectively. The diffusive energy flux Γ_ε on the LHS is the mesoscopic spreading of turbulence due to the three wave coupling. It represents local diffusion of the potential enstrophy ε. The potential enstrophy flux is written as: $\Gamma_\varepsilon = -D_\varepsilon\partial_x\varepsilon = -l_{mix}^2\sqrt{\varepsilon}\partial_x\varepsilon$, where $l_{mix} = \tilde{v}_x\tau_c$ is the turbulent mixing length and τ_c is the turbulence correlation time. The first term on the RHS of eq.(4.10) accounts for direct mean flow-fluctuation coupling, and converts the mean potential enstrophy into fluctuation potential enstrophy. This coupling term relates variations of the turbulent potential enstrophy to those in the mean profile of $\bar{n}$ and $\bar{v}_y$, via the particle flux $\Gamma_n = \langle\tilde{v}_x\tilde{n}\rangle$ and the vorticity flux $\Pi = \langle\tilde{v}_x\nabla^2\tilde{\phi}\rangle$. The second term on the RHS of eq.(4.10) dissipates the fluctuation potential enstrophy at a rate $\sqrt{\varepsilon}$. This dissipation is due to the collisional coefficients D_0 and μ_0. Lastly, the production term P represents an input of the potential enstrophy due to linear growth, driven by the mean profiles. It is proportional to ε and linear in γ_{DW}, the growth rate of the DW instability: $P = \gamma_{DW}\varepsilon$. Dropping

the neutral damping term from the vorticity equation, as well as the $\bar{.}$ sign, we simplify the notation by writing $u = \overline{\nabla^2\phi}$ to obtain:

$$\partial_t n = -\partial_x \Gamma_n + D_0 \nabla^2 n \tag{4.11a}$$

$$\partial_t u = -\partial_x \Pi + \mu_0 \nabla^2 u \tag{4.11b}$$

$$\partial_t \varepsilon + \partial_x \Gamma_\varepsilon = -(\Gamma_n - \Pi)(\partial_x n - \partial_x u) - \varepsilon^{3/2} + P \tag{4.11c}$$

Written in 1D (in radius), this system models the evolution of DW intensity and the formation of zonal flows in the plasma. For this purpose, an expression for the mixing length l_{mix} is required. One approach consists of considering a mixing length that exhibits a turbulence suppression through the azimuthal shear $u = \nabla v_y$:

$$l_{mix} = \frac{l_0}{\left(1 + \dfrac{(l_0 \nabla u)^2}{\varepsilon}\right)^{\delta}} \tag{4.12}$$

where δ is a free parameter and l_0 is an external dynamical turbulence production scale length. Eq.(4.12) exhibits a decorrelation of the turbulent structures by the flow shear $u = \nabla v_y$ [BDT90]: when the flow shear increases, the mixing length decreases. When l_{mix} is reduced, the production of potential enstrophy ε also drops, the mean profiles steepen, and a closed feedback loop is obtained. In the particular case of weak or collapsed flow shear, $u = \nabla v_y \simeq 0$ so a constant mixing length $l_{mix} \simeq l_0$ results.

4.4 Expressions for the Turbulent Fluxes

In addition to the expression for l_{mix}, expressions for the turbulent fluxes $\langle \tilde{v}_x \tilde{n} \rangle$ and $\langle \tilde{v}_x \tilde{v}_y \rangle$ are needed to close the model and solve eqs.(4.11a-4.11c). In this section, we use quasi linear theory to calculate the expressions for the particle flux and vorticity flux.

4.4.1 The Particle Flux: $\langle \tilde{n}\tilde{v}_x \rangle$

To calculate the expression for the particle flux $\langle \tilde{n}\tilde{v}_x \rangle$, we write the electron density fluctuation as $\tilde{n} = \tilde{\phi} + h$, where h is the deviation from the adiabatic response. Plugging in eq.(4.2a), we obtain:

$$h = \frac{\omega^\star - \omega}{\omega + i\hat{\alpha}}\tilde{\phi}, \qquad\qquad \tilde{n} = \tilde{\phi} + h = \left(\frac{\omega^\star + i\hat{\alpha}}{\omega + i\hat{\alpha}}\right)\tilde{\phi}$$

In the adiabatic limit, $\omega \simeq \omega^\star$ and the following relation between $\tilde{n}$ and $\tilde{\phi}$ is recovered: $\tilde{n} = \Big(1 - i(\omega^\star - \omega)/\hat{\alpha}\Big)\tilde{\phi} \simeq \tilde{\phi}$ [LDXT16]. For $\tilde{v}_x = -ik_m\rho_s c_s \delta\phi$, the expression for the particle flux $\langle \tilde{n}\tilde{v}_x \rangle$ is:

$$\begin{aligned}
\Gamma_n &= -\left[\frac{(\hat{\alpha} + |\gamma_m|)}{|\omega + i\hat{\alpha}|^2}\frac{d\ln n}{dx} + \frac{\hat{\alpha}\omega^r}{k_m\rho_s c_s|\omega + i\hat{\alpha}|^2}\right]\langle \delta v_x^2 \rangle \\
&\simeq -\frac{(\hat{\alpha} + |\gamma_m|)}{|\omega + i\hat{\alpha}|^2}\frac{d\ln n}{dx}\langle \delta v_x^2 \rangle \\
&= -\frac{D}{n_0}\frac{d\bar{n}}{dx}
\end{aligned} \tag{4.13}$$

The particle diffusion coefficient is: $D = \Big[(\hat{\alpha} + |\gamma_m|)/|\omega + i\hat{\alpha}|^2\Big]\langle \delta v_x^2 \rangle$. The expression for the particle diffusion coefficient D depends on $\hat{\alpha}$, and changes as the plasma passes from the adiabatic to the hydrodynamic regime. We introduce next the factor f that represents the fraction of the fluctuation energy εl_{mix}^2 which is in the kinetic energy of radial motion:

$$\langle \delta v_x^2 \rangle = f\varepsilon l_{mix}^2 = \frac{\langle \delta v_x^2 \rangle}{\langle \delta n^2 \rangle + \langle \delta v_x^2 \rangle}\varepsilon l_{mix}^2 \tag{4.14}$$

Using the expressions for $\tilde{n}$ and $\tilde{v}_x$, the expression for f is equal to:

$$f = \frac{k_\perp^2 \rho_s^2}{\left|\frac{\omega^* + i\hat{\alpha}}{\omega + i\hat{\alpha}}\right|^2 + k_\perp^2 \rho_s^2} = \begin{cases} \frac{k_\perp^2 \rho_s^2}{1 + k_\perp^2 \rho_s^2}, & \text{in the adiabatic regime} \\ \frac{1}{|\omega^*/\hat{\alpha}| + 1}, & \text{in the hydrodynamic regime} \end{cases} \tag{4.15}$$

In the adiabatic regime, the kinetic energy $\langle \delta v_x^2 \rangle$ is less then $\langle \delta n^2 \rangle$, and the electron total energy is mostly thermal/internal energy. Therefore, the factor $f \ll 1$. However, in the hydrodynamic regime, the kinetic energy of the electrons rises as compared to $\langle \delta n^2 \rangle$, reflecting an increase in the screening of ion diamagnetic oscillations such that $f \to 1$. For small values of $k_\perp^2 \rho_s^2 \ll 1$, the two limits of f are:

$$\begin{cases} f \to k_\perp^2 \rho_s^2 \simeq 0, & \text{in the adiabatic regime} \\ f \to 1, & \text{in the hydrodynamic regime} \end{cases}$$

Finally, for purely adiabatic DWs, the relation $\langle \delta v_x^2 \rangle \simeq k_\perp^2 \rho_s^2 \varepsilon l_{mix}^2$ is recovered.

4.4.2 The Vorticity Flux: $\langle \tilde{v}_x \nabla_\perp^2 \phi \rangle$

In addition to Γ_n, we calculate the vorticity flux $\Pi = \langle \tilde{v}_x \nabla_\perp^2 \tilde{\phi} \rangle$. This flux relates to the Reynolds force that controls the relation between turbulence and zonal flows via the Taylor identity: $-\partial_x \langle \tilde{v}_x \tilde{v}_y \rangle = \langle \tilde{v}_x \nabla_\perp^2 \tilde{\phi} \rangle$. The Taylor identity directly links the zonal flow momentum conservation to potential enstrophy balance [DGH$^+$08]. To calculate Π, we use the vorticity equation and drop the neutral drag term, as it is significant only at the edge. The vorticity flux

then follows as:

$$\begin{aligned}\Pi &= \sum_m -\frac{k_m^2\rho_s^2c_s^2|\gamma_m|}{|\omega|^2}|\tilde{\phi}^2|\frac{d^2\bar{v}_y}{dx^2} + 2Re\Big[\frac{k_m\rho_s c_s\hat{\alpha}}{\omega}\Big(\frac{\omega^\star-\omega}{\omega+i\hat{\alpha}}\Big)|\tilde{\phi}|^2\Big] \\ &= -\chi_y\frac{d\langle\nabla_\perp^2\phi\rangle}{dx} + \Pi^{res} \\ &= -\chi_y\frac{d^2\bar{v}_y}{dx^2} + \Pi^{res}\end{aligned} \tag{4.16}$$

The first term of eq.(4.16) represents the diffusive flux, while the second term is the residual stress, i.e., the non-diffusive flux driven by ∇n. The turbulent viscosity χ_y relating the mean vorticity gradient $d(\nabla\bar{v}_y)/dx$ to the vorticity flux Π is equal to:

$$\chi_y = \sum_m \frac{k_m^2\rho_s^2c_s^2|\gamma_m|}{|\omega|^2}|\tilde{\phi}^2| = \frac{|\gamma_m|\langle\delta v_x^2\rangle}{|\omega|^2} \tag{4.17}$$

Here χ_y depends on the adiabaticity parameter, as both $|\gamma_m|$ and $|\omega|$ are $\hat{\alpha}$-dependent.

The residual stress Π^{res} resulting from coupling between the density and vorticity profiles is equal to:

$$\Pi^{res} = \frac{k_m\rho_s c_s\omega_{ci}\hat{\alpha}\Big[(\omega^r)^2(\omega^\star-\omega^r) - |\gamma_m|^2(\omega^r+\omega^\star) - \omega^\star\hat{\alpha}|\gamma_m|\Big]}{|\omega|^2\times|\omega+i\hat{\alpha}|^2}\langle\tilde{\phi}^2\rangle \tag{4.18}$$

Π^{res} converts the driving particle flux into zonal (azimuthal) flow, and accelerates $\bar{v}_y$ from rest. Similar to the expression for χ_y, Π^{res} varies as $\hat{\alpha}$ changes, affecting thereby the character of the flow in both plasma limits. In the adiabatic limit, an examination of the expression for Π^{res} shows that the residual stress is inversely proportional to $\hat{\alpha}$, i.e., $\Pi^{res}_{adia} \propto 1/\hat{\alpha}$. In the hydrodynamic limit however, the residual stress is directly proportional to $\sqrt{\hat{\alpha}}$, i.e. $\Pi^{res}_{hydro} \propto \sqrt{\hat{\alpha}}$, for $\alpha \ll 1$.

4.4.3 Fluxes and Reynolds Work in Adiabatic and Hydrodynamic Limits.

The expressions for the particle and vorticity flux can be simplified depending on the value of $\hat{\alpha}$, i.e., depending on the electron plasma response.

In the adiabatic limit: ($\hat{\alpha} \gg |\omega|$)

In this limit, $\alpha \gg 1$. The growth rate $|\gamma_m| \simeq 1/\alpha \ll 1$, and $|\omega|^2 \simeq (\omega^r)^2 = \Big[\omega^\star/(1+k_\perp^2\rho_s^2)\Big]^2$. The expressions for the particle and vorticity fluxes in the adiabatic limit are:

$$n_0\Gamma_n = -\frac{\langle\delta v_x^2\rangle}{\hat{\alpha}}\frac{d\bar{n}}{dx} \simeq -\frac{\varepsilon l_{mix}^2}{\hat{\alpha}}\frac{d\bar{n}}{dx} \tag{4.19a}$$

$$\begin{aligned}\Pi &= -\frac{|\gamma_m|\langle\delta v_x^2\rangle}{|\omega|^2}\frac{d^2\bar{v}_y}{dx^2} - \frac{\omega_{ci}\langle\delta v_x^2\rangle}{\hat{\alpha}}\frac{d\bar{n}}{dx}\Big(\frac{k_\perp^2\rho_s^2}{1+k_\perp^2\rho_s^2}\Big)\\ &\simeq -\frac{\varepsilon l_{mix}^2}{\hat{\alpha}}\frac{d^2\bar{v}_y}{dx^2} - \frac{\omega_{ci}\varepsilon l_{mix}^2}{\hat{\alpha}}\frac{d\bar{n}}{dx}\end{aligned} \tag{4.19b}$$

Here $\langle\delta v_x^2\rangle_{adiabatic} = f_{adiabatic}\varepsilon l_{mix}^2 = k_\perp^2\rho_s^2\varepsilon l_{mix}^2/(1+k_\perp^2\rho_s^2)$. Scalings of the particle flux Γ_n, the turbulent viscosity χ_y and the residual stress Π^{res} in the adiabatic limit are:

$$\Gamma_n \simeq -(\varepsilon l_{mix}^2/\hat{\alpha})\nabla\bar{n} \tag{4.20a}$$

$$\chi_y \simeq \varepsilon l_{mix}^2/\hat{\alpha} \tag{4.20b}$$

$$\Pi^{res} \simeq -(\omega_{ci}\varepsilon l_{mix}^2/\hat{\alpha})\nabla\bar{n} \tag{4.20c}$$

Here, Γ_n, χ_y and Π^{res} are all inversely proportional to α In addition, both Γ_n and Π^{res} are proportional to ∇n. The expression for the Reynolds power density P_{Re} that represents the power exerted by the turbulence on the flow $\bar{v}_y$, is obtained by multiplying the Reynolds force $F_{Re} = -\partial_x\langle\tilde{v}_x\tilde{v}_y\rangle$ by the azimuthal flow $\bar{v}_y$. In the adiabatic limit, P_{Re} is equal to:

$$P_{Re} = -\partial_x\langle\tilde{v}_x\tilde{v}_y\rangle\bar{v}_y \simeq \Big(-\frac{\varepsilon}{\hat{\alpha}}\frac{d^2\bar{v}_y}{dx^2} - \frac{\omega_{ci}\varepsilon}{\hat{\alpha}}\frac{d\bar{n}}{dx}\Big)\bar{v}_y l_{mix}^2 \tag{4.21}$$

In the (likely case of) absence of an external azimuthal momentum source, and for a vanishing Reynolds power density $P_{Re} = 0$, the mean vorticity gradient is independent of $\hat{\alpha}$ and is given by:

$$\frac{d^2\bar{v}_y}{dx^2} = \frac{\Pi^{res}}{\chi_y} = -\omega_{ci}\frac{d\bar{n}}{dx} \tag{4.22}$$

In the hydrodynamic limit: ($\hat{\alpha} \ll |\omega|$)

For $\omega^r = |\gamma_m| = \sqrt{\omega^\star\hat{\alpha}/(2k_\perp^2\rho_s^2)}$, expressions for the particle and vorticity fluxes are equal to:

$$n_0\Gamma_n \simeq -\sqrt{\frac{k_\perp^2\rho_s^2}{2k_m\rho_s c_s}}\sqrt{\frac{|d\bar{n}/dx|}{\hat{\alpha}}}\langle\delta v_x^2\rangle \simeq -\frac{\varepsilon l_{mix}^2}{\sqrt{\hat{\alpha}|\omega^\star|}}\frac{d\bar{n}}{dx} \tag{4.23a}$$

$$\begin{aligned}\Pi &= -\frac{|\gamma_m|\langle\delta v_x^2\rangle}{|\omega|^2}\frac{d^2\bar{v}_y}{dx^2} - \frac{\omega_{ci}\langle\delta v_x^2\rangle}{k_m\rho_s c_s}\cdot\sqrt{\frac{k_\perp^2\rho_s^2}{2}}\sqrt{\frac{\hat{\alpha}}{|\omega^\star|}} \\ &\simeq -\frac{\varepsilon l_{mix}^2}{\sqrt{\hat{\alpha}|\omega^\star|}}\frac{d^2\bar{v}_y}{dx^2} - \frac{\omega_{ci}\varepsilon\sqrt{\hat{\alpha}}l_{mix}^2}{|\omega^\star|^{3/2}}\frac{d\bar{n}}{dx}\end{aligned} \tag{4.23b}$$

Here we used $\langle\delta v_x^2\rangle_{hydrodynamic} = f_{hydrodynamic}\varepsilon l_{mix}^2 = \varepsilon l_{mix}^2/\left[|\omega^*/\hat{\alpha}| + 1\right] < \varepsilon l_{mix}^2$. Scalings of the turbulent fluxes are then:

$$\Gamma_n \simeq -(\varepsilon l_{mix}^2/\sqrt{\hat{\alpha}|\omega^\star|})\nabla\bar{n} \tag{4.24a}$$

$$\chi_y \simeq \varepsilon l_{mix}^2/\sqrt{\hat{\alpha}|\nabla\bar{n}|} \tag{4.24b}$$

$$\Pi^{res} \simeq -(\omega_{ci}\varepsilon\sqrt{\hat{\alpha}}l_{mix}^2/|\omega^\star|^{3/2})\nabla\bar{n} \tag{4.24c}$$

While Γ_n and χ_y are inversely proportional to $\sqrt{\hat{\alpha}}$ in the hydrodynamic limit, the residual stress Π^{res} scales proportionally with $\sqrt{\hat{\alpha}}$. We note here that in the hydrodynamic limit, the particle flux Γ_n^{hydro} is proportional to $\sqrt{|\nabla\bar{n}|}$, and the residual stress Π_{hydro}^{res} is proportional to $1/\sqrt{|\nabla\bar{n}|}$. Such superficially unusual scalings with $|\nabla\bar{n}|$ result from neglecting the contributions

of the diffusive damping related to D_0 and μ_0 in the density and vorticity equations, while performing the linear analysis. Obviously these should not be extrapolated to regimes of very weak ∇n drive. In the hydrodynamic limit, the Reynolds power density is equal to:

$$P_{Re} = -\partial_x \langle \tilde{v}_x \tilde{v}_y \rangle \bar{v}_y \simeq \Big(- \frac{\varepsilon}{\sqrt{\hat{\alpha}|\nabla \bar{n}|}} \frac{d^2 \bar{v}_y}{dx^2} - \omega_{ci} \varepsilon \sqrt{\frac{\hat{\alpha}}{|\nabla \bar{n}|}} \Big) \bar{v}_y l_{mix}^2 \tag{4.25}$$

and the vorticity gradient for $P_{Re} = 0$ is directly proportional to $\hat{\alpha}$ and is equal to:

$$\frac{d^2 \bar{v}_y}{dx^2} = - \frac{\omega_{ci} \hat{\alpha}}{|\omega^\star|} \frac{d\bar{n}}{dx} \tag{4.26}$$

4.5 Simplification by Slaving: A Predator-Prey Model

When the eddy turnover time $\tau_c = l_{mix}/\tilde{v}_x$ is smaller than the particle confinement time $[D\nabla^2 \bar{n}/\bar{n}]^{-1}$, the model can be reduced to a 2-field predator-prey model that evolves the preys ($\bar{n}$) and predators ($\bar{v}_y$) according to eqs.(4.11a-4.11b). Clearly, these predators do not exist without the prey. A simplification of the previous model is achieved by slaving the expression for ε to the mean profiles, and solving the equations for $\bar{n}$ and $\bar{v}_y$. For slaved turbulence, both potential enstrophy spreading and potential enstrophy production are dropped from the ε equation because the eddy turnover time is shorter than the confinement time. The potential enstrophy equation then reduces to the balance:

$$-(\Gamma_n - \Pi)(\partial_x n - \partial_x u) - \varepsilon^{3/2} = 0 \tag{4.27}$$

In the adiabatic limit: using eqs.(4.20a-4.20c), the expression for the potential enstrophy reduces to:

$$\sqrt{\varepsilon}_{adia} = \frac{\omega_{ci}^2 l_{mix}^2}{\hat{\alpha}} \left[\Big(\frac{dn}{dx} - \frac{du}{dx} \Big)^2 - \omega_{ci} \frac{dn}{dx} \Big(\frac{dn}{dx} - \frac{du}{dx} \Big) \right] \tag{4.28}$$

The second term on the RHS of eq.(4.28) arises from the contribution of the residual stress Π^{res}_{adia}. For a constant mixing length, $\sqrt{\varepsilon}_{adia}$ is proportional to $1/\hat{\alpha}$.

In the hydrodynamic limit: the expression for the turbulent potential enstrophy is obtained from eqs.(4.24a-4.24c) as:

$$\sqrt{\varepsilon}_{hydro} = \frac{\omega_{ci}^2 l_{mix}^2}{\sqrt{|\omega^\star|\hat{\alpha}}}\left(\frac{dn}{dx} - \frac{du}{dx}\right)^2 \propto \frac{1}{\sqrt{\hat{\alpha}}} \tag{4.29}$$

Here $\sqrt{\varepsilon}_{hydro}$ is proportional to $1/\sqrt{\hat{\alpha}}$. Note that in the hydrodynamic limit, the contribution of the residual stress to the expression for ε vanishes, as $\Pi^{res}_{hydro} \propto \sqrt{\hat{\alpha}} \to 0$. A comparison of eq.(4.28) and eq.(4.29) shows that, in the adiabatic limit, the potential enstrophy is low, while ε is enhanced in the hydrodynamic limit. This is one reason why mesoscocpic zonal flows are strong in the former case, while a state of enhanced turbulence dominates in the hydrodynamic limit. In summary, the equations of the simplified model in the adiabatic and hydrodynamic limits are:

$$\partial_t n = -\partial_x \Gamma_n + D_0 \nabla^2 n \tag{4.30a}$$

$$\partial_t u = -\partial_x \Pi + \mu_0 \nabla^2 u \tag{4.30b}$$

The expressions for the particle and vorticity fluxes are:

$$\Gamma_n^{adia} = -\frac{\varepsilon l_{mix}^2}{\hat{\alpha}}\frac{dn}{dx} \tag{4.31a}$$

$$\Pi^{adia} = -\frac{\varepsilon l_{mix}^2}{\hat{\alpha}}\frac{du}{dx} - \frac{\omega_{ci}\varepsilon l_{mix}^2}{\hat{\alpha}}\frac{dn}{dx} \tag{4.31b}$$

$$\sqrt{\varepsilon}_{adia} = \frac{l_{mix}^2}{\hat{\alpha}}\left[\left(\frac{dn}{dx} - \frac{du}{dx}\right)^2 - \omega_{ci}\frac{dn}{dx}\left(\frac{dn}{dx} - \frac{du}{dx}\right)\right] \tag{4.31c}$$

in the adiabatic limit, and:

$$\Gamma_n^{hydro} = -\frac{\varepsilon l_{mix}^2}{\sqrt{\hat{\alpha}|\omega^\star|}}\frac{dn}{dx} \tag{4.32a}$$

$$\Pi^{hydro} = -\frac{\varepsilon l_{mix}^2}{\sqrt{\hat{\alpha}|dn/dx|}}\frac{du}{dx} - \frac{\omega_{ci}\varepsilon\sqrt{\hat{\alpha}}l_{mix}^2}{|\omega^\star|^{3/2}}\frac{dn}{dx} \tag{4.32b}$$

$$\sqrt{\varepsilon}_{hydro} = \frac{l_{mix}^2}{\sqrt{|\omega^\star|\hat{\alpha}}}\left(\frac{dn}{dx} - \frac{du}{dx}\right)^2 \tag{4.32c}$$

in the hydrodynamic limit.

An examination of the turbulence suppression criterion R_{DT}, previously introduced in ref. [HDAT17] as:

$$R_{DT} = \frac{\int \partial_x \langle \tilde{v}_x \nabla^2 \tilde{\phi} \rangle \nabla \bar{v}_y dx}{-\int \langle \tilde{n}\tilde{v}_x \rangle dx}, \tag{4.33}$$

shows that R_{DT} decreases in the hydrodynamic limit. Here R_{DT} is interpreted as the ratio of the turbulent enstrophy destruction rate $1/\tau_{transfer}$ due to coupling to the zonal flow through the vorticity flux or the Reynolds stress, as compared the turbulent enstrophy production rate $1/\tau_{relax}$ due to the relaxation of the density gradient. In the hydrodynamic limit, $1/\tau_{transfer}$ decreases because zonal flow production weakens.

4.6 Fate of Zonal Flows in the Hydrodynamic Limit $\alpha \ll 1$

Numerical analyses of bifurcation phenomena in the resistive DW turbulence of the HW model show an enhancement of turbulence and a collapse of the zonal flows for hydrodynamic plasma electrons [NBD07]. As α decreases, the ratio of the kinetic energy of the zonal flow ($F \equiv 1/2\int(\partial\langle\phi\rangle/\partial x)^2 dxdy$) to the total kinetic energy ($E^k \equiv 1/2\int|\nabla\phi|^2 dxdy$) decreases, showing a transition of the plasma to a turbulence dominated state. In other words, when α drops below unity, zonal flows collapse and turbulent fluctuations are enhanced. To explain these observations,

we present a series of arguments that illustrate the sequence of events leading to the enhancement of turbulence and to the collapse of the shear layer in the hydrodynamic electron limit.

4.6.1 Physical Picture: Energy-Momentum Flux Physics

A useful insight into why zonal flow production is weaker in the hydrodynamic regime than in the adiabatic limit may be gleaned from the wave dispersion relation. In the adiabatic regime, the standard drift wave dispersion relation directly links radial propagation (related to group velocity) to Reynolds stress $\langle \tilde{v}_x \tilde{v}_y \rangle$. In this limit, $|\omega^r| \gg |\gamma_m|$, suggesting the range of wave propagation is large. The expression for the Reynolds stress is:

$$\langle \tilde{v}_x \tilde{v}_y \rangle = \sum_k i k_r i k_m \frac{c^2}{B^2} |\tilde{\phi}_k|^2 = -\sum_k k_r k_m \frac{c^2}{B^2} |\tilde{\phi}_k|^2 \tag{4.34}$$

where k_r and k_m are the radial and azimuthal wavenumbers, respectively. The wave energy density flux $\langle v_{gr} \varepsilon \rangle$ is obtained by multiplying the group velocity $v_{gr} = -2\rho_s^2 k_r k_m v_d / (1 + k_\perp^2 \rho_s^2)^2$ by the energy:

$$\begin{aligned} \langle v_{gr} \varepsilon \rangle &= \sum_k -2\rho_s^2 \frac{k_r k_m v_d}{(1 + k_\perp^2 \rho_s^2)^2} \times (1 + k_\perp^2 \rho_s^2) \Big(\frac{e\tilde{\phi}}{T_e} \Big)^2 \frac{\rho_s^2 c_s^2}{2} \\ &= \sum_k -\rho_s^4 c_s^2 \Big(\frac{e\tilde{\phi}}{T_e} \Big)^2 \frac{k_r k_m v_d}{1 + k_\perp^2 \rho_s^2} \end{aligned}$$

With the electron diamagnetic velocity $v_d < 0$ and the group velocity $v_{gr} > 0$ (by causality for $r > r_0$), the correlator $k_r k_m$ must be positive. The momentum flux is thus $\langle \tilde{v}_x \tilde{v}_y \rangle < 0$, while the energy flux is $\langle v_{gr} \varepsilon \rangle > 0$. The causality relation implies a counter flow spin-up, suggesting that for outgoing wave energy flux, there exists an incoming wave momentum flux, as shown in Fig.4.1.

In the hydrodynamic regime, however, the link of wave energy flux to Reynolds stress is

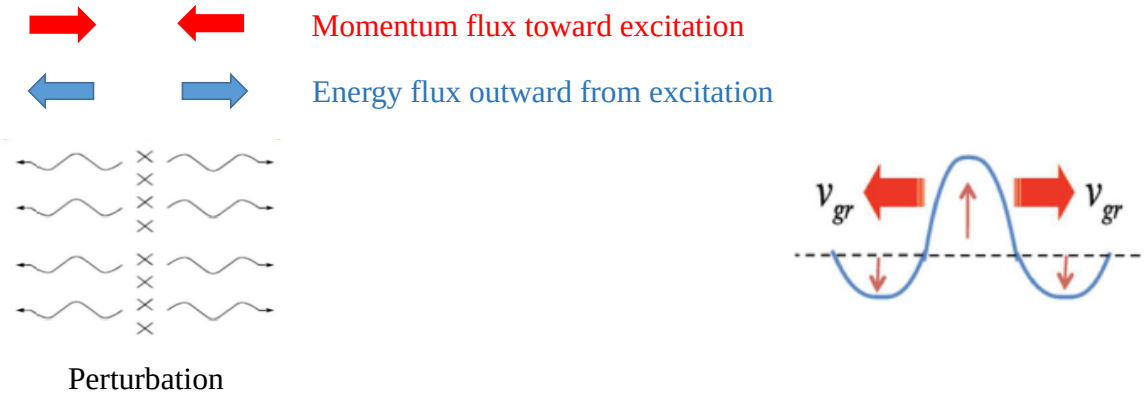

Figure 4.1: Outgoing wave energy flux and incoming momentum flux from/to perturbation.

broken. The momentum flux is still given by eq.(4.34), but the group velocity v_{gr} is:

$$v_{gr} = \frac{\partial \omega^r_{hydro}}{\partial k_r} = -\frac{k_r}{k_\perp^2}\omega^r_{hydro}$$

Note that here that causality has no implication for $\langle k_m k_r \rangle$, and thus for the momentum flux, since v_{gr} is independent of k_m (the wavenumber in the direction of symmetry). In the hydrodynamic limit, there is no causality constraint on eddy tilting, so the familiar tilt and stretch mechanism in not effective. Moreover, the waves have $|\omega^r| = |\gamma_m|$, suggesting limited propagation.

4.6.2 Scalings of Transport Fluxes with α

When the adiabaticity parameter α decreases below unity, the system passes from the adiabatic to the hydrodynamic regime. According to the scalings of eqs.(4.20) and eqs.(4.24), the particle flux scaling changes from $\Gamma_{adia} \propto 1/\alpha$ with $\alpha > 1$ to $\Gamma_{hydro} \propto \sqrt{1/\alpha}$ with $\alpha < 1$. The turbulent diffusivity χ_y that relates the vorticity flux to the vorticity gradient also exhibits the same scaling. The residual stress on the other hand, drops from $\Pi^{res}_{adia} \propto 1/\alpha$ to $\Pi^{res}_{hydro} \propto \sqrt{\alpha}$. Scalings of the transport fluxes are summarized in table (4.1). An interpretation of the analytical results shows that the Reynolds power (which generates the zonal flow underlying suppression)

Plasma Response	**Adiabatic** $\alpha \gg 1$	**Hydrodynamic** $\alpha \ll 1$
Turbulent enstrophy $\sqrt{\varepsilon}$	$\sqrt{\varepsilon} \propto 1/\alpha$	$\sqrt{\varepsilon} \propto 1/\sqrt{\alpha}$
Particle Flux Γ	eq.(4.20a) $\Gamma \propto 1/\alpha$	eq.(4.24a) $\Gamma \propto 1/\sqrt{\alpha}$
Turbulent Viscosity χ_y	eq.(4.20b) $\chi_y \propto 1/\alpha$	eq.(4.24b) $\chi_y \propto 1/\sqrt{\alpha}$
Residual Stress Π^{res}	eq.(4.20c) $\Pi^{res} \propto -1/\alpha$	eq.(4.24c) $\Pi^{res} \propto -\sqrt{\alpha}$
$\frac{\Pi^{res}}{\chi_y} = (\omega_{ci}\nabla\bar{n})\times$	$\left(\frac{\alpha}{\lvert\omega^\star\rvert}\right)^0$	$\left(\frac{\alpha}{\lvert\omega^\star\rvert}\right)$

Table 4.1: Scalings of the turbulent enstrophy ε, transport fluxes and vorticity gradient with α in both adiabatic and hydrodynamic regimes.

drops with α. In the absence of external momentum sources and for turbulence, the diffusive vorticity flux stress balances the residual stress. The mean vorticity gradient shown in Fig.4.2 then equals:

$$-\chi_y \frac{d^2\bar{v}_y}{dx^2} + \Pi^{res} = 0 \Longrightarrow \frac{d\nabla\bar{v}_y}{dx} = \frac{\Pi^{res}}{\chi_y} \tag{4.36}$$

In the adiabatic limit, the ratio between the residual stress and the turbulent viscosity is independent of α. In the hydrodynamic limit, Π^{res}/χ_y is directly proportional to α. As the plasma transitions from an adiabatic to a hydrodynamic regime, the residual stress Π^{res} weakens, while the turbulent diffusivity χ_y increases. As a result, the ratio Π^{res}/χ_y - which indicates the plasma capacity to produce mesoscopic flows - drops. When the plasma production of zonal

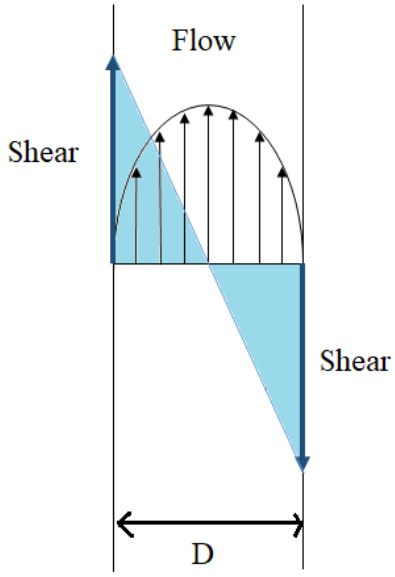

Figure 4.2: A jump in the flow shear (in blue) over a scale length D is equivalent to a vorticity gradient on that scale.

flows drops, turbulence is not effectively regulated and anomalous transport increases.

4.6.3 Potential Vorticity Mixing and Zonal Shear Collapse

It is useful to examine the flow generation in the adiabatic and hydrodynamic regimes from the perspective of potential vorticity (PV) dynamics. The key concept here is that zonal flows are formed as a consequence of PV mixing [Hor99], which in a system with mean inhomogeneity, necessitates trade-offs between mean and fluctuating PV. The classic example follows from the observation that for a rotating flow, the total vorticity: $\vec{\omega} + 2\vec{\Omega}$ is frozen in to the fluid. If $\vec{\Omega} = \vec{\Omega}(\mathbf{x})$ changes (due, say, to a variation in the axis of rotation through the plane of motion), a displacement of a mean vortex element in latitude forces a conversion of planetary vorticity ($\approx 2\vec{\Omega}$) to local flow vorticity ($\approx \vec{\omega}$), in order to conserve PV. This produces a change in vorticity, while conserving total PV. This reasoning is the underpinning of the β plane model,

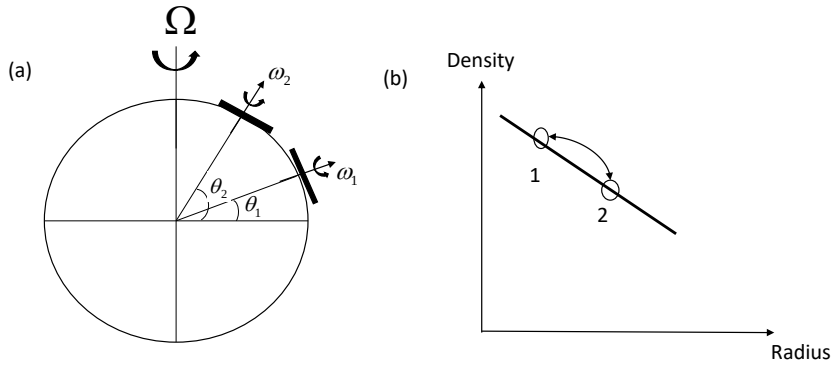

Figure 4.3: Analogy of PV conservation in geostrophic waves and drift waves: (a) change in local vorticity $\vec{\omega}$ of a fluid element between θ_1 and θ_2 forces a flow generation, (b) density variation along the ∇n line from position 1 to position 2 triggers a change in the flow (i.e., vorticity) so to conserve q.

for which the potential vorticity:

$$q = \nabla_\perp^2 \phi + \beta y$$

is conserved. That statement yields the familiar governing equation which is:

$$\partial_t \nabla_\perp^2 \phi + \nabla_\perp \phi \times \hat{z}.\nabla_\perp(\nabla_\perp^2 \phi) = -\beta V_y \tag{4.37}$$

In the Hasegawa-Wakatani system, the conserved PV is: $\ln(n) - \nabla^2\phi$ which may be expanded to:

$$q = \ln(n_0(x)) + \frac{\tilde{n}}{n_0} - \rho_s^2 \nabla^2 \left(\frac{|e|\phi}{T_e} \right)$$

Since $\tilde{n}/n_0 = |e|\tilde{\phi}/T_e + h$, it follows that:

$$q = \ln(n_0(x)) + \frac{|e|\tilde{\phi}}{T_e} + h - \rho_s^2 \nabla^2 \left(\frac{|e|\phi}{T_e} \right)$$

so that Γ_q, the PV flux, is equal to:

$$\Gamma_q = \langle \tilde{v}_x h \rangle - \rho_s^2 \left\langle \tilde{v}_x \nabla_\perp^2 \left(\frac{|e|\tilde{\phi}}{T_e} \right) \right\rangle \tag{4.38}$$

Observe that the adiabatic part of the density perturbation makes no contribution to the net PV flux or mixing. In the HW system, the displacement of a mean density element (analogous to the displacement of an element of planetary vorticity) induces a particle flux and a Reynolds force (from the vorticity flux), which drives a zonal flow. The latter follows from Taylor identity, assuming poloidal symmetry. Now in the adiabatic limit, density and vorticity fluctuations are tightly coupled. Indeed, both particle and vorticity fluctuations are proportional to $\alpha \gg 1$. Thus, it is not surprising that both particle flux and residual stress (i.e., the non-viscous component of the Reynolds force) scale identically ($\sim 1/\alpha$) and so zonal flows are robust. Both the particle flux and the vorticity flux support the PV flux. However, in the hydrodynamic regime, coupling of particle and PV fluctuations is weak ($\sim O(\alpha)$ with $\alpha < 1$), so the respective fluxes can decouple. The PV flux is supported primarily by the particle flux $\Gamma_n \sim 1/\sqrt{\alpha}$, while the residual stress $\Pi^{res} \sim \sqrt{\alpha}$ is insignificant, with $\alpha \ll 1$. Thus the non-diffusive Reynolds force drops with α, and so does flow production. Finally, the zonal vorticity gradient, an indication of the flow production, is proportional to α, suggesting that zonal flows and turbulence regulation are weak in the hydrodynamic regime. This is consistent with the findings of several numerical simulations, which note that zonal flows are robust for adiabatic electrons, but do not appear in the hydrodynamic regime [CBS95, KT13, NBD07]. However, PV mixing (resulting from convective cell instability) persists in the hydrodynamic regime, but it is supported primarily by the particle flux.

4.7 Relevance to Density Limit n_G

The Greenwald density limit n_G is an operational bound on the plasma density and pressure. It represents the maximum attainable density before the plasma develops strong disruptions and MHD activity [GTW$^+$88, Gre02]. Experiments in various toroidal devices including a recent experiment in the HL-2A tokamak [HTD$^+$18], indicate a reduction of the edge

shear flow layer and a strong enhancement of turbulent particle transport as $\bar{n} \rightarrow n_G$. The shearing rate of the mean $E \times B$ flow $\omega_{sh} = \nabla v_\theta$ drops, and the turbulent Reynolds power collapses in those ohmic L-mode discharges approaching n_G. In addition, both the core plasma density and the edge turbulent particle flux $\langle \tilde{v}_x \tilde{n} \rangle$ increase with $\bar{n}$. Meanwhile the cross-correlation between the velocity and the density fluctuations grows substantially inside the separatrix. The core plasma temperature T_e on the other hand, decreases with $\bar{n}$. Most importantly, the adiabaticity parameter α drops from 3 to 0.5 as $\bar{n}$ approaches n_G [HTD$^+$18]. Note that in this particular HL-2A experiment, the plasma $\beta = 2\mu_0 p_e / B^2$ was very low, in the range: $0.01 < \beta < 0.02$.

The aforementioned experimental findings can be interpreted according to the scalings of Section 4.6. When the local edge plasma density increases, the adiabaticity parameter α ($\propto 1/\bar{n}$) decreases below unity, thereby triggering a plasma transition from the adiabatic to the hydrodynamic drift wave regime. According to the scalings of the previous section, this transition is associated with an increase in the turbulent particle flux and turbulence. Consistent with this, the mean vorticity gradient $d\nabla\bar{v}_y/dx = \Pi^{res}/\chi_y$ drops. The production of zonal flows thus declines, so turbulence is no longer regulated effectively. Particle transport increases. So does the thermal diffusivity, as particle and heat losses are comparable for the case of collisional drift waves. Cooling of the edge plasma is triggered. For constant pressure p_e, this leads to a further increase in the density $\bar{n}$. A feedback loop between $\bar{n}$ and T_e is thus formed when α drops below unity. The provided scenario is summarized in fig.(4.4).

The uniqueness of this interpretation relies in considering the decrease of α below unity as the trigger for the drop in zonal flow production. Such interpretation does not require appeal to zonal flow damping effects, which are associated with collisionality, charge exchange etc. Most importantly, in contrast to ref. [RDZ98], which postulates the development of turbulence as due to yet another linear instability - such as the resistive ballooning mode - the current approach explains how variations of α affect the mean and turbulent plasma profiles within the context of generic drift wave theory. This mechanism is applicable to plasmas at low β, like that of the

HL-2A experiment [HTD+18], where resistive ballooning effects are not relevant.

4.8 Conclusion

This paper presents a theory of the collapse of a zonal shear layer in the hydrodynamic electron limit. It elucidates the evolution of the plasma flow and turbulence, as the electron response passes from the adiabatic to the hydrodynamic limit. In particular, the paper describes the variation of the turbulent fluxes and mean profiles with the adiabaticity parameter $\alpha = k_z^2 v_{th}^2/(\nu_{ei}|\omega|)$. The key result of this paper is its explanation of why the zonal shear layer weakens and disappears when the adiabaticity parameter drops below unity, and so allows an enhanced level of turbulence. Moreover, the paper highlights the importance of the ZF collapse in the hydrodynamic limit ($\alpha < 1$) as a key parameter and a general scenario for turbulence enhancement, even for plasmas with low β. We give a theoretical interpretation of the experimental and numerical results obtained in the hydrodynamic plasma limit. Findings of this paper are applicable to low β density limit experiments, where a weakening of the edge shear layer and a degradation of the thermal confinement are obtained when the plasma density increases sufficiently so that $\alpha < 1$.

The paper presents a 1D reduced model that self-consistently describes the spatiotemporal evolution of the mean density $\bar{n}$, the azimuthal flow $\bar{v}_y$, as well as the potential enstrophy $\varepsilon = \langle(\tilde{n} - \tilde{u})^2\rangle/2$. The model is derived from the Hasegawa-Wakatani system for turbulent drift waves, and exploits conservation of PV to constrain the relation between drift waves and zonal flows. Key results of this paper are:

1. The particle flux Γ_n and the vorticity flux Π are calculated as: $\Gamma_n = -D\nabla\bar{n}$ and $\Pi = -\chi_y \nabla^2 \bar{v}_y + \Pi^{res}$. The vorticity flux is related to the Reynolds force via the Taylor identity. Quasi-linear analysis shows that the scalings of Γ_n and Π with α change as the plasma passes from the adiabatic to the hydrodynamic limit. These scalings are summarized in

table (4.1), and reveal the enhancement of the particle flux Γ_n and the turbulent viscosity χ_y as α decreases. The residual stress Π^{res} on the other hand drops with α for $\alpha \ll 1$ as $\Pi^{res}_{hydro} \propto \sqrt{\alpha}$.

2. Variations in the turbulent fluxes are responsible for the change in the mesoscopic flow dynamics. When α drops, the mean vorticity gradient $d(\nabla \bar{v}_y)/dx = \Pi_{res}/\chi_y$ - which characterizes the zonal flow and the state of turbulence in the plasma - also drops. In the adiabatic limit, the mean vorticity gradient is independent of α. However, in the hydrodynamic limit, Π^{res}/χ_y is proportional to α, indicating weakened production of zonal flows for lower α. As the production of zonal flows decreases, the mechanism of self-regulation fails, and the turbulence intensity rises.

3. The findings of this paper illuminate the physics of the density limit. When the plasma density increases, the adiabaticity parameter decreases ($\alpha \propto 1/\bar{n}$). According to the scalings derived in Section 4.6, a decrease in the mean vorticity gradient results when $\bar{n}$ increases such that $\alpha \ll 1$. In this case, the *efficiency of the zonal flow production* drops. Thermal and particle losses thus increase, and the cross phase between the velocity and the density fluctuations also increases [HTD$^+$18]. Cooling of the plasma edge is then triggered causing T_e to drop further. Feedback between $\bar{n}$ and T_e is triggered. This mechanism does not invoke additional linear instabilities, such as resistive ballooning modes (in contrast to ref. [RDZ98]). This is particularly significant for discharges at low β, such as the experiment in ref. [HTD$^+$18].

4. Important results in this paper are the expressions for the fluxes Γ and Π. These expressions can be used to model the gradual plasma transition from the adiabatic to the hydrodynamic limit. While previous work simply presented numerical observations of the enhancement of turbulence [KT13, NBD07], as well as confirmation of the various power scaling laws of the turbulence energies in the hydrodynamic limit [GG15], no papers covering a complete

transition from one limit to the other are presented. The underlying physics was not explained.

5. The paper gives a simple physical picture of why ZF production drops in the hydrodynamic electron regime. There the dispersion relation is $\omega_r^{hydro} = \sqrt{\omega^\star \hat{\alpha}/(2k_\perp^2 \rho_s^2)}$, so $v_{gr} = -k_r \omega^r_{hydro}/k_\perp^2$. These are in contrast to the adiabatic case, for which $\omega_r^{adia} = \omega^\star(1 + k_\perp^2 \rho_s^2)^{-1}$ and $v_{gr} = -2\rho_s^2 k_r k_m v_d/(1 + k_\perp^2 \rho_s^2)^2$. Thus, in the hydrodynamic regime, the condition of outgoing waves ($v_{gr} > 0$) does not constrain the Reynolds stress $\langle \tilde{v}_x \tilde{v}_y \rangle \simeq \langle k_r k_m \rangle$, thus breaking the link between wave propagation and Reynolds stress. This link is fundamental to ZF production by DWs.

6. The paper explains why turbulence is enhanced in the hydrodynamic limit, and ascertains the physics of the Reynolds stress in regulating the drift wave - zonal flow relation. We show that PV mixing in the hydrodynamic electron limit is supported by the particle flux, i.e., $\langle \tilde{v}_x \tilde{q} \rangle = \langle \tilde{v}_x h \rangle - \langle \tilde{v}_x \nabla^2 \tilde{\phi} \rangle \simeq \langle \tilde{v}_x h \rangle$. The vorticity flux drops and the particle flux rises with α in this regime. This explains why zonal flow formation is weak in the hydrodynamic regime.

Future work includes numerical investigation of the slow evolution of a plasma transition from one limit to the other. Moreover, it would be instructive to investigate experimentally the causality relation between the drop in α and the drop in ZF production. In particular, it is useful to determine what occurs first. This would probe the predictions of the theory. One suggestion would be to verify the decrease of the calculated total Reynolds work, as $\bar{n}/n_G$ is raised. When the total Reynolds work decreases, energy transfer to the mean flow structures drops, so the fluctuations should grow. Another possible experiment consists of increasing the plasma density $\bar{n}$ and temperature T_e, such that the adiabaticity parameter $\alpha \propto T_e^{5/2}/\bar{n}$ remains constant (assuming the variations of the Coulomb logarithm are negligible). According to the theory presented above, no collapse of the zonal shear layer should be observed, simply because

α does not change. One can also investigate the contribution of collisional damping effects by comparing the response with and without the damping factor. This is particularly useful to confirm the pivotal role of the Reynolds stress in the collapse of the zonal shear layer at the density limit. Additional work also should include investigation of the role of high edge ∇p and high β values in H-modes on the enhancement of turbulence and profile evolution in density limit experiments.

4.9 Acknowledgments

The text and data in chapter 4 is a reprint of the material as currently being prepared for submission for publication in Zonal Shear Layer Collapse in the Hydrodynamic Electron Limit in the Journal of Physics of Plasmas 2018. Hajjar R. J., Diamond P. H., Malkov M., American Institute of Physics, 2018. The dissertation author was the primary investigator and author of this paper.

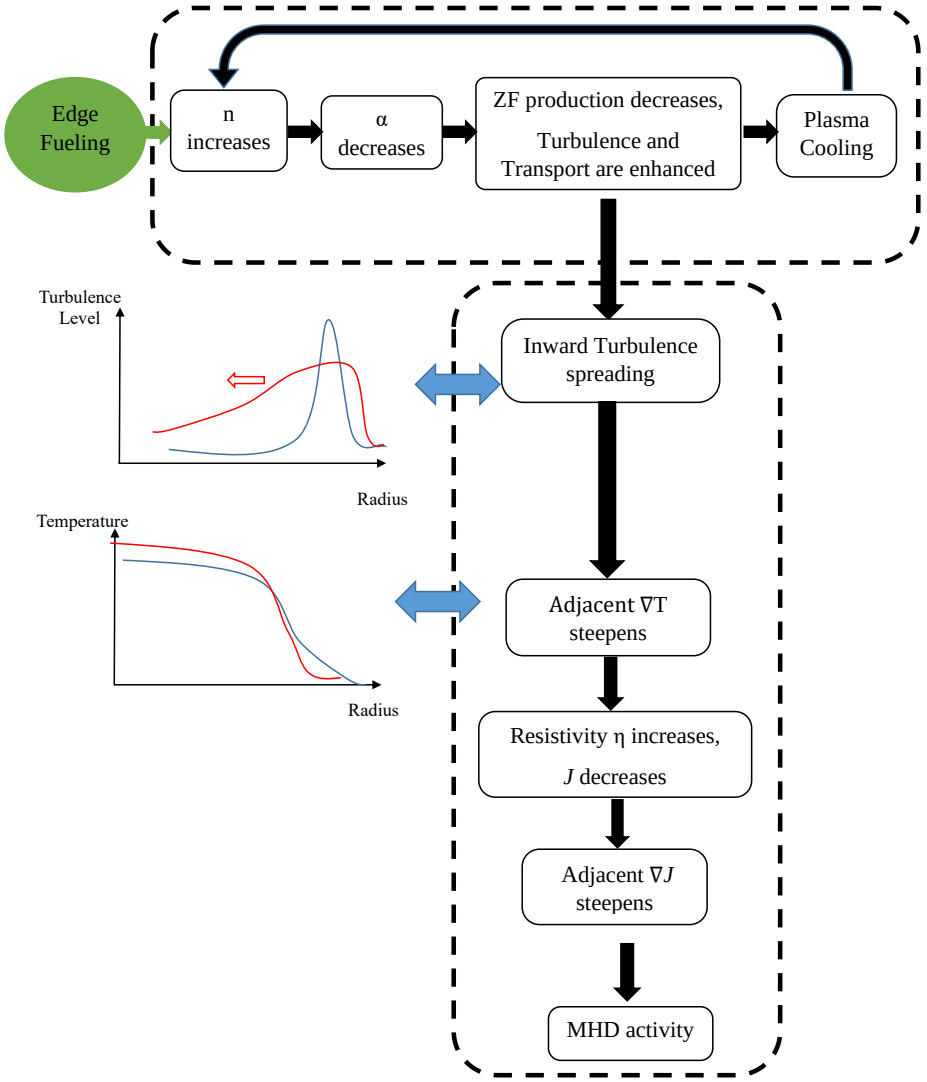

Figure 4.4: Profile evolution in the hydrodynamic limit. The diagram shows a feedback loop between the density and temperature via variations of α. A potential path for the development of MHD modes is also indicated. Inward turbulence spreading and steepening of adjacent ∇T from a state ① (in blue) to a state ② (in red) are shown on the left.

Chapter 5

SUMMARY AND FUTURE DIRECTIONS

In this dissertation, the relationship between the microscopic drift wave turbulence and the macroscopic zonal (perpendicular) and axial (parallel) flows was investigated. The dissertation included a presentation of two analytical reduced models, as well as some simulation results that validate and verify the previously published experimental data obtained from CSDX linear plasma. In addition, one of these models explains the collapse of the zonal shear layer in the plasma hydrodynamic electron limit closely related to the density limit experiments performed on HL-2A tokamak. The models formulated in this dissertation are 1D (in radius) reduced models that describe the physics of a multi-scale plasma. Such models are appropriate and essential to understand the physics behind the feedback loops that exist between the microscopic level and the macroscopic level in a multi-scale plasma. Moreover, reduced models generally provide a better and more elaborate physical interpretation of the experimental results than Direct Numerical Simulations (DNS), which have a high computational cost, and often fail to provide a detailed insight into the actual physics of the plasma. Most importantly, reduced models such as the ones presented in this dissertation can be easily coupled to other models

in the framework of future Plasma Material Interaction (PMI) studies. Such models provide a useful new intermediate approach for the simulation of self-consistent evolution edge and SOL plasma profiles, transverse and parallel flows and turbulence, and would allow the study of main plasma and impurity dynamics across timescales ranging from a few turbulent correlation times up to system equilibrium timescales. When modified to include toroidal and open-field line effects, and extended to a 2D geometry along the magnetic field and binormal directions, the proposed models bridge the gap between the existing time averaged fluid codes of the edge and SOL region of confinement device, and fully turbulent direct numerical simulations. Here DNS self-consistently capture the evolution of the plasma profile and its flow, but are computationally expensive to use for long time scales. Such a new capability might be useful to study the entrainment and transport of eroded wall impurities in flowing edge and SOL plasma, and the long-time migration of these materials in the SOL and divertor regions of confinement devices. This dissertation sought to investigate three topics:

1. How are axial flows generated in CSDX plasma, and is there a direct relation between the axial and the perpendicular flow dynamics in the adiabatic plasma of CSDX? Moreover, what is the analytical framework that describes the energy transfer between the flows and turbulence in CSDX? (Chapter 2)

2. What is the appropriate analytical model that describes the turbulent potential energy exchange between drift wave turbulence and zonal flows in CSDX plasma? (Chapter 3)

3. How is the predator/prey relation between drift waves and zonal flows previously discussed in Chapter 2 and 3 affected in the hydrodynamic electron limit? (Chapter 4)

The conclusions reached after investigating each topic are presented at the end of each chapter. In summary, the dissertation presents a comprehensive description of the theory behind the drift wave turbulence and both zonal and axial flows. The presented numerical results highlight the crucial role the Reynolds stresses play in regulating turbulence. Not only does this dissertation

formulate appropriate reduced models that describe the interactions between the mean profiles and the fluctuations in the adiabatic electron limit, but also extends this description to the hydrodynamic electron limit. The latter describes the behavior and dynamics of a plasma characterized by a high density and low temperature. The constants introduced in Chapter 2 (σ_{VT}) and Chapter 3 (R_{DT}) are novel criteria that describe parallel to perpendicular flow coupling, as well as suppression of drift wave turbulence by the zonal flows.

In addition to what was presented in this dissertation, recommended future work includes:

1. Performing numerical simulations of the comprehensive model presented in Chapter 2, and analyzing the numerical data in order to pinpoint the parallel to perpendicular flow coupling in CSDX. It is thus recommended to calculate a numerical value for the coupling constant σ_{VT} from the simulation profiles, and compare it to the value recovered from the experimental data. In addition, it is also useful to perform numerical studies for the slaved 2-field model also presented in Chapter 2.

2. Adding an axial momentum source to the model of Chapter 2, in an attempt to mimic the torque exerted on the plasma in toroidal devices. Adding an axial momentum source to the model could be used to compare the relative magnitude of the intrinsic parallel flows to the externally imposed ones. This is particularly helpful for studying the scaling of the parallel intrinsic flow with the plasma characteristics in future plasma devices.

3. Simulating a full and complete plasma transition from the adiabatic to the hydrodynamic limit. Such step is essential to characterize the changes in the mean and turbulent profiles of the plasma. The numerical results should be ultimately compared to the experimental data retrieved from various toroidal devices.

4. A study of the evolution of the plasma temperature, in addition to the variations in density and flow as presented in Chapter 4. Accounting for temperature variations aims at exploring the predator/prey relation in H-mode hydrodynamic limit plasmas.

5. Accounting for the effects of both charge-exchange reactions, as well as the ion-neutral collisions in a hydrodynamic plasma. This step aims at studying the importance of collisional zonal flow damping from a numerical perspective.

Bibliography

[AD16] A. Ashourvan and P. H. Diamond. How mesoscopic staircases condense to macroscopic barriers in confined plasma turbulence. Phys. Rev. E, 94:051202, 2016.

[ADG16] A. Ashourvan, P. H. Diamond, and O. D. Gurcan. Transport matrix for particles and momentum in collisional drift waves turbulence in linear plasma devices. Physics of Plasmas, 23(2), 2016.

[AKI+09] H. Arakawa, K. Kamataki, S. Inagaki, T. Maruta, Y. Nagashima, T. Yamada, S. Shinohara, K. Terasaka, S. Sugita, M. Yagi, Nl Kasuya, Al Fujisawa, S-I. Itoh, and K. Itoh. Observations of abrupt changes in the fluctuation spectrum on LMD-U. Plasma Physics and Controlled Fusion, 51(8):085001, 2009.

[AYT07] G. Y. Antar, J. H. Yu, and G. Tynan. The origin of convective structures in the scrape-off layer of linear magnetic fusion devices investigated by fast imaging. Physics of Plasmas, 14(2), 2007.

[BDT90] H. Biglari, P. H. Diamond, and P. W. Terry. Influence of sheared poloidal rotation on edge turbulence. Physics of Fluids B: Plasma Physics, 2(1):1–4, 1990.

[BLSY98] N. J. Balmforth, S. G. Llewellyn Smith, and W. R. Young. Dynamics of interfaces and layers in a stratified turbulent fluid. Journal of Fluid Mechanics, 355:329–358, 1 1998.

[BMT12] L. Biferale, S. Musacchio, and F. Toschi. Inverse energy cascade in three-dimensional isotropic turbulence. Phys. Rev. Lett., 108:164501, Apr 2012.

[BTA+05] M. J. Burin, G. R. Tynan, G. Y. Antar, N. A. Crocker, and C. Holland. On the transition to drift turbulence in a magnetized plasma column. Physics of Plasmas, 12(5), 2005.

[CAT+16] L. Cui, A. Ashourvan, S. C. Thakur, R. Hong, P. H. Diamond, and G. R. Tynan. Spontaneous profile self-organization in a simple realization of drift-wave turbulence. Physics of Plasmas, 23(5), 2016.

[CBS95] S. J. Camargo, D. Biskamp, and B. D. Scott. Resistive drift-wave turbulence. Physics of Plasmas, 2(1):48–62, 1995.

[Che84] F. F. Chen. Plasma Physics and Controlled Fusion. Plenum Press, New York, 1984.

[CLGD93] B. A. Carreras, V. E. Lynch, L. Garcia, and P. H. Diamond. Resistive pressure gradient driven turbulence with self consistent flow profile evolution. Physics of Fluids B, 5(5):1491–1505, 1993.

[CTD+15] L. Cui, G. R. Tynan, P. H. Diamond, S. C. Thakur, and C. Brandt. Up-gradient particle flux in a drift wave-zonal flow system. Physics of Plasmas, 22(5), 2015.

[DGH+08] P. H. Diamond, O. D. Gurcan, T. S. Hahm, K. Miki, Y. Kosuga, and X. Garbet. Momentum theorems and the structure of atmospheric jets and zonal flows in plasmas. Plasma Physics and Controlled Fusion, 50(12):124018, 2008.

[DIIH05] P. H. Diamond, S. I. Itoh, K. Itoh, and T. S. Hahm. Zonal flows in plasma; a review. Plasma Physics and Controlled Fusion, 47(5):R35–R161, 2005.

[DKG+13] P.H. Diamond, Y. Kosuga, .D. Grcan, C.J. McDevitt, T.S. Hahm, N. Fedorczak, J.E. Rice, W.X. Wang, S. Ku, J.M. Kwon, G. Dif-Pradalier, J. Abiteboul, L. Wang, W.H. Ko, Y.J. Shi, K. Ida, W. Solomon, H. Jhang, S.S. Kim, S. Yi, S.H. Ko, Y. Sarazin, R. Singh, and C.S. Chang. An overview of intrinsic torque and momentum transport bifurcations in toroidal plasmas. Nuclear Fusion, 53(10):104019, 2013.

[DLCT94] P. H. Diamond, Y.-M. Liang, B. A. Carreras, and P. W. Terry. Self-regulating shear flow turbulence: A paradigm for the l to h transition. Phys. Rev. Lett., 72:2565–2568, Apr 1994.

[DMG+09] P. H. Diamond, C.J. McDevitt, .D. Grcan, T.S. Hahm, W. X. Wang, E.S. Yoon, I. Holod, Z. Lin, V. Naulin, and R. Singh. Physics of non-diffusive turbulent transport of momentum and the origins of spontaneous rotation in tokamaks. Nuclear Fusion, 49(4):045002, 2009.

[EHH+10] T. Estrada, T. Happel, C. Hidalgo, E. Ascasbar, and E. Blanco. Experimental observation of coupling between turbulence and sheared flows during L-H transitions in a toroidal plasma. EPL (Europhysics Letters), 92(3):35001, 2010.

[FII+04] A. Fujisawa, K. Itoh, H. Iguchi, K. Matsuoka, S. Okamura, A. Shimizu, T. Minami, Y. Yoshimura, K. Nagaoka, C. Takahashi, M. Kojima, H. Nakano, S. Ohsima, S. Nishimura, M. Isobe, C. Suzuki, T Akiyama, K. Ida, K. Toi, S.-I. Itoh, and P. H. Diamond. Identification of zonal flows in a toroidal plasma. Phys. Rev. Lett., 93:165002, Oct 2004.

[Gar01] X. Garbet. Turbulence in fusion plasmas: key issues and impact on transport modelling. Plasma Physics and Controlled Fusion, 43(12A):A251, 2001.

[GDH06] Ö. D. Grcan, P. H. Diamond, and T. S. Hahm. Radial transport of fluctuation energy in a two-field model of drift-wave turbulence. Physics of Plasmas, 13(5):052306, 2006.

[GDH07] Ö. D. Gurcan, P. H. Diamond, and T. S. Hahm. Spatial and spectral evolution of turbulence. Physics of Plasmas, 14(5), 2007.

[GDH08] Ö. D. Gurcan, P. H. Diamond, and T. S. Hahm. Turbulent equipartition and homogenization of plasma angular momentum. Phys. Rev. Lett., 100:135001, Apr 2008.

[GDHS07] Ö. D. Gurcan, P. H. Diamond, T. S. Hahm, and R. Singh. Intrinsic rotation and electric field shear. Physics of Plasmas, 14(4):042306, 2007.

[GG15] K. Ghantous and Ö. D. Gürcan. Wave-number spectrum of dissipative drift waves and a transition scale. Phys. Rev. E, 92:033107, 2015.

[GKP+03] P. Gohil, J. Kinsey, V. Parail, X. Litaudon, T. Fukuda, T. Hoang, for the ITPA Group on Transport, ITB Physics: J. Connor, E.J. Doyle, Yu. Esipchuk, T. Fujita, T. Fukuda, P. Gohil, J. Kinsey, S. Lebedev, X. Litaudon, V. Mukhovatov, J. Rice, E. Synakowski, K. Toi, B. Unterberg, V. Vershkov, M. Wakatani, J. Weiland, for the International ITB Database Working Group: T. Aniel, Yu.F. Baranov, E. Barbato, A. Bcoulet, C. Bourdelle, G. Bracco, R.V. Budny, P. Buratti, E.J. Doyle, L. Ericsson, Yu. Esipchuk, B. Esposito, T. Fujita, T. Fukuda, P. Gohil, C. Greenfield, M. Greenwald, T. Hahm, T. Hellsten, T. Hoang, D. Hogeweij, S. Ide, F. Imbeaux, Y. Kamada, J. Kinsey, N. Kirneva, X. Litaudon, P. Maget, A. Peeters, K. Razumova, F. Ryter, Y. Sakamoto, H. Shirai, G. Sips, T. Suzuki, E. Synakowski, and T.Takizuka. Increased understanding of the dynamics and transport in itb plasmas from multi-machine comparisons. Nuclear Fusion, 43(8):708, 2003.

[GmcHP+06] B. Gonçalves, C. Hidalgo, M. A. Pedrosa, R. O. Orozco, E. Sánchez, and C. Silva. Role of turbulence on edge momentum redistribution in the tj-ii stellarator. Phys. Rev. Lett., 96:145001, Apr 2006.

[Gre02] M. Greenwald. Density limits in toroidal plasmas. Plasma Phys. Control. Fusion, 44:R27, 2002.

[GTA+99] A. M. Garofalo, A. D. Turnbull, M. E. Austin, J. Bialek, M. S. Chu, K. J. Comer, E. D. Fredrickson, R. J. Groebner, R. J. La Haye, L. L. Lao, E. A. Lazarus, G. A. Navratil, T. H. Osborne, B. W. Rice, S. A. Sabbagh, J. T. Scoville, E. J. Strait, and T. S. Taylor. Direct observation of the resistive wall mode in a tokamak and its interaction with plasma rotation. Phys. Rev. Lett., 82:3811–3814, May 1999.

[GTW+88] M. Greenwald, J. L. Terry, S. M. Wolfe1, S. Ejima, M. G. Bell, S. M. Kaye, and G.H. Neilson. Nuclear Fusion, 28:2199, 1988.

[HB95] T. S. Hahm and K. H. Burrell. Flow shear induced fluctuation suppression in finite aspect ratio shaped tokamak plasma. Physics of Plasmas, 2(5):1648–1651, 1995.

[HDAT17] R. J. Hajjar, P. H. Diamond, A. Ashourvan, and G. R. Tynan. Modelling enhanced confinement in drift-wave turbulence. Physics of Plasmas, 24(6):062106, 2017.

[Hin91] F. L. Hinton. Thermal confinement bifurcation and the L to H mode transition in tokamaks. Physics of Fluids B, 3(3):696–704, 1991.

[HLH+17] R. Hong, J. C. Li, R. J. Hajjar, S. Thakur, P. H. Diamond, and G. R. Tynan. Generation of parasitic axial flow by drift wave turbulence with broken symmetry: Theory and experiment. submitted to Physics of Plasmas, 2017.

[HLT+17] R. Hong, J. C. Li, S. Thakur, R. J. Hajjar, P. H. Diamond, and G. R. Tynan. Tracing the pathway from drift-wave turbulence with broken symmetry to the production of sheared axial mean flow. submitted to Physical Review Letters, 2017.

[HM77] A. Hasegawa and K. Mima. Stationary spectrum of strong turbulence in magnetized nonuniform plasma. Phys. Rev. Lett., 39:205–208, 1977.

[Hol16] C. Holland. Validation metrics for turbulent plasma transport. Physics of Plasmas, 23(6), 2016.

[Hor99] W. Horton. Drift waves and transport. Rev. Mod. Phys., 71:735–778, 1999.

[HS93] F. L. Hinton and G. M. Staebler. Particle and energy confinement bifurcation in tokamaks. Physics of Fluids B: Plasma Physics, 5(4):1281–1288, 1993.

[HTD+18] R. Hong, G.R. Tynan, P.H. Diamond, L. Nie, D. Guo, T. Long, R. Ke, Y. Wu, B. Yuan, M. Xu, and The HL-2A Team. Edge shear flows and particle transport near the density limit of the HL-2A tokamak. Nuclear Fusion, 58(1):016041, 2018.

[HW83] A. Hasegawa and M. Wakatani. Plasma edge turbulence. Phys. Rev. Lett., 50:682, 1983.

[HW87] A. Hasegawa and M. Wakatani. Self-organization of electrostatic turbulence in a cylindrical plasma. Phys. Rev. Lett., 59:1581–1584, Oct 1987.

[II96] K. Itoh and S.-I Itoh. Plasma Phys. Control. Fusion, 38:1, 1996.

[IIFY99] K. Itoh, S. I. Itoh, A. Fukuyama, and M. Yagi. Transport and structural formation in plasmas. IOP, 1999.

[IKI+16] S. Inagaki, T. Kobayashi, S. I. Itoh, T. Mitsuzono, H. Arakawa, T. Yamada, Y. Miwa, N. Kasuya, M. Sasaki, M Lesur, A. Fujisawa, and K. Itoh. A concept of cross-ferroic plasma turbulence. Scientific Reports, 6(22189), 2016.

[ite] Iter official website. https://www.iter.org/. Accessed: 2018-02-10.

[KD03] E. J. Kim and P. H. Diamond. Zonal flows and transient dynamics of the L-H transition. Phys. Rev. Lett., 90:185006, 2003.

[KDG10] Y. Kosuga, P. H. Diamond, and . D. Grcan. On the efficiency of intrinsic rotation generation in tokamaks. Physics of Plasmas, 17(10):102313, 2010.

[KII16] Y. Kosuga, S.-I. Itoh, and K. Itoh. Turbulence dynamics with the coupling of density gradient and parallel velocity gradient in the edge plasmas. Contributions to Plasma Physics, 56(6-8):511–515, 2016.

[KII17] Y. Kosuga, S.-I. Itoh, and K. Itoh. Zonal flow generation in parallel flow shear driven turbulence. Physics of Plasmas, 24(3):032304, 2017.

[KIIe5] Y. Kosuga, S-I. Itoh, and K. Itoh. Density peaking by parallel flow shear driven instability. Plasma and Fusion Research, 10:3401024–3401024, 201the5.

[KIK+16] T. Kobayashi, S. Inagaki, Y. Kosuga, M. Sasaki, Y. Nagashima, T. Yamada, H. Arakawa, N. Kasuya, A. Fujisawa, S.-I. Itoh, and K. Itoh. Structure formation in parallel ion flow and density profiles by cross-ferroic turbulent transport in linear magnetized plasma. Physics of Plasmas, 23(10), 2016.

[KJD+11] S. S. Kim, H. Jhang, P. H. Diamond, L. Terzolo, S. Yi, and T.S. Hahm. Intrinsic rotation, hysteresis and back transition in reversed shear internal transport barriers. Nuclear Fusion, 51(7):073021, 2011.

[KLP+97] T. Klinger, A. Latten, A. Piel, G. Bonhomme, and T. Pierre. Chaos and turbulence studies in low-β plasmas. Plasma Phys. Control. Fusion, 39:B145, 1997.

[KT13] J. Kim and P. W. Terry. Numerical investigation of frequency spectrum in the Hasegawa-Wakatani model. Physics of Plasmas, 20(10):102303, 2013.

[LD17] J. C. Li and P. H. Diamond. Negative viscosity from negative compressibility and axial flow shear stiffness in a straight magnetic field. Physics of Plasmas, 24(3):032117, 2017.

[LDXT16] J. C. Li, P. H. Diamond, X. Q. Xu, and G. R. Tynan. Dynamics of intrinsic axial flows in unsheared, uniform magnetic fields. Physics of Plasmas, 23(5), 2016.

[LL94] M. A. Lieberman and A. J. Lichtenberg. Principles of Plasma Discharges and Materials Processing. Wiley Interscience Publication, New York, 1994.

[MAP09] P. D. Mininni, A. Alexakis, and A. Pouquet. Scale interactions and scaling laws in rotating flows at moderate rossby numbers and large reynolds numbers. Physics of Fluids, 21(1):015108, 2009.

[MBB+11] S. H. Muller, J. A. Boedo, K. H. Burrell, J. S. deGrassie, R. A. Moyer, D. L. Rudakov, W. M. Solomon, and G. R. Tynan. Intrinsic rotation generation in ELM-free H-mode plasmas in the DIII-D tokamak - experimental observations. Physics of Plasmas, 18(7), 2011.

[MD10] K. Miki and P. H. Diamond. Role of the geodesic acoustic mode shearing feedback loop in transport bifurcations and turbulence spreading. Physics of Plasmas, 17(3):032309, 2010.

[MDG+12] K. Miki, P. H. Diamond, O. D. Gurcan, G. R. Tynan, T. Estrada, L. Schmitz, and G. S. Xu. Spatio-temporal evolution of the L-I-H transition. Physics of Plasmas, 19(9), 2012.

[MDM+15] M. A. Malkov, P. H. Diamond, K. Miki, J. E. Rice, and G. R. Tynan. Linking the micro and macro: *L* - *H* transition dynamics and threshold physics. Physics of Plasmas, 22(3), 2015.

[MRS09] P. Manz, M. Ramisch, and U. Stroth. Physical mechanism behind zonal-flow generation in drift-wave turbulence. Phys. Rev. Lett., 103:165004, 2009.

[MXTT11] P. Manz, M. Xu, S. C. Thakur, and G. R. Tynan. Nonlinear energy transfer during the transition to drift-interchange turbulence. Plasma Physics and Controlled Fusion, 53(9):095001, 2011.

[NBD07] R. Numata, R. Ball, and R. L. Dewar. Bifurcation in electrostatic resistive drift wave turbulence. Physics of Plasmas, 14(10):102312, 2007.

[OT] W. L. Oberkampf and T. G. Trucano. Some specific features of atmospheric turbulence. Progress in Aerospace Sciences, 38(3):209–272.

[PBN13] A. V. Pushkarev, W. J. T. Bos, and S. V. Nazarenko. Zonal flow generation and its feedback on turbulence production in drift wave turbulence. Physics of Plasmas, 20(4):042304, 2013.

[Pec13] H. Pecseli. Waves and Oscillations in PLasmas. CRC Press, Abingdon-U.K., first edition edition, 2013.

[Pop08] S. Pope. Turbulent Flows. Cambridge University Press, Cambridge, UK, 2008.

[RDZ98] B. N. Rogers, J. F. Drake, and A. Zeiler. Phase space of tokamak edge turbulence, the $L-H$ transition, and the formation of the edge pedestal. Phys. Rev. Lett., 81:4396–4399, 1998.

[RHD+11] J. E. Rice, J. W. Hughes, P. H. Diamond, Y. Kosuga, Y. A. Podpaly, M. L. Reinke, M. J. Greenwald, Ö. D. Gürcan, T. S. Hahm, A. E. Hubbard, E. S. Marmar, C. J. McDevitt, and D. G. Whyte. Edge temperature gradient as intrinsic rotation drive in alcator *c*-mod tokamak plasmas. Phys. Rev. Lett., 106:215001, May 2011.

[Rhi75] P. B. Rhines. Waves and turbulence on a beta-plane. Journal of Fluid Mechanics, 69:417–443, 6 1975.

[RMRP92] T. D. Rognlien, J. L. Milovich, M. E. Rensink, and G. D. Porter. A fully implicit, time dependent 2-D fluid code for modeling tokamak edge plasmas. Journal of Nuclear Materials, 196-198(Supplement C):347 – 351, 1992. Plasma-Surface Interactions in Controlled Fusion Devices.

[Sco05] B. D. Scott. Energetics of the interaction between electromagnetic E $\times$ B turbulence and zonal flows. New Journal of Physics, 7(1):92, 2005.

[SDSK13] T. Stoltzfus-Dueck, B. D. Scott, and J. A. Krommes. Nonadiabatic electron response in the hasegawa-wakatani equations. Physics of Plasmas, 20(8):082314, 2013.

[SGK+99] U. Stroth, T. Geist, J. P. T. Koponen, H.-J. Hartfuß, P. Zeiler, ECRH, and W7-AS team. Evidence for convective inward particle transport in a stellarator. Phys. Rev. Lett., 82:928–931, Feb 1999.

[SM00] W. D. Smyth and J. N. Moum. Length scales of turbulence in stably stratified mixing layers. Physics of Fluids, 12(6):1327–1342, 2000.

[Sta05] W. M. Stacey. Fusion Plasma Physics. Wiley VCH, Weinheim, Germany, 2005.

[SZR+12] L. Schmitz, L. Zeng, T. L. Rhodes, J. C. Hillesheim, E. J. Doyle, R. J. Groebner, W. A. Peebles, K. H. Burrell, and G. Wang. Role of zonal flow predator-prey oscillations in triggering the transition to H-mode confinement. Phys. Rev. Lett., 108:155002, Apr 2012.

[Tay15] G. I. Taylor. Eddy motion in the atmosphere. Philosophical Transactions of the Royal Society of London A: Mathematical, Physical and Engineering Sciences, 215(523-537):1–26, 1915.

[TBC+14] S. C. Thakur, C Brandt, L. Cui, J. J. Gosselin, A. D. Light, and G. R. Tynan. Multi-instability plasma dynamics during the route to fully developed turbulence in a helicon plasma. Plasma Sources Science and Technology, 23(4):044006, 2014.

[TBI+04] T. Tala, C. Bourdelle, F. Imbeaux, D. Moreau, V. Parail, G. Corrigan, F. Crisanti, X. Garbet, D. Heading., E. Joffrin, L. Laborde, X. Litaudon, P. et al Mantica, Pr Strand, and Jan Weiland. Progress in transport modeling of internal transport

barrier plasmas in jet. In 20th IAEA Fusion Energy Conference, Villamoura, Portugal November 1-6, IAEA, pages Paper TH / P2–9, 2004.

[Ter00] P. W. Terry. Suppression of turbulence and transport by sheared flow. Rev. Mod. Phys., 72:109–165, 2000.

[TGM+16] S. C. Thakur, J. J. Gosselin, J. McKee, E. E. Scime, S. H. Sears, and G. R. Tynan. Development of core ion temperature gradients and edge sheared flows in a helicon plasma device investigated by laser induced fluorescence measurements. Physics of Plasmas, 23(8):082112, 2016.

[TGT+10] P. Tamain, Ph. Ghendrih, E. Tsitrone, V. Grandgirard, X. Garbet, Y. Sarazin, E. Serre, G. Ciraolo, and G. Chiavassa. Tokam-3d: A 3d fluid code for transport and turbulence in the edge plasma of tokamaks. Journal of Computational Physics, 229(2):361 – 378, 2010.

[THY+06] G. R. Tynan, C. Holland, J. H. Yu, A. James, D. Nishijima, M. Shimada, and N. Taheri. Observation of turbulent-driven shear flow in a cylindrical laboratory plasma device. Plasma Physics and Controlled Fusion, 48(4):S51, 2006.

[TKE+99] P. L. Taylor, A. G. Kellman, T. E. Evans, D. S. Gray, D. A. Humphreys, A. W. Hyatt, T. C. Jemigan, R. L. Lee, J. A. Leur, S. C. Luckhardt, P. B. Prks, M. J. Schaffer, D. G. Whyte, and J. Zhang. Disruption mitigation studies in diii-d. Physics of Plasma, 6:1872, 1999.

[TKL05] M. Z. Tokar, F. A. Kelly, and X. Loozen. Role of thermal instabilities and anomalous transport in threshold of detachment and multifacetted asymmetric radiation from the edge (MARFE). Physics of Plasmas, 12(5):052510, 2005.

[Tok03] M. Z. Tokar. Synergy of anomalous transport and radiation in the density limit. Phys. Rev. Lett., 91:095001, 2003.

[TXD+13] G. R. Tynan, M. Xu, P.H. Diamond, J.A. Boedo, I. Cziegler, N. Fedorczak, P. Manz, K. Miki, S. Thakur, L. Schmitz, L. Zeng, E.J. Doyle, G. M. McKee, Z. Yan, G. S. Xu, B. N. Wan, H. Q. Wang, H. Y. Guo, J. Dong, K. Zhao, J. Cheng, W. Y. Hong, and L. W. Yan. Turbulent-driven low-frequency sheared $E \times B$ flows as the trigger for the h-mode transition. Nuclear Fusion, 53(7):073053, 2013.

[WDH12] L. Wang, P. H. Diamond, and T. S. Hahm. How does drift wave turbulence convert parallel compression into perpendicular flows? Plasma Physics and Controlled Fusion, 54(9):095015, 2012.

[Wes04] J. Wesson. Tokamaks. Clarendon Press, Oxford,UK, third edition, 2004.

[WGE+17] W. X. Wang, B. A. Grierson, S. Ethier, J. Chen, E. Startsev, and P. H. Diamond. Understanding and predicting profile structure and parametric scaling of intrinsic rotation. Physics of Plasmas, 24(9):092501, 2017.

[WRK+15] S. Wiesen, D. Reiter, V. Kotov, M. Baelmans, W. Dekeyser, A.S. Kukushkin, S.W. Lisgo, R.A. Pitts, V. Rozhansky, G. Saibene, I. Veselova, and S. Voskoboynikov. The new solps-iter code package. Journal of Nuclear Materials, 463(Supplement C):480 – 484, 2015. PLASMA-SURFACE INTERACTIONS 21.

[XBFS11] H. Xia, D. Byrne, G. Falkovich, and M. Shats. Upscale energy transfer in thick turbulent fluid layers. Nature Physics, 7:321–324, 2011.

[XTD+12] M. Xu, G. R. Tynan, P. H. Diamond, P. Manz, C. Holland, N. Fedorczak, S. Chakraborty Thakur, J. H. Yu, K. J. Zhao, J. Q. Dong, J. Cheng, W. Y. Hong, L. W. Yan, Q. W. Yang, X. M. Song, Y. Huang, L. Z. Cai, W. L. Zhong, Z. B. Shi, X. T. Ding, X. R. Duan, and Y. Liu. Frequency-resolved nonlinear turbulent energy transfer into zonal flows in strongly heated L-mode plasmas in the HL-2A tokamak. Phys. Rev. Lett., 108:245001, 2012.

[XTH+09] M. Xu, G. R. Tynan, C. Holland, Z. Yan, S. H. Muller, and J. H. Yu. Study of nonlinear spectral energy transfer in frequency domain. Physics of Plasmas, 16(4):042312, 2009.

[XWW+11] G. S. Xu, B. N. Wan, H. Q. Wang, H. Y. Guo, H. L. Zhao, A. D. Liu, V. Naulin, P. H. Diamond, G. R. Tynan, M. Xu, R. Chen, M. Jiang, P. Liu, N. Yan, W. Zhang, L. Wang, S. C. Liu, and S. Y. Ding. First evidence of the role of zonal flows for the L-H transition at marginal input power in the EAST tokamak. Phys. Rev. Lett., 107:125001, Sep 2011.

[YII03] A. Yoshizawa, S. Itoh, and K. Itoh. Plasma and Fluid Turbulence: Theory and Modeling. Institute of Physics Publishing, London, 2003.

[YTH+10] Z. Yan, G. R. Tynan, C. Holland, M. Xu, S. H. Muller, and J. H. Yu. Scaling properties of turbulence driven shear flow. Physics of Plasmas, 17(1):012302, 2010.

[ZHB+10] S. Zhou, W. W. Heidbrink, H. Boehmer, R. McWilliams, T. Carter, S. Vincena, S. K. P. Tripathi, P. Popovich, B. Friedman, and F. Jenko. Turbulent transport of fast ions in the large plasma device. Physics of Plasmas, 17(9), 2010.

[ZMH+10] S. J. Zweben, R. J. Maqueda, R. Hager, K. Hallatschek, S. M. Kaye, T. Munsat, F. M. Poli, A. L. Roquemore, Y. Sechrest, and D. P. Stotler. Quiet periods in edge turbulence preceding the L-H transition in the national spherical torus experiment. Physics of Plasmas, 17(10), 2010.